DIPLOMARBEIT

Master's Thesis

BONE FIBRILLOGENESIS AND MINERALIZATION: QUANTITATIVE ANALYSIS AND IMPLICATIONS FOR TISSUE ELASTICITY

FIBRILLOGENESE UND MINERALISIERUNG IN KNOCHEN: QUANTITATIVE ANALYSE UND AUSWIRKUNGEN AUF DIE GEWEBSELASTIZITÄT

ausgeführt zum Zwecke der Erlangung
des akademischen Grades einer Diplom-Ingenieurin

unter der Leitung von

Ao.Univ.Prof.Dipl.-Ing. Dr.techn. **Christian Hellmich**
E202
Institut für Mechanik der Werkstoffe und Strukturen

eingereicht an der Technischen Universität Wien
Fakultät für Bauingenieurwesen

von

Jenny VUONG, BSc
Sechshauserstraße 68-70/1/2/8
A-1150 Wien, Österreich

Wien, im Jänner 2011

Abstract

The purpose of this master's thesis is to investigate the mineralization and fibrillogenesis mechanism of bone, by interpreting published experimental data in a new way. Corresponding experiments were carried out in different laboratories ranging from the year 1925 up to 2003, using biochemical, biophysical and biomechanical techniques. The first Chapter gives a rough introduction of the topic, while the main part of this thesis consists of an article, which was written in cooperation with Christian Hellmich (this article makes up Chapter 2). The third Chapter summarizes the results, discusses various related scientific papers on biological research, and gives an outlook to future research. The evaluation of the data was done with the software Matlab, and respective source codes with description can be found in the appendix section.

Extracellular bone matrix is a tough material consisting mainly of three types of matter. The organic matter is made up of about 90% collagen, the mineral matter is made up of hydroxyapatite crystals, and the rest of the tissue is made up by water. The goal of our research was to find an inherent 'universal' rule in bone mineralization and fibrillogenesis during growth, adulthood, and finally senescence of humans and various mammals. The first step was to collect data from experiments on bone. We classified the experiments into three different measurement methods: dehydration-demineralization, dehydration-deorganification, and dehydration-ashing tests. All considered experimental protocols covered determination of the overall tissue mass density through Archimedes' principle, and they give access to the weight fractions of the three bone components. We calculated the apparent mass densities of the elementary components of bone, which represent the mass of the respective component per unit volume of the entire tissue. By putting the apparent mass densities of the organic and of the mineral matter in relation, we discovered an astonishing correlation between those two quantities. It becomes evident that the mineral concentration increases linearly with the organic concentration during growth from a young individual until it reaches puberty. After reaching a turning point, the reverse can be seen. At very old age, we may face a decrease of the organic matter with progressing mineralization, and also a decline of water is shown by our results. These findings are consistent with what is known about the cooperation of the biological cells responsible for bone formation and resorption, namely the osteocytes, osteoblasts and osteoclasts, which are guided by growth factors and other stimuli. With the mechanical four-step elastic homogenization scheme developed by Fritsch *et al.* (2009), we could also determine mechanical properties of the extracellular bone matrix on the basis of only one variable

— the overall mass density of the bone sample. Such relations can be suitably expressed by polynomial functions. These findings are also essential in biomaterial design and Computer Tomography based biomedical engineering.

Zusammenfassung

Der Zweck dieser Diplomarbeit ist die Erforschung der Knochenmineralisierung und -fibrillogenese durch Neuinterpretation bereits vorhandener Daten von verschiedenen Experimenten, die in den Jahren 1925 bis 2003 durchgeführt wurden. Biochemische, biophysikalische und biomechanische Techniken wurden hierbei für die Datenerhebung verwendet. Das erste Kapitel umfasst eine kurze Einführung in die Thematik. Kapitel 2 beinhaltet einen wissenschaftlichen Artikel, der in Kooperation mit Christian Hellmich verfasst wurde, welcher den Hauptteil dieser Diplomarbeit ausmacht. Das dritte Kapitel besteht aus einer Zusammenfassung der erzielten Resultate, diskutiert verschiedene wissenschaftliche Artikel, die einen biologischen Bezug zur Thematik aufweisen, und gibt einen Ausblick auf zukünftige Forschungsarbeiten. Die Auswertung der Daten wurde mit Hilfe der Software Matlab durchgeführt, und die dazugehörigen Quelltexte mit genauer Beschreibung befinden sich im Appendix.

Die extrazelluläre Knochenmatrix ist ein widerstandsfähiges Material, welches aus drei Hauptbestandteilen besteht. Der organische Teil besteht hauptsächlich (nämlich zu 90%) aus Kollagen, der Mineralanteil besteht aus Hydroxyapatit-Kristallen, und der Rest des Gewebes besteht aus Wasser. Motivation für unsere Forschung ist es, eine inhärente 'universelle' Regel für Knochenmineralisierung und -fibrillogenese während des Wachstums, des Erwachsenenalters, und schließlich der Vergreisung von Menschen und unterschiedlichen Säugetieren zu finden. Der erste Schritt ist das Sammeln der Daten verschiedenster Knochenexperimente. Die Experimente können nach drei verschiedene Messmethoden klassifiziert werden: Dehydrierung-Demineralisierung, Dehydrierung-Deorganifizierung und Dehydrierung-Verbrennung. Alle berücksichtigten Messprotokolle beinhalteten das Archimedische Prinzip, um die Dichte des Knochenmaterials zu messen. Aus diesen Werten können dann die prozentuellen Gewichtsanteile der drei Knochenkomponenten abgeleitet werden. Wir berechnen die apparente Massendichte (Rohdichte) der drei Knochenkomponenten, welche als die Masse der entsprechenden Knochenkomponente pro Volumseinheit des gesamten Gewebes definiert ist. Wir setzen die apparente Massendichte des organischen und mineralischen Materials in Beziehung und entdecken eine erstaunliche Korrelation zwischen diesen zwei Größen. Die chemische Konzentration des Minerals steigt linear mit der Konzentration des organischen Anteils — während der Wachstungsphase des jungen Individuums bis zur Pubertät. Nach dem Erreichen eines Wendepunktes geschieht beim Umbau des organischen Materials genau das Gegenteil: Im hohen Alter stehen wir einer Abnahme des organischen Anteils bei fortschreitender Mineralisierung gegenüber, und auch eine Verminderung des Wasseranteils

wird aus unseren Resultaten ersichtlich. Diese Ergebnisse passen gut zusammen mit dem aktuellen Wissen über die Kooperation der biologischen Zellen, die für den Knochenaufbau und -abbau verantwortlich sind, nämlich den Osteozyten, den Osteoblasten und den Osteoklasten, die durch Wachstumsfaktoren und anderen *Stimuli* gesteuert werden. Mit Hilfe des mechanischen 4-Stufen Homogenisierungsmodells von Fritsch *et al.* (2009) können wir dann auch die mechanischen Eigenschaften der extrazellulären Knochenmatrix auf Basis einer einzigen Variable bestimmen, nämlich der Massendichte des jeweiligen Knochenstückes. Entsprechende Zusammenhänge können durch Polynome ausgedrückt werden. Diese Erkenntnisse sind auch wichtig beim Entwurf von Biomaterialen, sowie bei auf Computertomographie aufbauender biomedizinischer Technik.

Danksagung

Zuallererst möchte ich meinem Betreuer ao. Univ-Prof. DI Dr. Christian Hellmich für seine Unterstützung bei der Verfassung meiner Diplomarbeit bedanken. Ohne seine kompetente Hilfestellung und Ratschläge hätte die Fertigstellung dieser Arbeit mindestens doppelt so lang gedauert und der Output wäre weniger erfolgreich gewesen. Ich möchte mich auch besonders für die Chance bedanken die mir Prof. Hellmich geboten hat, dass ich am Institut für Mechanik der Werkstoffe und Strukturen als Projektassistentin mitarbeiten durfte. Ich konnte dadurch nicht nur eigene Erfahrungen sammeln, sondern auch von Prof. Hellmichs langjährigen Erfahrungen profitieren und konnte dadurch meinen Horizont für das wissenschaftliche Arbeiten erweitern.

Ich möchte mich auch bei meinem Arbeits- und Bürokollegen DI Dr. Andreas Fritsch für seinen herzlichen Empfang am Institut bedanken. Er hat mir nicht nur bei diversen administrativen Fragen geholfen, sondern mich auch bei Verständnisfragen zur Mechanik und mit der Bereitstellung diverser Unterlagen unterstützt. Der Einstieg in den Arbeitsalltag am Institut wurde mir dadurch wesentlich erleichtert.

Weiters möchte ich mich bei meiner gesamten Familie, insbesondere bei meinen Eltern, bedanken. Egal welche Entscheidung ich in schulischer, beruflicher und akademischer Hinsicht getroffen habe, meine Eltern haben mich nicht nur finanziell, sondern auch seelisch unterstützt. Ich möchte mich auch bei meinen drei Schwestern Xuan, Monika und Martina bedanken, denn auch ihnen verdanke ich finanzielle und seelische Unterstützung. Ohne die Zusprüche, Lebensweisheiten und Aufmunterungen ihrerseits, hätte die Vervollständigung dieser Arbeit nur halb so viel Spaß gemacht und hätte weitaus mehr Krisen verursacht.

Table of Contents

1. Introduction

Bone can be classified as a connective tissue. It consists of a collagen matrix, with a mineral (hydroyapatite) and a water phase (Parfitt, 1983) and is known to give structure to our body, provides supporting functions, protects our organs, has metabolic functions, and also stores minerals. These are only a few examples of the many tasks which our bones should fulfill at normal functionality. It has drawn a lot of attention and encouraged scientists to do various experiments to help them understand the biological, chemical, and physical properties of this biological material. Yet a lot of facts are not understood or cannot be explained, some parts of the big puzzle are incomplete, and some pieces still remain undiscovered.

The main focus of this paper is to help bringing light into fibrillogenesis and mineralization of bone, throughout the growing and aging process of different bones stemming from various mammals. Bone consists mainly of three major components: water (H_2O), hydroxyapatatite minerals (HA) and organics (org). The latter are made up by 90% of collagen (Biltz & Pellegrino, 1969; Urist *et al.* , 1983; Lees, 1987; Weiner & Wagner, 1998; Teitelbaum, 2000; Kazuhiko *et al.* , 2009).

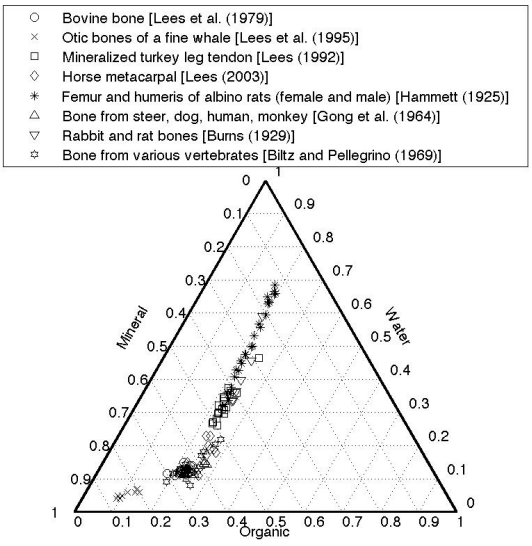

Figure 1.1.: Mineral, water, and organic weight fractions in different mammalian bones

The apparent mass densities, which represent the concentrations of these three bone components, vary among different animals (Lees, 1987; Lees & Page, 1992; Gong *et al.* , 1964; Burns, 1929; Biltz & Pellegrino, 1969) and among animals at different age groups (Lees, 2003; Hammett, 1925). Age being the key factor of enormous chemical composition changes, which is also responsible for changes in mechanical characteristics of bone, was the motivation of several researchers to carry out experiments to find an answer to the question of how aging affects our bones (Kiebzak, 1991; Jowsey, 1960; Frost, 1960; Smith, 1963; Bailey *et al.* , 1998). Even now still a lot of inconsistency exist in the determination of age changes of bone composition between different experiments and researchers. The aim is to define a consistent determination and find a possible explanation with regards to bone biology.

Fritsch & Hellmich (2007) developed a 'universal' five-step micromechanical homogenization model to predict the stiffness of the extravascular bone material. Fritsch & Hellmich (2007) not only developed a model to predict bone stiffness with a high accuracy (mean relative error smaller than 10% between predicted and experimental data), but also pointed out how big the influence of a different composition of water, organics and mineral on the mechanical characteristics of bone is. This is primarily important in designing biomaterials, which should reflect the exact biological and mechanical characteristics of the bone material.

To quantify the mixture of the three bone componentes at different overall mass densities, we aim to define a 'universal' rule of bone mineralization and fibrillogenesis throughout different age groups and density changes as the key factor. To reach this goal, we needed a comprehensive data base from the literature and calculated the concentrations of organic, water and hydroxyapatite minerals by means of quantifying the density and the weight and volume fractions of different bones at different age and from different mammalians. On relating these concentrations to the overall mass density, we could define a general pattern of bone samples going through age and density changes. With the knowledge of this growing and aging pattern of bone, the volume fractions of the samples and the 5-step micromechanical homogenization scheme of Fritsch *et al.* (2009), we could predict the mechanical properties by means of the overall mass density with an even higher accuracy as attained by Fritsch & Hellmich (2007).

2. Article: Bone fibrillogenesis and mineralization: Quantitative analysis and implications for tissue elasticity

This article was submitted to *The Journal of Theoretical Biology* in January 2011.

Bone fibrillogenesis and mineralization: Quantitative analysis and implications for tissue elasticity

Jenny Vuong*, Christian Hellmich**

Institute for Mechanics of Materials and Structures, Vienna University of Technology (TU Wien), A-1040 Wien (Vienna), Austria

Abstract

Data from bone drying, demineralization, and deorganification tests, collected over a time span of more than eighty years, evidence a myriad of different chemical compositions of different bone materials. However, careful analysis of the data, as to extract the chemical concentrations of hydroxyapatite, of water, and of organic material (mainly collagen) in the extracellular bone matrix, reveals an astonishing fact: it appears that there exists a unique bilinear relationship between organic concentration and mineral concentration, across different species, organs, and age groups, from early childhood to senility: During organ growth, the mineral concentration increases linearly with the organic concentration (which increases during fibrillogenesis), while from adulthood on, further increase of the mineral concentration is accompanied by a decrease in organic concentration. These relationships imply unique mass density-concentration laws for fibrillogenesis and mineralization, which - in combination with micromechanical models - deliver 'universal' mass density-elasticity relationships in extracellular bone matrix – valid across different species, organs, and ages. They turn out as quantitative reflections of the well-instrumented interplay of osteoblasts, osteoclasts, osteocytes, and their precursors, controlling, in a fine-tuned fashion, the chemical genesis and continuous transformation of the extracellular bone matrix. Considerations of the aformentioned rules may strongly affect the potential success of tissue engineering strategies, in particular when translating, via micromechanics, the aformentioned growth and mineralization characteristics into tissue-specific elastic properties.

Keywords: bone, fibrillogenesis, mineralization, elasticity, continuum micromechanics, Computer Tomography, biomaterials, tissue engineering

*Tel: +43 1 58801 20265; fax: +43 1 58801 20299

**Corresponding author. Tel: +43 1 58801 20220; fax: +43 1 58801 20299

Email addresses: jenny.vuong@tuwien.ac.at (Jenny Vuong), christian.hellmich@tuwien.ac.at (Christian Hellmich)

Nomenclature

A	...	regression parameter for function $\mathscr{F}_{\rho^*_{org}}(\rho^*_{HA})$
b	...	average (rigid) collagen crosslink length valid for all mineralized tissues
B	...	regression parameter for function $\mathscr{F}_{\rho^*_{org}}(\rho^*_{HA})$
$\mathbb{c}_r$	...	elasticity tensor of phase r
$\mathbb{c}_s$	...	elasticity tensor of phase s
$\mathbb{C}^{ec}$	...	elasticity tensor of extracellular matrix
$\mathbb{C}^{hom}$	...	homogenized elasticity tensor
$\mathbb{C}^0$	...	elasticity tensor of matrix in Eshelby's matrix-inclusion problem
C^{ec}_{ijkl}	...	components of elasticity tensor of extracellular matrix
C^{exp}_{ijkl}	...	experimental value for component *ijkl* of elasticity tensor
C^{pred}_{ijkl}	...	model-predicted value for component *ijkl* of elasticity tensor
d_s	...	equatorial diffraction spacing of molecular collagen
D	...	axial macroperiod of staggered assemblies of type I collagen
D^{ec}_{ijkl}	...	components of compliance tensor of extracellular matrix
$\bar{e}$	...	mean of relative errors between experimental and model-predicted values
e_s	...	standard deviation of relative errors between experimental and model-predicted values
E^{ec}_1	...	Young's modulus in transverse direction
E^{ec}_3	...	Young's modulus in axial direction
f_{col}	...	volume fraction of collagen in extracellular bone matrix
$\mathring{f}_{col}$	...	volume fraction of (molecular) collagen at the wet collagen level
f_{ef}	...	volume fraction of the extrafibrillar space
f_{fib}	...	volume fraction of the fibrillar space
f_{HA}	...	volume fraction of hydroxyapatite in extracellular matrix
$\breve{f}_{HA}$	...	volume fraction of hydroxyapatite in the fibrillar space
$\check{f}_{HA}$	...	volume fraction of hydroxyapatite in the extrafibrillar space
f_{H_2O}	...	volume fraction of water in extracellular matrix
f_{org}	...	volume fraction of organic matter in extracellular matrix
f_r	...	volume fraction of the phase r

f_s	...	volume fraction of the phase s
$\breve{f}_{wetcol}$	...	volume fraction wet collagen in the fibrillar space
$\mathscr{F}_{\rho^*_{org}}(\rho^*_{HA})$	...	bilinear relationship between ρ^*_{org} and ρ^*_{HA}
$\mathfrak{F}(A, B, \rho^{*,crit}_{HA})$	...	sum of squares of the differences between experimental and predicted values
g	...	standard average gravity
G^{ec}_{12}	...	shear modulus in isotropic plane $1-2$, of extracellular bone material
i	...	index (numbering of experimental values)
$\mathbb{I}$	...	fourth-order unity tensor
m_0	...	mass constant in diffraction-density relation
M_{air}	...	mass of (millimeter-sized) wet bone sample in air (with empty vascular pores)
M_{dry}	...	mass of (millimeter-sized) dehydrated bone sample
M_{HA}	...	mass of hydroxyapatite in (millimeter-sized) bone sample
M_{H_2O}	...	mass of water in (millimeter-sized) bone sample
M_{org}	...	mass of organic material in (millimeter-sized) bone sample
N	...	number of experimental values
$\mathbb{P}^0_r$	...	fourth-order Hill tensor
R^2	...	coefficient of determination
SS_{err}	...	sum of squares of the residuals, total sum of squares
SS_{tot}	...	total sum of squares
v_{fib}	...	volume of one rhomboidal fibrillar unit
v_1	...	velocitiy of acoustic plane wave travelling in transverse direction
v_3	...	velocitiy of acoustic plane wave travelling in axial direction
V^{ec}	...	volume of the extracellular tissue within (millimeter-sized) bone sample
$W_{submerged}$	...	weight of (millimeter-sized) bone sample when fully submerged in liquid
WF^{dry}_{ash}	...	weight fraction of ash in dried bone samples
WF_{HA}	...	weight fraction of hydroxyapatite in extracellular bone matrix
WF_{H_2O}	...	weight fraction of water in extracellular bone matrix
WF_{org}	...	weight fraction of organic material in extracellular bone matrix

$x_{exp,i}$	...	i^{th} experimentally obtained value
$x_{pred,i}$	...	i^{th} predicted value
μ^{ec}	...	X-ray attenuation coefficient of the extracellular bone material
μ_{HA}	...	X-ray attenuation coefficient of hydroxyapatite
μ_{H_2O}	...	X-ray attenuation coefficient of water
μ_{org}	...	X-ray attenuation coefficient of organic matter
ν_{12}	...	Poisson's ratio in isotropic plane
ν_{13}	...	Poisson's ratio in axial direction
ρ^{ec}	...	mass density of extracellular bone matrix
ρ_{liquid}	...	mass density of liquid
ρ_{HA}	...	real mass density of hydroxyapatite
ρ_{H_2O}	...	real mass density of water
ρ_{org}	...	real mass density of organic matter
ρ^*_{HA}	...	apparent mass density of hydroxyapatite (mass of hydroxyapatite per volume of extracellular bone matrix)
$\rho^*_{H_2O}$	...	apparent mass density of water (mass of water per volume of extracellular bone matrix)
ρ^*_{org}	...	apparent mass density of organic matter (mass of organic matter per volume of extracellular bone matrix)
$\phi_{HA,ef}$	...	relative amount of hydroxyapatite in the extrafibrillar space, with respect to total amount of hydroxyapatite per volume of extracellular matrix
:	...	second-order tensor contraction

1. Introduction

Bone tissue engineering has become a huge field, both in terms of scientific production and medical potential (Cancedda et al., 2007), and ever since the pioneering work of Langer and Vacanti (1993), a great variety of different material systems have been explored for their potential use as bone tissue engineering scaffolds (Karageorgiou and Kaplan, 2005; Perry, 2002; Komlev et al., 2010; Verma et al., 2008). Quite naturally among all these materials, such based on the actual elementary components of bone, i.e. on hydroxyapatite, collagen and water, may play an important role among all the aformentioned material classes, since one might well expect that such materials might tend to be able to reproduce both the astonishing mechanical properties of bone and the material's biological features (Ficai et al., 2009; Green, 2008; Pramatarova et al., 2005; Roeder, 2008). But even if the materials' basic components are chosen, the questions regarding their mixing characteristics, i.e. of the concentration of the individual components, remain to be answered. A close inspection of century-long chemical investigations clearly shows that there is a larger variety of compositions, ranging all the way from (almost) unmineralized osteoid in early deposition stages to tissues consisting mainly of hydroxyapatite (Hammett, 1925; Lees et al., 1995). To somehow simplify this truly complicated matter, one might hope for general inherent 'rules', quantifying natural relationships between constituent concentrations stemming from sophistically orchestrated activity of biological cells, hormones and growth factors (Lemaire et al., 2004; Gajjeraman et al., 2007; Filvaroff and Derynck, 1998; Pivonka et al., 2010). It is the very focus of this paper to check for the existence of such 'universal' rules in bone fibrillogenesis [when more and more organic matter, mostly collagen, is accumulated in a material volume of bone (Hammett, 1925; Parry and Craig, 1978)] and in bone mineralization [when hydroxyapatite precipitates in the extracollagenous spaces (Hellmich and Ulm, 2003; Höhling, 1969; Landis et al., 1996)]. Therefore, we aim at quantification of relations between the concentrations of the elementary components within a piece of extracellular bone matrix, being expressed as the masses of these constituents per volume of extraellular bone matrix ("apparent mass densities"). In order to reach this aim, we perform the following steps, as described in the sequel of the paper: We collect a comprehensive data base from the literature, related to tissue mass density and composition measurements from a great variety of tissues, belonging either to the same tissue type at different ages of the organism, or to tissues from different organisms at only one age per organism, or both. Subsequently, we describe how to derive constituent concentrations (i.e. apparent mass densities of mineral, collagen and water) from these experimental data base (Section 2). The results of this derivation, 'universal' rules for bone fibrillogenesis and mineralization, are given thereafter (Section 3). Then, the aformentioned bone composition rules are converted, through micromechanics laws, into composition-elasticity relations, which may be used as a prerequisite for biomaterial design (Section 4). Finally, the results are discussed in view of their relation to modern bone biology, as well as with respect to biomaterial design and exploitation of Computer Tomographic Data (Section 5).

2. Evaluation of mass and volume, demineralization and ashing experiments - mass densities and concentrations

2.1. Mass and volume measurements - mass densities

The experimental data of Lees et al. (1979a, 1995, 1983); Lees (1987, 2003); Lees and Page (1992); Biltz and Pellegrino (1969); Gong et al. (1964a); Burns (1929); Hammett (1925) refer to mass density determination according to Archimedes' principle: The mass of samples with a typical size of a few millimeters is measured in air. Hence, the respective value M_{air} refers to a state of empty vascular and lacunar pores, but with wet extracellular (ec) bone matrix. This mass is related to the volume of the extracellular bone matrix V^{ec}, as to arrive at the extracellular tissue mass density

$$\rho^{ec} = \frac{M_{air}}{V^{ec}}. \tag{1}$$

The important feature of Archimedes' principle lies in the mode of determination of V^{ec}. It is determined from M_{air}, together with the weight $W_{submerged}$ of the sample when submerged into a liquid with mass density ρ_{liquid}, according to

$$V^{ec} = \frac{M_{air} - \frac{W_{submerged}}{g}}{\rho_{liquid}}, \tag{2}$$

with g as the standard average gravity, $g = 9.81$ m/s^2. Eq. (2) is valid once the pressure in the vascular and lacunar pores follows the hydrostatic pressure distribution in the container where the sample is submerged. Given the characteristic size of vascular and lacunar pores, this requirement is standardly fulfilled. Still, care has to be taken that no air bubbles are entrapped when submerging the samples (Gong et al., 1964a). The extracellular bone tissue mass densities have been documented by Lees et al. (1979a, 1983); Lees (1987); Lees and Page (1992); Lees et al. (1995); Lees (2003); Biltz and Pellegrino (1969); Broz et al. (1995); Gong et al. (1964a); Burns (1929); Hammett (1925), see Tables 1–5.

2.2. Dehydration and demineralization tests - Concentration of hydroxyapatite, organics and water

According to the protocols of Lees et al. (1979a, 1983); Lees (1987); Lees and Page (1992), Lees et al. (1995); Lees (2003), bone samples are dried in a vacuum dessicator at room temperature, until a constant mass is observed (typically after 7 days). This mass is the mass of the dehydrated extracellular bone tissue, M_{dry}. The difference between the wet tissue mass in air, M_{air}, and the dehydrated tissue mass, M_{dry}, equals the mass of water contained in the extracellular matrix,

$$M_{H_2O} = M_{air} - M_{dry}. \tag{3}$$

The water content is typically given in terms of the weight fraction of water,

$$WF_{H_2O} = \frac{M_{H_2O}}{M_{air}}, \tag{4}$$

or in terms of the apparent mass density

$$\rho^*_{H_2O} = \frac{M_{H_2O}}{V^{ec}}, \tag{5}$$

which is proportional to the chemical concentration of water, with the molar mass of water as the proportionality factor. Next, the samples are re-hydrated and then demineralized in a 0.5 M EDTA solution at pH 7.5, until no calcium is detected anymore by an atomic absorption spectrometer. After drying such a demineralized sample in vaccum, one is left with the organic mass contained in the tissue, M_{org}. The respective organic content is typically given in terms of the organic weight fraction

$$WF_{org} = \frac{M_{org}}{M_{air}}, \tag{6}$$

or in terms of the apparent mass density

$$\rho^*_{org} = \frac{M_{org}}{V^{ec}}, \tag{7}$$

which is proportional to the chemical concentration of organic matter within the extracellular bone matrix, with the molar mass of the osteoid organic material as the proportionality factor. Finally, knowledge of mass and concentrations of both organic and water gives access to the hydroxyapatite masses, weight fractions, and apparent mass densities, as

$$M_{HA} = M_{air} - M_{org} - M_{H_2O}, \tag{8}$$

$$WF_{HA} = \frac{M_{HA}}{M_{air}}, \tag{9}$$

$$\rho^*_{HA} = \frac{M_{HA}}{V^{ec}}, \tag{10}$$

and the subsequent relations follow from Eqs. (3)–(10)

$$WF_{HA} + WF_{org} + WF_{H_2O} = 1, \tag{11}$$

$$\rho^*_{HA} + \rho^*_{org} + \rho^*_{H_2O} = \rho^{ec}, \tag{12}$$

with the apparent mass densities calculated via

$$\rho^*_{org} = WF_{org} \times \rho^{ec}, \tag{13}$$

$$\rho^*_{HA} = WF_{HA} \times \rho^{ec}, \tag{14}$$

$$\rho^*_{H_2O} = WF_{H_2O} \times \rho^{ec}. \tag{15}$$

Such weight fractions have been documented by Lees et al. (1979a, 1983); Lees (1987); Lees and Page (1992); Lees et al. (1995); Lees (2003), and Eqs. (13) to (15) were used to compute the apparent mass densities, as given in Tables 1 and 2. The extracellular mass densities ρ^{ec} are not explicitly given in Lees (2003). In this case, the weight fractions provide access to ρ^{ec}, via

$$\begin{aligned} \rho^{ec} &= \left(\frac{WF_{org}}{\rho_{org}} + \frac{WF_{HA}}{\rho_{HA}} + \frac{WF_{H_2O}}{\rho_{H_2O}} \right)^{-1} \\ &= \left(\frac{WF_{org}}{\rho_{org}} + \frac{WF_{HA}}{\rho_{HA}} + \frac{1 - WF_{org} - WF_{HA}}{\rho_{H_2O}} \right)^{-1} \end{aligned} \tag{16}$$

with the real mass densities of water, of organics, and of hydroxyapatite reading as $\rho_{H_2O} = 1$ g/cm^3, $\rho_{org} = 1.41$ g/cm^3 (Lees, 1987), and $\rho_{HA} = 3$ g/cm^3 (Gong et al., 1964b; Lees, 1987; Hellmich, 2005). Corresponding values are documented in Table 3.

Table 1: Bone compositions from dehydration-demineralization experiments of Lees et al. (1979a); Lees and Page (1992)

Tissue	ρ^{ec}	WF_{HA}	WF_{org}	WF_{H_2O}	ρ^*_{HA}	ρ^*_{org}	$\rho^*_{H_2O}$
	[g/cm^3]	-	-	-	[g/cm^3]	[g/cm^3]	[g/cm^3]
	given	given	given	given	Eq. (14)	Eq. (13)	Eq. (15)
Bovine tibia[a]	2.060	0.66	0.22	0.12	1.355	0.451	0.253
Bovine tibia[a]	2.050	0.66	0.22	0.13	1.345	0.449	0.258
Bovine tibia[a]	2.020	0.62	0.24	0.14	1.254	0.483	0.283
Bovine tibia[a]	2.020	0.63	0.23	0.14	1.267	0.469	0.283
Bovine tibia[a]	2.000	0.64	0.23	0.13	1.286	0.454	0.258
Bovine tibia[a]	2.050	0.64	0.23	0.13	1.318	0.471	0.260
Bovine tibia[a]	2.100	0.67	0.21	0.12	1.409	0.443	0.248
Bovine tibia[a]	2.080	0.66	0.22	0.12	1.381	0.449	0.250
Bovine tibia[a]	2.020	0.66	0.22	0.12	1.329	0.442	0.248
Bovine tibia[a]	1.990	0.66	0.22	0.13	1.305	0.436	0.251
Bovine tibia[a]	1.950	0.64	0.23	0.13	1.248	0.445	0.255
Bovine tibia[a]	2.010	0.66	0.22	0.12	1.325	0.438	0.247
Bovine tibia[a]	2.040	0.64	0.24	0.12	1.302	0.494	0.247
Bovine tibia[a]	2.050	0.70	0.21	0.12	1.433	0.430	0.238
Bovine tibia[a]	2.120	0.66	0.21	0.12	1.401	0.456	0.261
Bovine tibia[a]	2.080	0.66	0.22	0.12	1.379	0.460	0.241
Bovine tibia[a]	2.100	0.65	0.22	0.13	1.359	0.470	0.271
Bovine tibia[a]	1.980	0.65	0.22	0.13	1.295	0.430	0.253
Bovine tibia[a]	2.050	0.64	0.23	0.13	1.320	0.465	0.264
Bovine tibia[a]	2.110	0.65	0.23	0.12	1.369	0.483	0.257
Bovine tibia[a]	2.030	0.64	0.21	0.12	1.295	0.432	0.250
Bovine tibia[a]	2.060	0.70	0.18	0.12	1.440	0.379	0.241
Mineralized turkey leg tendon[b]	1.332	0.29	0.25	0.46	0.380	0.333	0.619
Mineralized turkey leg tendon[b]	1.498	0.45	0.24	0.32	0.667	0.358	0.473
Mineralized turkey leg tendon[b]	1.498	0.41	0.22	0.37	0.614	0.325	0.560
Mineralized turkey leg tendon[b]	1.507	0.44	0.22	0.35	0.658	0.326	0.522
Mineralized turkey leg tendon[b]	1.520	0.45	0.24	0.31	0.690	0.363	0.468
Mineralized turkey leg tendon[b]	1.523	0.44	0.22	0.34	0.666	0.334	0.523
Mineralized turkey leg tendon[b]	1.524	0.40	0.24	0.36	0.603	0.372	0.549
Mineralized turkey leg tendon[b]	1.533	0.44	0.22	0.34	0.678	0.341	0.514
Mineralized turkey leg tendon[b]	1.541	0.46	0.24	0.30	0.707	0.376	0.457
Mineralized turkey leg tendon[b]	1.577	0.47	0.23	0.30	0.746	0.359	0.472
Mineralized turkey leg tendon[b]	1.581	0.46	0.22	0.32	0.730	0.343	0.508
Mineralized turkey leg tendon[b]	1.589	0.48	0.23	0.30	0.756	0.362	0.471
Mineralized turkey leg tendon[b]	1.597	0.49	0.23	0.28	0.777	0.368	0.452
Mineralized turkey leg tendon[b]	1.610	0.46	0.23	0.31	0.739	0.371	0.500
Mineralized turkey leg tendon[b]	1.614	0.49	0.24	0.26	0.799	0.394	0.421
Mineralized turkey leg tendon[b]	1.619	0.50	0.23	0.27	0.810	0.369	0.440
Mineralized turkey leg tendon[b]	1.643	0.51	0.23	0.27	0.831	0.374	0.438

[a] Lees et al. (1979a)
[b] Lees and Page (1992)

Table 2: Bone compositions from dehydration-demineralization experiments of Lees et al. (1995)

Tissue	ρ^{ec}	WF_{HA}	WF_{org}	WF_{H_2O}	ρ^*_{HA}	ρ^*_{org}	$\rho^*_{H_2O}$
	[g/cm^3]	-	-	-	[g/cm^3]	[g/cm^3]	[g/cm^3]
	given	given	given	given	Eq. (14)	Eq. (13)	Eq. (15)
Whale malleus [a]	2.490	0.86	0.10	0.04	2.141	0.249	0.100
Whale malleus [a]	2.450	0.80	0.13	0.07	1.960	0.319	0.172
Whale incus [a]	2.500	0.86	0.09	0.05	2.150	0.225	0.125
Whale stapes [a]	2.420	0.81	0.13	0.06	1.960	0.315	0.145
Whale stapes [a]	2.360	0.80	0.14	0.06	1.888	0.330	0.142
Whale periotic[a]	2.400	0.81	0.13	0.07	1.944	0.312	0.168
Whale periotic[a]	2.480	0.83	0.11	0.06	2.058	0.273	0.149
Whale periotic[a]	2.520	0.85	0.10	0.05	2.142	0.252	0.126
Whale periotic[a]	2.520	0.85	0.10	0.05	2.142	0.252	0.126
Whale periotic[a]	2.580	0.87	0.09	0.04	2.245	0.232	0.103
Whale t. bulla[a]	2.480	0.85	0.10	0.05	2.108	0.248	0.124

Table 3: Bone compositions from dehydration-demineralization experiments of Lees (2003)

Tissue	WF_{HA}	WF_{org}	WF_{H_2O}	ρ^{ec}	ρ^*_{HA}	ρ^*_{org}	$\rho^*_{H_2O}$
	-	-	-	[g/cm^3]	[g/cm^3]	[g/cm^3]	[g/cm^3]
	given	given	given	Eq. (16)	Eq. (14)	Eq. (13)	Eq. (15)
Horse metacarpal	0.54	0.25	0.20	1.784	0.981	0.446	0.357
Horse metacarpal	0.53	0.26	0.17	1.837	1.047	0.478	0.312
Horse metacarpal	0.54	0.26	0.19	1.793	0.986	0.466	0.341
Horse metacarpal	0.63	0.28	0.18	1.790	0.967	0.501	0.322
Horse metacarpal	0.62	0.26	0.12	1.957	1.213	0.509	0.235
Horse metacarpal	0.62	0.27	0.11	1.968	1.220	0.531	0.216
Horse metacarpal	0.64	0.26	0.12	1.957	1.213	0.509	0.235
Horse metacarpal	0.62	0.26	0.13	1.932	1.178	0.502	0.251
Horse metacarpal	0.66	0.25	0.13	1.946	1.206	0.486	0.253
Horse metacarpal	0.63	0.23	0.23	1.745	0.942	0.401	0.401
Horse metacarpal	0.54	0.24	0.23	1.733	0.919	0.416	0.399
Horse metacarpal	0.53	0.27	0.19	1.781	0.962	0.481	0.338
Horse metacarpal	0.54	0.22	0.15	1.938	1.221	0.426	0.291
Horse metacarpal	0.63	0.25	0.13	1.946	1.206	0.486	0.253
Horse metacarpal	0.62	0.26	0.12	1.957	1.213	0.509	0.235
Horse metacarpal	0.62	0.23	0.13	1.975	1.264	0.454	0.257
Horse metacarpal	0.64	0.26	0.12	1.957	1.213	0.509	0.235
Horse metacarpal	0.62	0.23	0.12	1.988	1.312	0.457	0.239
Horse metacarpal	0.66	0.24	0.13	1.960	1.235	0.470	0.255

2.3. Dehydration-deorganification tests of Gong et al. - Concentration of hydroxyapatite, organics and water

According to the protocol of Gong et al. (1964a), bone samples with original weight of M_{air} are dried at 80 °C for 72 hours, after which they exhibit mass M_{dry}. Through Eqs. (3)–(5), these masses give access to the water concentration in the extracellular bone matrices. Next, the samples are freed from fat and other organic material, using, in a soxhlet apparatus, a mixture of 80% ethyl ether and 20% ethyl alcohol, as well as an 80% aqueous solution of ethylene diamine, respectively.
After drying such a de-organified sample at 80 °C until a constant weight is attained, one is left with the hydroxyapatite mass contained in the tissue, M_{HA}. Through Eqs. (9)–(10), this mass gives access to the hydroxyapatite concentrations in the extracellular bone matrices. Finally, when knowing M_{HA}, M_{air}, and M_{H_2O}, Eq. (8), together with Eq. (6) and (7), delivers the organic concentration. Corresponding apparent mass densities are given in Gong et al. (1964a), see Table 4.

Table 4: Bone composition from dehydration-deorganification experiments of Gong et al. (1964a)

Tissue	ρ^{ec}	ρ^*_{org}	$\rho^*_{H_2O}$	ρ^*_{HA}
	[g/cm^3]	[g/cm^3]	[g/cm^3]	[g/cm^3]
	given	given	given	Eq. (12)
Steer tibial shaft	1.995	0.486	0.252	1.257
Dog femoral shaft	2.003	0.519	0.223	1.261
Human femur and tibia	1.991	0.476	0.237	1.278
Monkey femur diaphysis	2.035	0.487	0.239	1.309
Steer atlas bone	1.93	0.51	0.28	1.14
Dog lumbar vertebral body	1.91	0.51	0.29	1.11
Human 12th thoracic, 1st and 2nd lumbar vertebral body	1.92	0.50	0.27	1.16
Monkey lumbar vertebrae	1.88	0.51	0.27	1.09

2.4. Dehydration-ashing tests - Concentration of hydroxyapatite, organics and water

According to the protocols of Burns (1929) and Hammett (1925), whole bones of rats with fresh weight M_{air} are dried at 105-110 °C for 24 hours (Hammett, 1925; Chick et al., 1926) and at 96 °C for seven days (Hammett, 1925, 1924), respectively. Thereafter, the bones exhibit masses M_{dry}. Through Eqs. (3) and (4), these masses give access to the water weight fractions WF_{H_2O}. Next, the dried bones are gently incinerated until all organic matter is burned off. Subsequent weighing results in the hydroxyapatite mass M_{HA}, giving access to mineral and organic weight fractions according to Eqs. (9), (8) and (6) . These weight fractions, in turn, provide access to the mean mass density of the extracellular matrix of the investigated bones, through Eq. (16). Together with Eqs. (16), Eqs. (13)–(15) deliver the apparent mass densities of organics, water and hydroxyapatite. Corresponding values are documented in Table 5.

Table 5: Bone compositions from dehydration-ashing experiments of Hammett (1925) and Burns (1929)

Tissue	WF_{HA}	WF_{org}	WF_{H_2O}	ρ^{ec}	ρ^*_{HA}	ρ^*_{org}	$\rho^*_{H_2O}$
	-	-	-	[g/cm^3]	[g/cm^3]	[g/cm^3]	[g/cm^3]
	given	given	given	Eq. (16)	Eq. (10)	Eq. (7)	Eq. (5)
Rabbit femur, fibula, tibia, humerus, radius and ulna[a]	0.31	0.23	0.45	1.381	0.428	0.324	0.628
Rabbit femur, fibula, tibia, humerus, radius and ulna[a]	0.21	0.20	0.59	1.250	0.266	0.246	0.737
Rat leg bones[a]	0.42	0.25	0.34	1.54	0.64	0.38	0.52
Rat leg bones[a]	0.37	0.24	0.40	1.45	0.53	0.35	0.58
Rat leg bones[a]	0.42	0.24	0.34	1.54	0.65	0.38	0.52
Rat leg bones[a]	0.40	0.23	0.36	1.52	0.62	0.35	0.54
Rat leg bones[a]	0.40	0.24	0.36	1.50	0.59	0.36	0.54
Humerus of rat[b]	0.18	0.19	0.63	1.209	0.155	0.212	0.798
Humerus of rat[b]	0.18	0.19	0.63	1.213	0.169	0.225	0.784
Humerus of rat[b]	0.26	0.20	0.53	1.308	0.249	0.253	0.738
Humerus of rat[b]	0.32	0.21	0.48	1.372	0.379	0.290	0.668
Humerus of rat[b]	0.36	0.21	0.43	1.433	0.433	0.288	0.651
Humerus of rat[b]	0.42	0.22	0.36	1.524	0.509	0.311	0.610
Humerus of rat[b]	0.45	0.23	0.32	1.580	0.628	0.349	0.543
Humerus of rat[b]	0.17	0.18	0.65	1.199	0.169	0.233	0.779
Humerus of rat[b]	0.18	0.19	0.63	1.209	0.178	0.231	0.777
Humerus of rat[b]	0.23	0.20	0.57	1.273	0.300	0.266	0.711
Humerus of rat[b]	0.31	0.21	0.48	1.372	0.387	0.285	0.669
Humerus of rat[b]	0.34	0.21	0.46	1.398	0.475	0.301	0.629
Humerus of rat[b]	0.38	0.21	0.41	1.459	0.601	0.333	0.564
Humerus of rat[b]	0.42	0.22	0.35	1.532	0.666	0.364	0.520
Femur of rat[b]	0.14	0.20	0.66	1.180	0.205	0.215	0.779
Femur of rat[b]	0.15	0.19	0.65	1.186	0.213	0.230	0.766
Femur of rat[b]	0.24	0.21	0.56	1.277	0.299	0.253	0.721
Femur of rat[b]	0.29	0.21	0.50	1.341	0.432	0.288	0.652
Femur of rat[b]	0.34	0.21	0.45	1.404	0.471	0.290	0.637
Femur of rat[b]	0.40	0.22	0.38	1.497	0.552	0.314	0.594
Femur of rat[b]	0.43	0.23	0.34	1.550	0.650	0.340	0.542
Femur of rat[b]	0.13	0.18	0.68	1.165	0.212	0.234	0.763
Femur of rat[b]	0.14	0.19	0.67	1.178	0.218	0.234	0.761
Femur of rat[b]	0.20	0.20	0.59	1.240	0.345	0.268	0.695
Femur of rat[b]	0.28	0.22	0.50	1.337	0.432	0.287	0.652
Femur of rat[b]	0.32	0.21	0.47	1.372	0.519	0.300	0.614
Femur of rat[b]	0.36	0.22	0.43	1.429	0.640	0.334	0.550
Femur of rat[b]	0.41	0.23	0.36	1.520	0.713	0.361	0.506

[a] Burns (1929), weight fraction of the fat was given separately, therefore recalculation of the fatless weight fractions necessary
[b] Hammett (1925)

According to the protocol of Biltz and Pellegrino (1969), bone samples with original weight of M_{air}, are dried at 105 °C until a constant mass, M_{dry}, is attained. Thereafter, they are incinerated at 600 °C, for sixteen hours, being transformed into ash with weight M_{ash}. Biltz and Pellegrino (1969) documented the volume fraction of water

$$f_{H_2O} = \frac{(M_{air} - M_{dry})}{V^{ec}}, \tag{17}$$

as well as the weight fraction of ash in dried samples,

$$WF_{ash}^{dry} = \frac{M_{ash}}{M_{dry}}. \tag{18}$$

Gong et al. (1964b) showed that, at 600 °C, not only organic matter, but also part of the hydroxyapatite becomes volatile during incineration. In quantitative terms, 6.6% of the ash weight is the weight of volatile inorganic. Hence, the weight fraction of hydroxyapatite in a dried bone sample reads as

$$WF_{HA}^{dry} = WF_{ash}^{dry} \times 1.066. \tag{19}$$

WF_{HA}^{dry} gives access to the apparent mass density of hydroxyapatite, via

$$\rho_{HA}^{*} = WF_{HA}^{dry} \times (\rho_{exp}^{ec} - \rho_{H_2O}^{*}), \tag{20}$$

with the apparent mass density of water following from

$$\rho_{H_2O}^{*} = f_{H_2O} \times \rho_{H_2O}. \tag{21}$$

Finally, the apparent mass density of organic matter follows from Eq. (12). Corresponding values are documented in Table 6.

Table 6: Bone compositions from dehydration-ashing experiments of Biltz and Pellegrino (1969)

Tissue	ρ^{ec}	f_{H_2O}	WF_{ash}^{dry}	WF_{HA}^{dry}	WF_{HA}^{ec}	WF_{org}^{ec}	$WF_{H_2O}^{ec}$	ρ_{HA}^{*}	ρ_{org}^{*}	$\rho_{H_2O}^{*}$
Cortical bone of	[g/cm^3]	-	-	-	-	-	-	[g/cm^3]	[g/cm^3]	[g/cm^3]
femora and tibia:	given	given	given	Eq. (19)	Eq. (14)	Eq. (13)	Eq. (15)	Eq. (20)	Eq. (12)	Eq. (21)
Fish	1.800	0.40	0.61	0.65	0.51	0.27	0.22	0.913	0.491	0.396
Turtle	1.810	0.37	0.62	0.67	0.53	0.27	0.20	0.958	0.482	0.370
Frog	1.930	0.35	0.66	0.70	0.57	0.25	0.18	1.103	0.475	0.352
Polar Bear	1.920	0.33	0.66	0.70	0.58	0.25	0.17	1.119	0.471	0.330
Man	1.940	0.15	0.67	0.71	0.66	0.26	0.08	1.275	0.510	0.155
Elephant	2.000	0.20	0.69	0.73	0.66	0.24	0.10	1.316	0.484	0.200
Monkey	2.090	0.23	0.69	0.73	0.65	0.24	0.11	1.364	0.496	0.230
Cat	2.050	0.24	0.69	0.74	0.65	0.23	0.12	1.336	0.478	0.236
Horse	2.020	0.25	0.69	0.74	0.65	0.23	0.12	1.309	0.461	0.250
Chicken	2.040	0.24	0.70	0.74	0.65	0.23	0.12	1.332	0.463	0.245
Dog	1.940	0.28	0.70	0.74	0.64	0.22	0.14	1.235	0.425	0.280
Goose	2.040	0.23	0.71	0.75	0.67	0.22	0.11	1.365	0.445	0.230
Cow	2.000	0.26	0.71	0.76	0.66	0.21	0.13	1.315	0.423	0.262
Guinea Pig	2.100	0.25	0.71	0.76	0.67	0.21	0.12	1.404	0.446	0.250
Rabbit	2.120	0.24	0.73	0.77	0.69	0.20	0.12	1.453	0.422	0.245
Rat	2.240	0.20	0.73	0.78	0.71	0.20	0.09	1.597	0.441	0.202

3. 'Universal' rules in bone fibrillogenesis and mineralization

The concentrations (apparent mass densities) of organics, mineral, and water in bone tissues from a great variety of species, organs, and ages [as determined through Eqs. (1) –(21)], strongly correlate mutually, and they also correlate with the bone tissue mass density, as seen in Figures 1–4, plotted on the basis of the data evaluated in Tables 1–6.

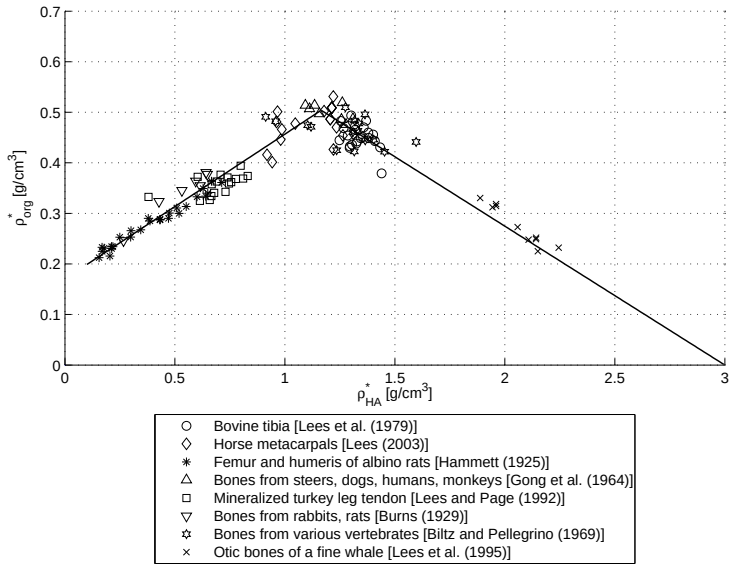

Figure 1: Relation between apparent mass densities of hydroxyapatite and organic matter in extracellular bone matrix, across different species, organs and ages (see Tables 1 to 6 for numerical values and specification of bone types)

Interestingly, all these correlations can be represented by bilinear functions. As for the relationship between organics and mineral concentration, an increase of organic concentration with increasing mineral concentration (up to a critical value $\rho_{HA}^{*,crit}$ of about 1.20 g/m^3) is followed by a decrease of organic concentration with increasing mineral concentration (larger than about 1.20 g/m^3), see Figure 1. The bilinear relationship can be represented by two linear branches,

$$\mathscr{F}_{\rho_{org}^*}(\rho_{HA}^*) = A \times \rho_{HA}^* + B \qquad \text{for } 0 < \rho_{HA}^* \leqslant \rho_{HA}^{*,crit}, \tag{22}$$

$$\mathscr{F}_{\rho_{org}^*}(\rho_{HA}^*) = \left[A \times \rho_{HA}^{*,crit} + B\right] \times \left[1 - \frac{\rho_{HA}^* - \rho_{HA}^{*,crit}}{\rho_{HA} - \rho_{HA}^{*,crit}}\right] \tag{23}$$
$$\text{for } \rho_{HA}^{*,crit} < \rho_{HA}^* < \rho_{HA}.$$

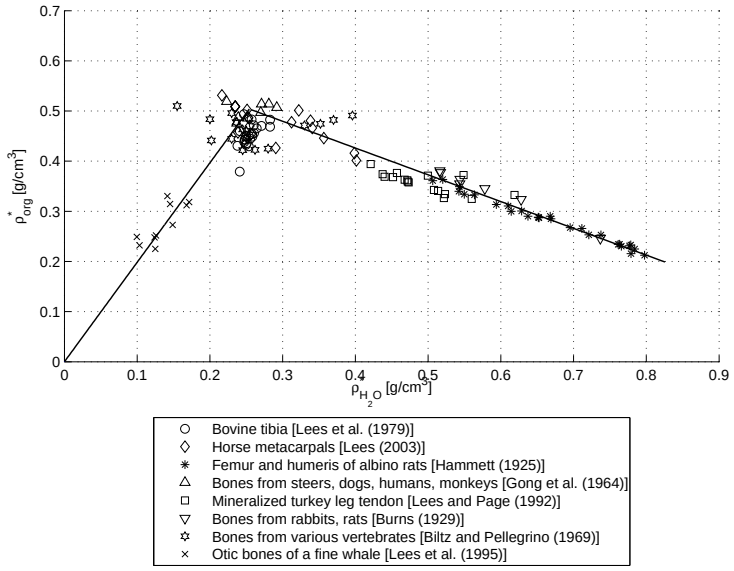

Figure 2: Relation between apparent mass densities of water and organic matter in extracellular bone matrix, across different species, organs and ages (see Tables 1 to 6 for numerical values and specification of bone types)

In Eq. (22) and (23), A, B, and $\rho_{HA}^{*,crit}$ are determined such that the sum of squares of the differences between the N experimental values $\rho_{org,i}^{*}$ (corresponding to hydroxyapatite concentrations $\rho_{HA,i}^{*}$) and corresponding fitted values $\mathscr{F}_{\rho_{org}^{*}}(\rho_{HA,i}^{*})$, according to Eqs. (22) and (23), is minimized,

$$\mathfrak{F}(A,B,\rho_{HA}^{*,crit}) = \sum_{i=1}^{N} \left[\rho_{org,i}^{*} - \mathscr{F}_{\rho_{org}^{*}}(\rho_{HA,i}^{*})\right]^2 \rightarrow min. \tag{24}$$

This yields $A = 0.29$ g/cm^3, $B = 0.17$ g/cm^3, and $\rho_{HA}^{*,crit} = 1.18$ g/cm^3. The maximum apparent mass density of organic matter follows as $\mathscr{F}_{\rho_{org}^{*}}(\rho_{HA}^{*,crit}) = 0.51$ g/cm^3. The quality of the bilinear representation expressed through Eq. (22) and (23) is underlined by the coefficient of determination

$$R^2 = 1 - \left(\frac{SS_{err}}{SS_{tot}}\right), \tag{25}$$

with

$$SS_{tot} = \sum_{i=1}^{N} \left(\rho_{org,i}^{*} - \frac{1}{N}\sum \rho_{org,i}^{*}\right)^2, \tag{26}$$

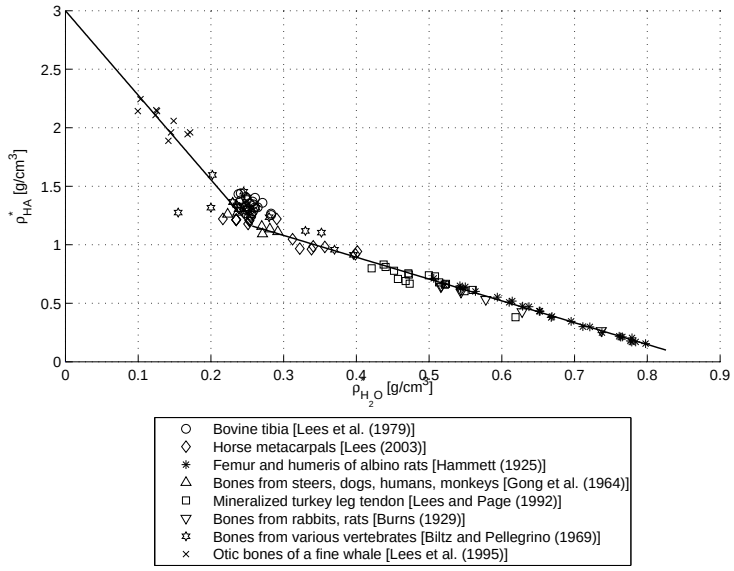

Figure 3: Relation between apparent mass densities of water and hydroxyapatite matter in extracellular bone matrix, across different species, organs and ages (see Tables 1 to 6 for numerical values and specification of bone types)

and

$$SS_{err} = \sum_{i=1}^{N} (\rho^*_{org,i} - \mathscr{F}_{\rho^*_{HA,i}})^2, \tag{27}$$

amounting to $R^2 = 0.94$.
The apparent mass densities of hydroxyapatite and organics can be transformed into volume fractions (volume of hydroxyapatite or organics within a piece of extracellular bone matrix, over volume V_{ec} of this piece), through

$$f_{HA} = \frac{\rho^*_{HA}}{\rho_{HA}}, \tag{28}$$

$$f_{org} = \frac{\rho^*_{org}}{\rho_{org}}. \tag{29}$$

Since the remaining space in the aformentioned piece of extracellular bone tissue is occupied by water, the volume fraction of the latter follows as

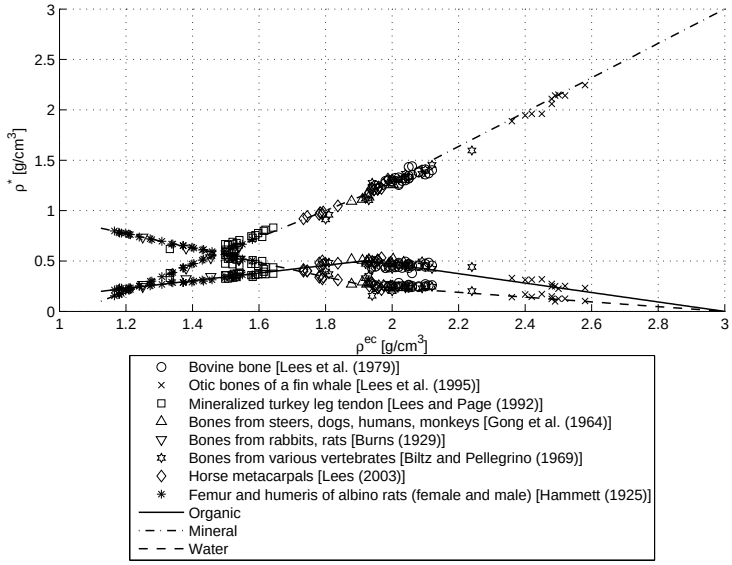

Figure 4: Apparent mass densities of water, hydroxyapatite, and organic matter versus overall mass density ρ^{ec} of extracellular bone matrix, across different species, organs and ages (see Tables 1 to 6 as in Figures 1 to 3

$$f_{H_2O} = 1 - f_{HA} - f_{org}, \tag{30}$$

which gives acess to the apparent mass density of water as

$$\rho^*_{H_2O} \quad = \quad f_{H_2O} \times \rho_{H_2O}. \tag{31}$$

When representing ρ^*_{org} through function $\mathscr{F}_{\rho^*_{org}}$ [see Eqs. (22) and (23)], Eqs. (28) to (31) define bilinear relations involving the apparent mass density of water, $\rho^*_{H_2O}$, depicted in Figures 2 and 3. These relationships are characterized by coefficients of determination amounting to $R^2 = 0.75$ and $R^2 = 0.95$, respectively. Alternatively, the apparent mass densities can be given as a function of the extracellular bone tissue mass density

$$\rho^{ec} \quad = \quad f_{H_2O} \times \rho_{H_2O} + f_{org} \times \rho_{org} + f_{HA} \times \rho_{HA}, \tag{32}$$

see Figure 4. Corresponding coefficients of determination for water, organics, and hydroxyapatite amount to $R^2 = 0.97$, $R^2 = 0.90$, and $R^2 = 0.99$, respectively. Alternatively, with the help of Eqs. (28), (29), and (30), the extracellular mass density ρ^{ec} can be related to volume fractions of hydroxyapatite, organics, and water (see Figure 5).

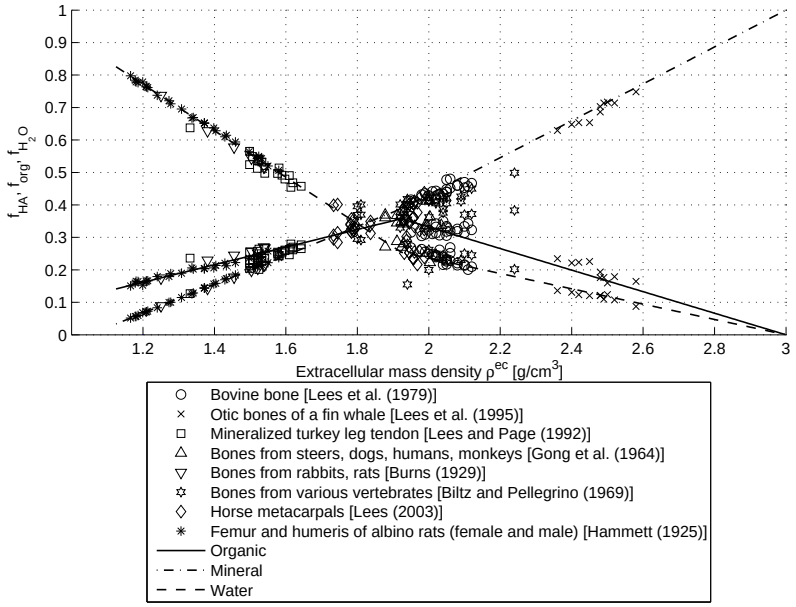

Figure 5: Volume fractions of hydroxyapatite, organs, and water in extracellular bone matrix, as function of the mass density of the latter

4. 'Universal' relations between extracellular mass density and tissue elasticity

Recently, hierarchical material models for bone (Hellmich et al., 2004; Fritsch and Hellmich, 2007; Fritsch et al., 2009a), developed within the framework of continuum micromechanics (Zaoui, 2002) and validated through a multitude of biochemical, biophysical and biomechanical experiments (Bonar et al., 1985; Lees, 1987; Ashman et al., 1984; McCarthy et al., 1990), have opened the way to translate the chemical composition of extracellular bone material (i.e. the volume fractions of organics, water, and hydroxyapatite, as seen in Figure 5) into the tissue's anisotropic elasticity. In the following, we will combine the aforementioned micromechanics models with the relations depicted in Figure 5, as to provide 'universal' relations between extracellular mass density and tissue elasticity (such relations are of interest for biomaterial design or simulation-based biomedical engineering, as discussed later, see Section 5). In more detail, we employ the four-step elastic homogenization scheme reported in (Fritsch and Hellmich, 2007; Fritsch et al., 2009a), see Figure 6, based on the tissue-independent 'universal' elastic properties of the elementary building blocks of extracellular bone material, namely hydroxyapatite, collagen, and water with some insignificant amount of non-collagenous organics. These properties given in (Hellmich et al., 2004; Fritsch and Hellmich, 2007), are accessible through ultrasonic techniques (Katz and Ukraincik, 1971; Cusack and Miller, 1979) or *ab initio* simultations (Ching et al., 2009). The aforementioned multilevel homogenization scheme relates the stiffness of material phases (i.e. quasi-homogeneous subdomains) within a representative volume element (RVE) [e.g. molecular collagen within RVE of wet collagen in Figure 6 (a), or mineralized

collagen fibril within RVE of extracellular bone matrix in Figure 6 (d)], to the stiffness of the RVE itself, as a function of the phase stiffnesses and of the phase volume fractions in all RVEs. On a mathematical level, this is achieved by setting the phase strain equal to those in ellipsoidal inclusions in infinitely extending matrices of stiffness $\mathbb{C}^0$ subjected to remote strains, and by combining respective semi-analytical relationships (Eshelby, 1957; Laws, 1977) with stress and strain average rules (Hashin, 1983; Zaoui, 2002). For all four RVEs depicted in Figure 6, the phase elasticities are related to the overall RVE-specific ("homogenized") elasticity through the standard expression of matrix-inclusion-problem-based continuum micromechanics (Benveniste, 1987; Zaoui, 2002)

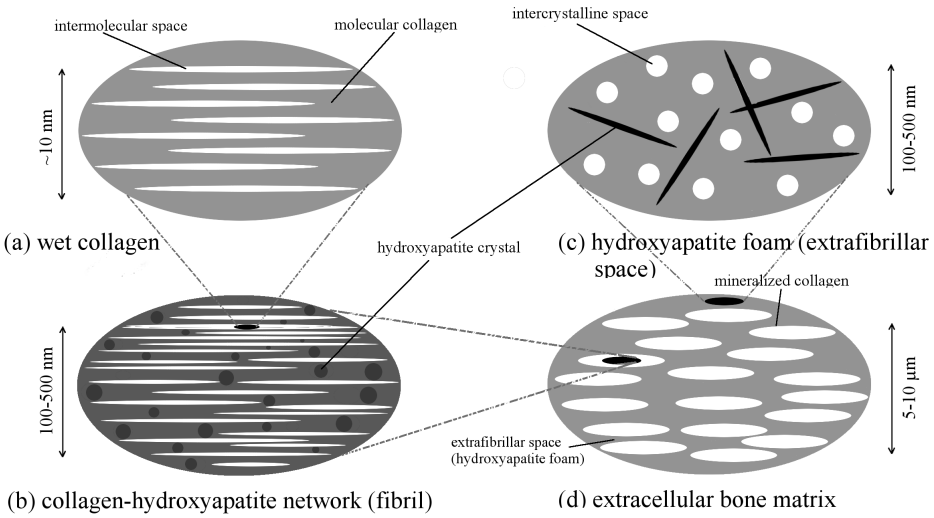

Figure 6: Four-step homogenization scheme after Fritsch and Hellmich (2007), Fritsch et al. (2009a)

$$\begin{aligned}\mathbb{C}^{hom} = &\sum_r f_r \mathbb{c}_r : [\mathbb{I} + \mathbb{P}_r^0 : (\mathbb{c}_r - \mathbb{C}^0)]^{-1} \\ &: \left\{ \sum_s f_s [\mathbb{I} + \mathbb{P}_s^0 : (\mathbb{c}_s - \mathbb{C}^0)]^{-1} \right\}^{-1},\end{aligned} \tag{33}$$

where f_r and $\mathbb{c}_r$ are the volume fraction and the elastic stiffness of phase r, $\mathbb{I}$ is the fourth-order unity tensor, $\mathbb{P}_r^0$ the fourth-order Hill tensor of the characteristic shape of phase r and $\mathbb{C}^0$ is the matrix stiffness. Choice of this stiffness describes the interactions between the phases: for $\mathbb{C}^0$ coinciding with one of the phase stiffnesses [Mori-Tanaka scheme, (Mori and Tanaka, 1973; Wakashima and Tsukamoto, 1991)], a composite material is represented [contiguous matrix with inclusions - see Figure 6 (d)]; for $\mathbb{C}^0 = \mathbb{C}^{hom}$ (self-consistent scheme Hershey (1954); Hill (1963)), a dispersed arrangement

of the phases is considered [typical for polycrystals - see Figure 6 (a),(b),(c)]). In case of the extrafibrillar space [Figure 6 (c)], with infinitely many crystal phases oriented in all directions, the sums in Eq. (33) need to be replaced by integrals over the unit sphere, as detailled in Fritsch et al. (2009a,b).

The volume fractions of the four RVEs of Figure 6 need to be derived from f_{org}, f_{HA}, and f_{H_2O}: first, the volume fraction of collagen is determined from the organic volume fraction, through the fact that 90% of the organic matter in extracellular bone matrix is collagen,

$$f_{col} = 0.9 \times f_{org}. \tag{34}$$

The volume fraction of the fibrils and the extrafibrillar space [see Figure 6 (b),(c),(d)], f_{fib} and f_{ef} can be quantified on the basis of the generalized packing model of Lees et al. (1984b); Lees (1987), through

$$f_{fib} = f_{col} \times \frac{v_{fib}}{v_{col}}, \qquad v_{fib} = b d_s 5D, \tag{35}$$

where f_{col} is determined according to Eq. (34). In Eq. (35), $v_{col} = 335.6$ nm^3 is the volume of a single collagen molecule (Lees, 1987); v_{fib} is the volume of one rhomboidal fibrillar unit with length $5D$, width b, and height d_s; $b = 1.47$ nm is an average (rigid) collagen crosslink length valid for all mineralized tissues (Lees et al., 1984b), $D \approx 64$ nm is the axial macroperiod of staggered assemblies of type I collagen, and d_s is the tissue-specific neutron diffraction spacing between collagen molecules, which depends on the mineralization and the hydration state of the tissue (Lees et al., 1984a; Bonar et al., 1985; Lees et al., 1994b). For wet tissues, d_s can be given in a dimensionless form (Hellmich and Ulm, 2003), as a function of ρ^{ec} only

$$d_s = \text{const} \times m_0^{\frac{1}{3}} \rho^{ec^{-\frac{1}{3}}}, \tag{36}$$

for (const $\times m_0^{\frac{1}{3}}$) $= 1.57 \times 10^{-10}$ kg$^{\frac{1}{3}}$.

The volume fractions for scales below the ultrastructure can be derived directly from f_{fib} and f_{col}, on the basis of the finding of Hellmich and Ulm (2001, 2003) that the average hydroxyapatite concentration in the extra-collagenous space of the extracellular wet mineralized tissues is the same inside and outside the fibrils. Accordingly, the relative amount of hydroxyapatite in the extrafibrillar space reads as (Hellmich and Ulm, 2001, 2003)

$$\phi_{HA,ef} = \frac{1 - f_{fib}}{1 - f_{col}}. \tag{37}$$

With this value at hand, the mineral volume fractions in the fibrillar and the extrafibrillar space follow as [see Figure 6 (b),(c),(d)]

$$\breve{f}_{HA} = \frac{f_{HA}(1-\phi_{HA,ef})}{f_{fib}}, \tag{38}$$

$$\breve{f}_{HA} = \frac{\phi_{HA,ef} f_{HA}}{f_{ef}}. \tag{39}$$

Within the fibril, comprising the phases hydroxyapatite and wet collagen [see Figure 6 (b)], the volume fraction of the latter reads as

$$\breve{f}_{wetcol} = 1 - \breve{f}_{HA}. \tag{40}$$

Finally, the volume fraction of (molecular) collagen [see Figure 6 (a)] at the wet collagen level can be calculated from $\bar{f}_{col}$, through

$$\mathring{f}_{col} = \frac{f_{col}}{\breve{f}_{wetcol}}. \tag{41}$$

Eqs. (33) and (36), together with Eqs. (34)–(41), deliver the extracellular elasticity tensor components C^{ec}_{ijkl} as a function of the extracellular mass density ρ^{ec} [see Figures 8(a) and 8(b)]. These elasticity tensor components give access to the Young's moduli [see Figures 9(a) and 9(b)] via

$$E^{ec}_1 = \frac{1}{D^{ec}_{1111}}, \tag{42}$$

$$E^{ec}_3 = \frac{1}{D^{ec}_{3333}}, \tag{43}$$

with compliance tensor $\mathbb{D}^{ec}$ being the inverse of $\mathbb{C}^{ec}$; and the Poisson's ratio and the shear modulus of the bone material [see Figures 10(a), 10(b), 9(a) and 9(b)] read as

$$\nu^{ec}_{12} = -D^{ec}_{1122} \times E^{ec}_1, \tag{44}$$

$$\nu^{ec}_{13} = -D^{ec}_{1133} \times E^{ec}_3, \tag{45}$$

$$G^{ec}_{12} = \frac{E^{ec}_1}{2(1+\nu^{ec}_{12})} = C^{ec}_{1212}. \tag{46}$$

see Figure 10.
These mass density-elasticity relations can be independently checked through ultrasonic experiments at a frequency of 10 MHz (Lees et al., 1979b, 1983, 1995), revealing the elastic properties of extracellular bone matrix as (Carcione, 2001; Fritsch and Hellmich, 2007)

$$C^{ec}_{1111} = \rho^{ec}\nu_1^2, \tag{47}$$

$$C^{ec}_{3333} = \rho^{ec}\nu_3^2, \tag{48}$$

with ν_1 and ν_3 being the velocity of the longitudinal acoustic waves travelling in the transverse and axial directions, respectively, see Tables 7 and 8 for experimental values. The mean $\bar{e}$ and the standard deviation e_s of the relative errors between stiffness prediction and experiments,

$$\bar{e} = \frac{1}{N}\sum e_i = \frac{1}{N}\sum \frac{C^{pred}_{ijkl} - C^{exp}_{ijkl}}{C^{exp}_{ijkl}}, \tag{49}$$

$$e_s = \left[\frac{1}{N-1}\sum (e_i - \bar{e})^2\right]^{1/2}, \tag{50}$$

are as low as $+5.47 \pm 10.17\%$ [mean value $\pm$ standard deviation] for the transverse normal stiffness C^{ec}_{1111}, and $+4.82 \pm 8.81\%$ [mean value $\pm$ standard deviation] for the longitudinal normal stiffness C^{ec}_{3333}, see Figure 7 for a comparison of model predictions and experiments. This is, to the authors' knowledge, the highest predictive precision ever attained in the field of bone microelasticity. The mass density-elasticity relationship of Figure 8 can be suitably approximated through higher order polynomials with mean relative errors below 0.25% (with respect to the micromechanical estimates). In a dimensionless form based on the normal elastic stiffness and the mass density of hydroxyapatite, $C^{HA}_{1111} = 137$ GPa (Katz and Ukraincik, 1971) and $\rho_{HA} = 3$ g/cm^3 (Lees, 1987), such polynomials read as

$$\begin{aligned} C^{ec}_{1111}(\rho^{ec})/C^{HA}_{1111} \simeq &+ 4.6826 \times (\rho^{ec}/\rho_{HA})^3 - 6.0171 \times (\rho^{ec}/\rho_{HA})^2 \\ &+ 2.8081 \times (\rho^{ec}/\rho_{HA}) - 0.4470, \end{aligned} \tag{51}$$

with a relative approximation error of $-0.17 \pm 1.64\%$ [mean value $\pm$ standard deviation according to Eq. (49) and (50)];

$$C^{ec}_{3333}(\rho^{ec})/C^{HA}_{1111} \simeq -6.8447 \times (\rho^{ec}/\rho_{HA})^4 + 17.6300 \times (\rho^{ec}/\rho_{HA})^3 - 13.5048 \times (\rho^{ec}/\rho_{HA})^2 + 4.2118 \times (\rho^{ec}/\rho_{HA}) - 0.4573, \quad (52)$$

with a relative approximation error of of $+0.2 \pm 5.5\%$ [mean value $\pm$ standard deviation];

$$C^{ec}_{1122}(\rho^{ec})/C^{HA}_{1111} \simeq -11.0152 \times (\rho^{ec}/\rho_{HA})^5 + 29.7474 \times (\rho^{ec}/\rho_{HA})^4 - 28.7144 \times (\rho^{ec}/\rho_{HA})^3 + 12.5870 \times (\rho^{ec}/\rho_{HA})^2 - 2.3375 \times (\rho^{ec}/\rho_{HA}) + 0.1188, \quad (53)$$

with a relative approximation of $-0.02 \pm 0.69\%$ [mean value $\pm$ standard deviation];

$$C^{ec}_{1133}(\rho^{ec})/C^{HA}_{1111} \simeq -5.0088 \times (\rho^{ec}/\rho_{HA})^4 + 13.7237 \times (\rho^{ec}/\rho_{HA})^3 - 12.4876 \times (\rho^{ec}/\rho_{HA})^2 + 4.8307 \times (\rho^{ec}/\rho_{HA}) - 0.6745, \quad (54)$$

with a relative approximation error of $-0.05 \pm 2.42\%$ [mean value $\pm$ standard deviation]; and finally

$$C^{ec}_{2323}(\rho^{ec})/C^{HA}_{1111} \simeq +4.1245 \times (\rho^{ec}/\rho_{HA})^5 - 14.9352 \times (\rho^{ec}/\rho_{HA})^4 + 21.9578 \times (\rho^{ec}/\rho_{HA})^3 - 15.1486 \times (\rho^{ec}/\rho_{HA})^2 + 4.9459 \times (\rho^{ec}/\rho_{HA}) - 0.6169, \quad (55)$$

with a relative approximation error of $-0.18 \pm 5.02\%$ [mean value $\pm$ standard deviation].

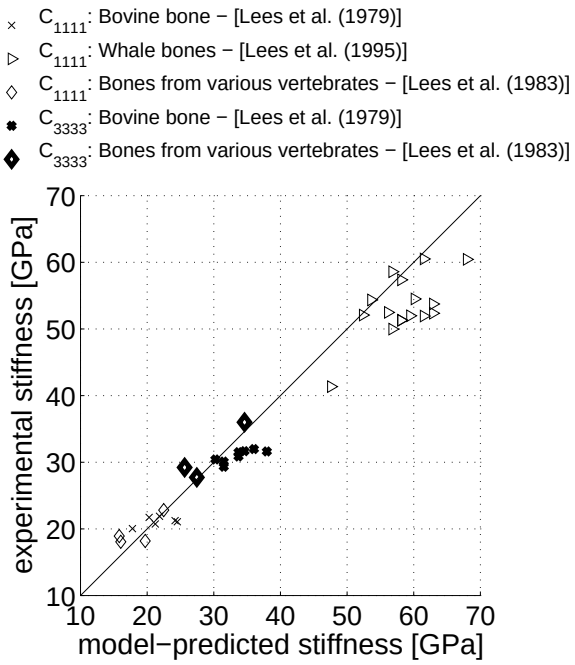

Figure 7: Extracellular tissue elasticity: Comparison between model-predicted and ultrasonic experiments at 10 MHz frequency

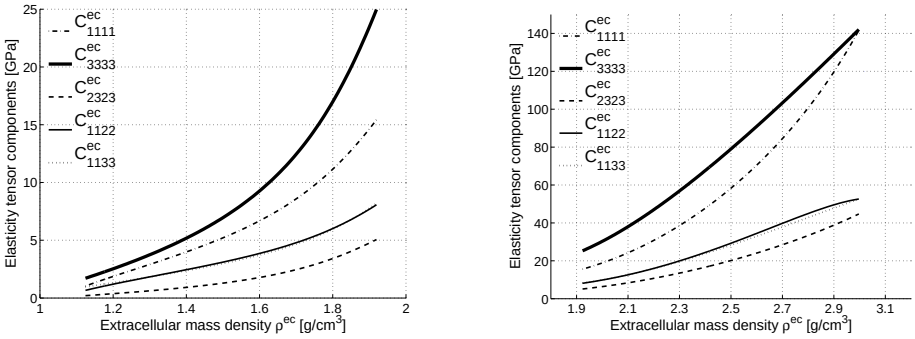

(a) Low mass density (b) High mass density

Figure 8: Elasticity tensor components of extracellular bone matrix, as a function of the mass density of the latter (3 . . . axial direction; 1,2 . . . transverse direction)

Table 7: Experimental ultrasound data in transverse direction

Tissue	ρ^{ec}	ν_1	$C^{ec}_{1111,exp}$	$C^{ec}_{1111,pre}$
	[g/cm^3]	[m/s]	[GPa]	[GPa]
	given	given	Eq. (47)	Eqs. (**??**)–(41)
Bovine tibia[a]	2.10	3.18	21.2	24.2
Bovine tibia[a]	1.98	3.18	20.0	17.8
Bovine tibia[a]	2.05	3.18	20.7	21.2
Bovine tibia[a]	2.11	3.16	21.1	24.5
Bovine tibia[a]	2.03	3.27	21.7	20.3
Bovine tibia[a]	2.06	3.26	21.9	21.9
Bovine tibia [b]	2.07	3.32	22.8	22.5
Dugong rib [b]	2.02	3.00	18.2	19.7
Elephant radius[b]	1.94	3.05	18.0	16.0
Human femur [b]	1.93	3.13	18.9	15.8
Whale malleus [c]	2.49	4.85	58.6	56.8
Whale malleus [c]	2.53	4.89	60.5	61.5
Whale malleus [c]	2.51	4.55	52.0	59.5
Whale malleus [c]	2.45	4.61	52.1	52.4
Whale incus [c]	2.50	4.79	57.4	58.1
Whale incus [c]	2.46	4.70	54.3	53.6
Whale stapes [c]	2.40	4.15	41.3	47.6
Whale stapes [c]	2.48	4.60	52.5	56.1
Whale periotic[c]	2.50	4.53	51.3	58.1
Whale periotic[c]	2.52	4.65	54.5	60.1
Whale periotic[c]	2.58	4.84	60.4	68.0
Whale periotic[c]	2.54	4.60	53.7	62.9
Whale periotic[c]	2.50	4.53	51.3	58.1
Whale t. bulla[c]	2.53	4.53	51.9	61.5
Whale t. bulla[c]	2.54	4.54	52.4	62.9
Whale t. bulla[c]	2.49	4.48	50.0	56.8

[a] Lees et al. (1979b)
[b] Lees et al. (1983)
[c] Lees et al. (1995)

Table 8: Experimental ultrasound data in axial direction

Tissue	ρ^{ec}	ν_3	$C^{ec}_{3333,exp}$	$C^{ec}_{3333,pre}$
	[g/cm^3]	[m/s]	[GPa]	[GPa]
	given	given	Eq. (48)	Eqs. (**??**)–(41)
Bovine tibia[a]	2.06	3.92	31.7	34.6
Bovine tibia[a]	2.05	3.92	31.5	33.7
Bovine tibia[a]	2.02	3.81	29.3	31.5
Bovine tibia[a]	2.02	3.86	30.1	31.5
Bovine tibia[a]	2.00	3.90	30.4	30.2
Bovine tibia[a]	2.05	3.88	30.9	33.7
Bovine tibia[a]	2.10	3.88	31.6	38.0
Bovine tibia[a]	2.08	3.92	32.0	36.0
Bovine tibia [b]	2.07	4.18	36.0	34.6
Elephant radius[b]	2.02	3.89	29.2	25.6
Human femur [b]	1.94	3.76	27.7	27.5

[a] Lees et al. (1979b)
[b] Lees et al. (1983)

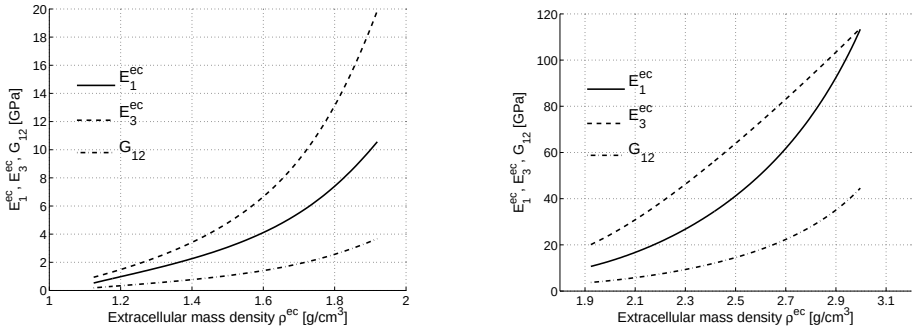

(a) Low mass density (b) High mass density

Figure 9: Young's and shear moduli of extracellular bone matrix, as a function of the mass density of the latter (3 . . . axial direction; 1,2 . . . transverse direction)

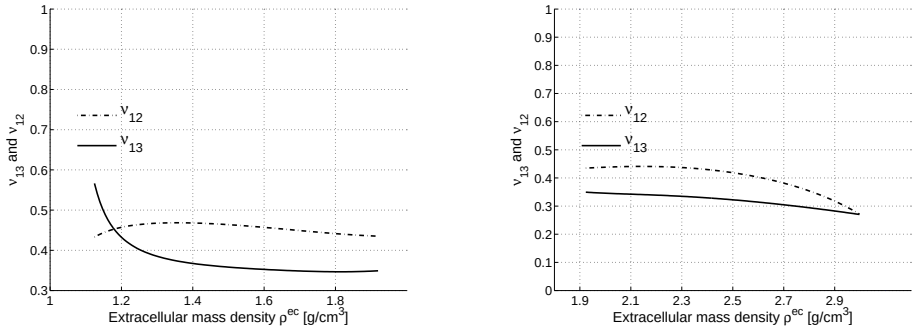

(a) Low mass density (b) High mass density

Figure 10: Poisson's ratio of extracellular bone matrix, as a function of the mass density of the latter (3 . . . axial direction; 1,2 . . . transverse direction)

5. Discussion

This contribution revealed inter-relation between the mineral, organics, and water concentrations in extracellular bone materials, inherent to tissues across different species, organs, and ages, see Figures 1–5. In this context, it is particularly noteworthy that the positive progression along the ρ^*_{HA}-axis in Figure 1, as well as along the ρ^{ec}-axis in Figure 4, relates to first growing and then to further aging of the bone tissues during adolescence of the respective animals or humans. In fact, the data of Hammett (1925) for rat femur and humeris allow for computation of an organic apposition rate, as $(d\rho^*_{org}/dt) = 0.0317$ g/cm^3 per month, see Figure 11(a), which is even constant throughout the time of animal growth, as is the growth rate in rat tail tendon, see Figure 11(b) for data of Parry and Craig (1978).

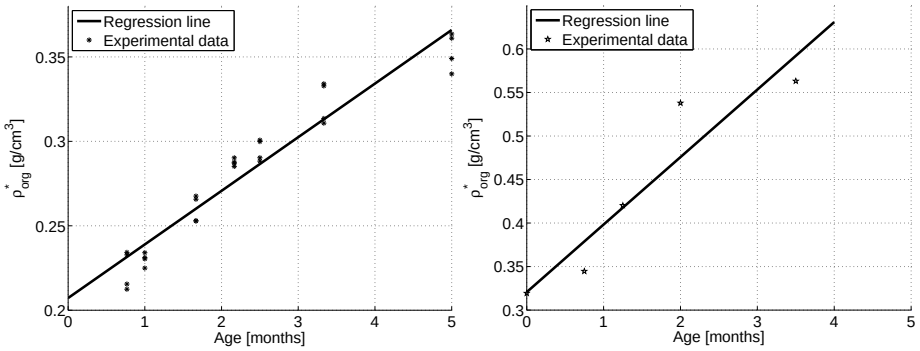

(a) Humeris and femur of an albino rat (Hammett, 1925)

(b) Rat-Tail Tendon (Parry and Craig, 1978)

Figure 11: Age-related organic apparent mass density

Thus, while organic matter is accumulated during animal or human growth (see e.g. rising branch in Figure 1), it may be continuously reduced once adulthood is reached (see e.g. declining branch in Figure 1). This reduction, however, may be considerably delayed, i.e. occuring only at very high age in specific organs, since it is known from imaging techniques, such as computerized quantitative contact microradiography (Boivin and Meunier, 2002), quantitative backscattered electron imaging (Roschger et al., 2003), Raman microscopy (Akkus et al., 2003), and Synchroton Micro Computer Tomography (Bossy et al., 2004), that the chemical compsitions of adult bone matrix remains, for a long time, constant throughout specific organs, and in particular with age (Hellmich et al., 2008). During this time span, measured mechanical properties of the extracellular bone matrix, such as indentation modulus and hardness, appear also as time-invariant (Weaver, 1966; Hoffler et al., 2000; Wolfram et al., 2010; Rho et al., 2002; Burket et al., 2011), while such mechanical properties increase during animal (or human) growth (Feng and Jasiuk, 2011; Weaver, 1966). It is interesting to discuss the mineral-organics concentration relation of Figure 1 from the viewpoint of cell biology: During growth, the ratio between a portion of newly deposited osteoid (i.e. unmineralized organic bone matrix) and the amount of mineral precipitating immediately after

osteoid deposition, is a constant,

$$\frac{d\rho^*_{HA}}{d\rho^*_{org}} = \frac{1}{A} = 3.5 \qquad \text{for } 0 < \rho^*_{HA} \leqslant \rho^{*,crit}_{HA}, \tag{56}$$

"universally" valid throughout different tissues of different growing species at different ages, see Figure 1. This constant expresses the working mode of osteoblasts (polygonal bone cells with several tens of micrometers characteristic length (Aaron, 1971; Noble, 2008), which deposit new osteoid, and afterward inject the latter, through filopodia (cell processes), with mineral, in a quasi-instantaneous fashion often referred to as primary mineralization with a characteristic time of hours at most (Buckwalter et al., 1995; Aaron, 1971; Parfitt, 1983). Thereby, initially meta-stable calcium phosphate solutions precipitate into hydroxyapatite crystals (Gajjeraman et al., 2007; Reddi, 2000; Höhling, 1969), thanks to the removal of mineralization-inhibitors such as decorin (Mochida et al., 2008; Hoshi et al., 1999) and to the enzymatic capacity of non-collagenous matrix proteins, often called bone matrix proteins (BMPs). Bone regeneration was successfully induced in biomaterial scaffolds loaded with BMPs (Schopper et al., 2008, 2009). The primary mineralization takes place in the matrix vesicles, round or oval shaped entities with a diameter of around 100 nm, which may be extruded by a budding from the processes of the osteoblasts (Wiesmann et al., 2005). The subsequent secondary mineralization, which is related to further growth of the primary crystals injected through the osteoblasts, would take several months to proceed - but this secondary mineralization is continuously interrupted through the high bone turnover rate in growing organisms (Jowsey, 1960): I.e. before the crystals can remarkably grow, the entire bone is resorbed by osteoclasts, followed by yet more newly osteoblast-formed osteoid, as described before. This leads to maintenance of a constant mineral-to-organics apposition ratio in growing organisms, as seen in Figure 1. The picture may change in adult organisms, and especially does so at very old age, where the osteoclasts [bone cells with several hundreds of micrometers characteristic length, Aaron (1971)] resorb more bone tissue than the osteoblasts can produce (Kiebzak, 1991), so that the organic concentration steadily decreases. Furthermore, bone turnover, i.e. amount of bone remodeling processes over space and tissue drastically decreases so that secondary mineralization, i.e. growth of existing crystals throughout months and years becomes the dominant process, being expressed by a (negative) mineral-growth-to-organic-removal ratio,

$$\frac{d\rho^*_{HA}}{d\rho^*_{org}} = -3.6 \qquad \text{for } \rho^{*,crit}_{HA} < \rho^*_{HA} \leqslant \rho_{HA}, \tag{57}$$

see Figure 1. Maintenance of a constant mineral-to-organic ratio in newly deposited bone during growth, as expressed in Eq. (56), is also supported by the activity of osteocytes, preventing mineralization of lacunae (Bonucci, 2009). However, at high age, this activity decreases, and with $d\rho^*_{HA}/d\rho^*_{org} < 0$, Eq. (57), lacunae may be filled with mineral, as evidenced by Frost (1960), Jowsey (1960), and Bell et al. (2008). We also remark that Figures 1–5 refer to physiologically normal conditions, while drug treatments (Lees et al., 1994a) may lead to considerable deviations from these rules for

fibrillogenesis and mineralization.

From a more practical viewpoint, relations of Figures 1–5, and 8–10 can be employed for enhanced exploitation of Computer Tomographic (CT) data (Komlev et al., 2010). Namely, the volume fractions of the tissue's components can be related to the X-ray attenuation coefficients quantifiable in a micro Computer Tomograph (Jackson and Hawkes, 1981; Hellmich et al., 2008; Scheiner et al., 2009)

$$\mu^{ec} = f_{H_2O}\mu_{H_2O} + f_{HA}\mu_{HA} + f_{org}\mu_{org}, \tag{58}$$

with $\mu_{H_2O} = 5.33$ cm^{-1}, $\mu_{HA} = 142$ cm^{-1}, $\mu_{org} = 5.71$ cm^{-1} as the attenuation coefficients of water, organics, and hydroxyapatite at a photon energy of 10 keV, which is typically used in bone micro CT imaging. The values for μ_{H_2O}, μ_{HA}, μ_{org} are accessible from the NIST database[1]. Combination of Eq. (58) with the miromechanics model Eqs. (33)–(41) yields attenuation coefficient-elasticity relations, see Fig. 12. They open interesting possibilities for CT-based, micromechanics-supported biomaterial design (Bertrand and Hellmich, 2009): Voxel-specific gray values guide the way to individuum- and location-specific elastic properties, which an implant is required to exhibit, as not to disturb the physiological force field, necessary for undisturbed biophysical functionality of the organism.

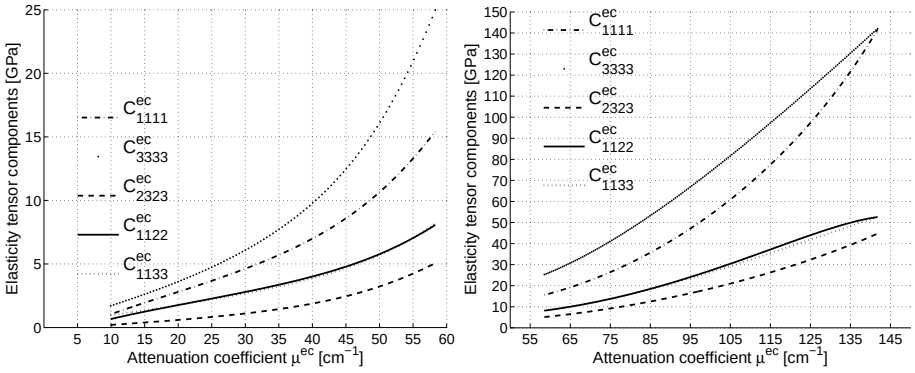

(a) Growing bone material (b) Aging bone material

Figure 12: Elasticity tensor components as a function of attenuation coefficient μ^{ec} at 10 keV photon energy (3 . . . axial direction; 1,2 . . . transverse direction)

[1]NIST XCOM database, US National Institute of Standards and Technology, http://physics.nist.gov/PhysRefData/Xcom/html/xcom1.html, 2010

Acknowledgments

This work was partially supported by the European Commission under the Theme FP7-2008-SME-1 of the 7^{th} Framework Program, project no. 232 164, BIO–CT–EXPLOIT. The authors gratefully acknowledge the support of Andreas Fritsch.

References

Aaron, J. (1971). Histology and micro-anatomy of bone. In Nordin, B., editor, *Calcium, Phosphate and Magnesium Metabolism: Clinical Physiology and Diagnostic Procedures*, pages 298–356. Churchill Livingstone, New York.

Akkus, O., Polyakova-Akkus, A., Adar, F., and Schaffler, M. (2003). Aging of microstructural compartments in human compact bone. *Journal of Bone and Mineral Research*, 18(6):1012 – 1019.

Ashman, R., Cowin, S., van Buskirk, W., and Rice, J. (1984). A continuous wave technique for the measurement of the elastic properties of cortical bone. *Journal of Biomechanics*, 17(5):349 – 361.

Bell, L., Kayser, M., and Jones, C. (2008). The mineralized osteocyte: a living fossil. *American Journal of Physical Anthropolgy*, 137:449–456.

Benveniste, Y. (1987). A new approach to the application of Mori-Tanaka's theory in composite materials. *Mechanics of Materials*, 6(2):147 – 157.

Bertrand, E. and Hellmich, C. (2009). Multiscale elasticity of tissue engineering scaffolds with tissue-engineered bone: A continuum micromechanics approach. *Journal of Engineering Mechanics (ASCE)*, 135:395–412.

Biltz, R. and Pellegrino, E. (1969). The chemical anatomy of bone. *Journal of Bone and Joint Surgery*, 51-A(3):456 – 466.

Boivin, G. and Meunier, P. (2002). The degree of mineralization of bone tissue measured by computerized quantitative contact microradiography. *Calcified Tissue International*, 70:503 – 511.

Bonar, L., Lees, S., and Mook, H. (1985). Neutron diffraction studies of collagen in fully mineralized bone. *Journal of Molecular Biology*, 181:265 – 270.

Bonucci, E. (2009). The osteocyte: the underestimated conductor of the bone orchestra. *Rendiconti Lincei: Scienze Fisiche e Naturali*, 20:237–254.

Bossy, E., Talmant, M., Peyrin, F., Akrout, L., Cloetens, P., and Laugier, P. (2004). In in vitro study of the ultrasonic axial transmission technique at the radius: 1 MHz velocity measurements are sensitive to both mineralization and introcortical porosity. *Journal of Bone and Mineral Research*, 19(9):1548 – 1556.

Broz, J. J., Simske, S. J., and Greenberg, A. R. (1995). Material and compositional properties of selectively demineralized cortical bone. *Journal of Biomechanics*, 28(11):1357 – 1368.

Buckwalter, J., Glimcher, M., Cooper, R., and Recker, R. (1995). Bone biology, Part I: Structure, blood supply, cells, matrix, and mineralization. *The Journal of Bone and Joint Surgery*, 77-A(8):1256 – 1275.

Burket, J., Gourion-Arsiquaud, S., Havill, L., Baker, S., Boskey, A., and van der Meulen M.C.H. (2011). Microstructure and nanomechanical properties in osteons relate to tissue and animal age. *Journal of Biomechanics*, 44:277 – 284.

Burns, C. M. (1929). XCIV. The effect of the continued ingestion of mineral acid on growth of body and bone and on the composition of bone and of the soft tissues. *Biochemical Journal*, 23(5):860 – 867.

Cancedda, R., Giannoni, P., and Mastrogiacomo, M. (2007). A tissue engineering approach to bone repair in large animal models and in clinical practice. *Biomaterials*, 28:4240 – 4250.

Carcione, J. (2001). Wave fields in real media: Wave propagation in anisotropic, anelastic and porous media. In Helbig, K. and Treitel, S., editors, *Handbook of Geophysical Exploration Seismic Exploration*, volume 31. Elsevier, Amsterdam, The Netherlands.

Chick, H., Korenchevsky, V., and Roscoe, M. (1926). LXXXIII. The difference in chemical composition of the skeletons of young rats fed (1) on diets deprived of fat-soluble vitamins and (2) on a low phosphorus rachitic diet, compared with those of normally nourished animals of same age. *Biochemical Journal*, 20(3):621 – 631.

Ching, W., Rulis, P., and Misra, A. (2009). Ab initio elastic properties and tensile strength of crystalline hydroxyapatite. *Acta Biomaterialia*, 5:3067 – 3075.

Cusack, S. and Miller, A. (1979). Determination of the elastic constants of collagen by Brillouin light scattering. *Journal of Molecular Biology*, 135:39 – 51.

Eshelby, J. (1957). The determination of the elastic field of an ellipsoidal inclusion, and related problems. *Proceedings of the Royal Society of London. Series A, Mathematical and Physical Sciences*, 241(1226):376 – 396.

Feng, L. and Jasiuk, I. (2011). Multi-scale characterization of swine femoral cortical bone. *Journal of Biomechanics*, 44:313 – 320.

Ficai, A., Andronescu, E., Voicu, G., Manzu, D., and Ficai, M. (2009). Layer by layer deposition of hydroxyapatite onto the collagen matrix. *Materials Science and Engineering: C*, 29(7):2217 – 2220.

Filvaroff, E. and Derynck, R. (1998). Bone remodelling: a signalling system for osteoclast regulation. *Current Biology*, 8:R679 – R682.

Fritsch, A., Dormieux, L., Hellmich, C., and Sanahuja, J. (2009a). Mechanical behaviour of hydroxyapatite biomaterials: An experimentally validated micromechanical model for elasticity and strength. *Journal of Biomedical Materials Research*, 88A:149 – 161.

Fritsch, A. and Hellmich, C. (2007). 'Universal' microstructural patterns in cortical and trabecular, extracellular and extravacular bone materials: Micromechanics-based prediction of anisotropic elasticity. *Journal of Theoretical Biology*, 244:597 – 620.

Fritsch, A., Hellmich, C., and Dormieux, L. (2009b). Ductile sliding between mineral crystals followed by rupture of collagen crosslinks: experimentally supported micromechanical explanation of bone strength. *Journal of Theoretical Biology*, 260:230 – 252.

Frost, H. (1960). Micropetrosis. *Journal of Bone and Joint Surgery*, 42:144 – 150.

Gajjeraman, S., Narayanan, K., Hao, J., Qin, C., and George, A. (2007). Matrix macromolecules in hard tissues control the nucleation and hierarchical assembly of hydroxyapatite. *The Journal of Biologial Chemistry*, 282(2):1193 – 1204.

Gong, J., Arnold, J., and Cohn, S, H. (1964a). Composition of trabecular and cortical bone. *The Anatomical Record*, 149:325 – 332.

Gong, J., Arnold, J., and Cohn, S, H. (1964b). The density of organic and volatile and non-volatile inorganic components of the bone. *The Anatomical Record*, 149:319 – 324.

Green, D. (2008). Tissue bionics: examples in biomimetic tissue engineering. *Biomedical Materials*, 3:1–11.

Hammett, F. S. (1924). Studies of the thyroid apparatus: XIV. the growth of the humerus and femur of male and female albino rats thyro-parathyroidectomized and parathyroidectomized when 100 days of age. *The Journal of Experimental Zoology*, 39(3):465 – 504.

Hammett, F. S. (1925). A biochemical study of bone growth. I. Changes in the ash, organic matter and water during growth (mus norvegicus albinus). *The Journal of Biological Chemistry*, 64:409 – 428.

Hashin, Z. (1983). Analysis of composite materials – a survey. *Journal of Applied Mechanics (ASME)*, 50(3):481 – 505.

Hellmich, C. (2005). Microelasticity of bone. In Dormieux, L. and Ulm, F.-J., editors, *Applied Micromechanics of Porous Media*, volume 480, pages 289 – 332. Springer, Wien - New York.

Hellmich, C., Kober, C., and Erdmann, B. (2008). Micromechanics-based conversion of CT data into anisotropic elasticity tensors, applied to FE simulations of a mandible. *Annals of Biomedical Engineering*, 36(1):108 – 122.

Hellmich, C. and Ulm, F.-J. (2001). Hydroxyapatite is uniformly concentrated in the extracollagenous ultrastructure of mineralized tissue. In Middleton, J., Shrive, N., and Jones, M., editors, *Proceedings of the Fifth International Symposium on Computer Methods in Biomechanics and Biomedical Engineering*, Rome, Italy.

Hellmich, C. and Ulm, F.-J. (2003). Average hydroxyapatite concentration is uniform in extracollageneous ultrastructure of mineralized tissue. *Biomechanics and Modeling in Mechanobiology*, 2:21 – 36.

Hellmich, C., Ulm, F.-J., and Dormieux, L. (2004). Can the diverse elastic properties of trabecular and cortical bone be attributed to only a few tissue-independent phase properties and their interactions? – arguments from a multiscale approach. *Biomechanics and Modeling in Mechanobiology*, 2:219 – 238.

Hershey, A. (1954). The elasticity of an isotropic aggregate of anisotropic cubic crystals. *Journal of Applied Mechanics (ASME)*, 21:236 – 240.

Hill, R. (1963). Elastic properties of reinfored solids: some theoretical principles. *Journal of the Mechanics and Physics of Solids*, 11:357 – 362.

Hoffler, C. E., Moore, K. E., Kozloff, K., Zysset, P. K., and Goldstein, S. A. (2000). Age, gender, and bone lamellae elastic moduli. *Journal of Orthopaedic Research*, 18:432–437.

Hoshi, K., Kemmotsu, S., Takeuchi, Y., Amizuka, N., and Ozawa, H. (1999). The primary calcification in bones follows removal of decorin and fusion of collagen fibrils. *Journal of Bone and Mineral Research*, 14(2):273 – 280.

Höhling, H. (1969). Collagen mineralization in bone, dentine, cementum and cartilage. *Naturwissenschaften*, 56(9):466.

Jackson, D. and Hawkes, D. (1981). X-ray attenuation coefficients of elements and mixtures. *Physics Letters*, 70(3):169 – 233.

Jowsey, J. (1960). Age changes in human bone. *Clinical Orthopaedics*, 17:210 – 218.

Karageorgiou, V. and Kaplan, D. (2005). Porosity of 3D biomaterial scaffolds and osteogenesis. *Biomaterials*, 26:5474 – 5491.

Katz, J. and Ukraincik, K. (1971). On the anisotropic elastic properties of hydroxyapatite. *Journal of Biomechanics*, 4:221 – 227.

Kiebzak, G. (1991). Age-related bone changes. *Experimental Gerontology*, 26:171 – 187.

Komlev, V., Mastrogiacomo, M., Pereira, R., Peyrin, F., Rustichelli, F., and Cancedda, R. (2010). Biodegradation of porous calcium phosphate scaffolds in an ectopic bone formation model studied by X-ray computed microtomography. *European Cells and Materials*, 19:136 – 146.

Landis, W., Hodgens, K., Song, M., Arena, J., Kiyonaga, S., Marko, M., Owen, C., and McEwen, B. (1996). Mineralization of collagen may occur on fibril surfaces: Evidence from conventional and high-voltage electron microscopy and three-dimensional imaging. *Journal of Structural Biology*, 117:24 – 35.

Langer, R. and Vacanti, J. (1993). Tissue engineering. *Science*, 260(5110):920–926.

Laws, N. (1977). The determination of stress and strain concentrations at an ellipsoidal inclusion in an anisotropic material. *Journal of Elasticity*, 7:91 – 97.

Lees, S. (1987). Considerations regarding the structure of the mammalian mineralized osteoid from viewpoint of the generalized packing model. *Connective Tissue Research*, 16:281 – 303.

Lees, S. (2003). Mineralization of type I collagen. *Biophysical Journal*, 85:204 – 207.

Lees, S., Ahern, J., and Leonard, M. (1983). Parameters influencing the sonic velocity in compact calcified tissues of various species. *Journal of the Acoustical Society of America*, 74(1):28 – 33.

Lees, S., Bonar, L., and Mook, H. (1984a). A study of dense mineralized tissue by neutron diffraction. *International Journal of Biological Macromolecules*, 6:321 – 326.

Lees, S., Cleary, P., Heeley, J., and Gariepy, E. (1979a). Distribution of sonic plesio-velocity in a compact bone sample. *Journal of Acoustic Society of America*, 66(3):641– 646.

Lees, S., Hanson, D., and Page, E. (1995). Some acoustical properties of the otic bones of a fin whale. *Journal of the Acoustical Society of America*, 99(4):2421 – 2427.

Lees, S., Hanson, D., Page, E., and Mook, H. (1994a). Comparison of dosage-dependent effects of beta-aminopropionitrile, sodium fluoride, and hydrocortisone on selected physical properties of cortical bone. *Journal of Bone and Mineral Research*, 9(9):1377 – 1389.

Lees, S., Heeley, J., and Cleary, P. (1979b). A study of some properties of a sample of bovine cortical bone using ultrasound. *Calcified Tissue International*, 29:107 – 117.

Lees, S. and Page, E. (1992). A study of some properties of mineralized turkey leg tendon. *Connective Tissue Research*, 28:263 – 287.

Lees, S., Pineri, M., and Escoubes, M. (1984b). A generalized packing model for type I collagen. *International Journal of Biological Macromolecules*, 6:133 – 136.

Lees, S., Prostak, K., Ingle, V., and Kjoller, K. (1994b). The loci of mineral in turkey leg tendon as seen by atomic force microscope and electron microscopy. *Calcified Tissue International*, 55:180 – 189.

Lemaire, V., Tobin, F., Greller, L., Cho, C., and Suva, L. (2004). Modeling the interactions between osteoblast and osteoclast activities in bone remodeling. *Journal of Theoretical Biology*, 229:293 – 309.

McCarthy, R., Jeffcott, L., and McCartney, R. (1990). Ultrasound speed in equine cortical bone: effects of orientation, density, porosity and temperature. *Journal of Biomechanics*, 23(11):1139 – 1143.

Mochida, Y., Parisuthiman, D., Pornprasertsuk-Damrongsri, S., Atsawasuwan, P., Sricholpech, M., Boskey, A., and Yamauchi, M. (2008). Decorin modulates collagen matrix assembly and mineralization. *Matrix Biology*, 28:44 – 52.

Mori, T. and Tanaka, K. (1973). Average stress in matrix and average elastic energy of materials with misfitting inclusions. *Acta Metallurgica*, 21(5):571 – 574.

Noble, B. (2008). The osteocyte lineage. *Archives of Biochemistry and Biophysics*, 473:106 – 111.

Parfitt, A. (1983). The physiologic and clinical significance of bone histomorphometric data. In Recker, R., editor, *Histomorphometry, Techniques and Interpretation*, pages 143–223. CRC Press Inc, Boca Raton, FL, USA.

Parry, D. and Craig, A. (1978). Collagen fibrils and elastic fibers in rat-tail tendon: an electron microscopic investigation. *Biopolymers*, 17:843 – 855.

Perry, C. (2002). Biomaterials, synthetic synthesis, fabrication, and applications. In Meyer, R., editor, *Encyclopedia of Physical Science and Technology, Volume 2*, pages 173 – 191. Academic Press, San Diego, USA.

Pivonka, P., Zimak, J., Smith, D., Gardiner, B., Dunstan, C., Sims, N., Martin, T., and Mundy, G. (2010). Theoretical investigation of the role of the RANK-RANKL-OPG system in bone remodeling. *Journal of Theoretical Biology*, 262:306 – 316.

Pramatarova, L., Pecheva, E., Presker, R., Pham, M., Maitz, M., and Stutzmann, M. (2005). Hydroxyapatite growth induced by native extracellular matrix deposition on solid surfaces. *European Cells and Materials*, 9:9 – 12.

Reddi, A. (2000). Morphogenetic messages are in the extracellular matrix: biotechnology from bench to bedside. *Biochemical Society Transactions*, 28(4):345 – 349.

Rho, J., Zioupos, P., Currey, J., and Pharr, G. (2002). Microstructural elasticity and regional heterogeneity in human femoral bone of various ages examined by nano-indentation. *Journal of Biomechanics*, 35:189 – 198.

Roeder, R. (2008). Hydroxyapatite-reinforced polymer biocomposites for synthetic bone substitutes. *Journal of the Minerals, Metals and Materials Society*, 60(3):38 – 45.

Roschger, P., Gupta, H., Berzlanovich, A., Ittner, G., Dempster, D., Fratzl, P., Cosman, F., Parisien, M., Lindsay, R., Nieves, J., and Klaushofer, K. (2003). Constant mineralization density distribution in cancellous human bone. *Bone*, 32:316 – 323.

Scheiner, S., Sinibaldi, R., Pichler, B., Komlev, V., Renghini, C., Vitale-Brovarone, C., Rustichelli, F., and Hellmich, C. (2009). Micromechanics of bone tissue-engineering scaffolds, based on resolution error-cleared computer tomography. *Biomaterials*, 30:2411–2419.

Schopper, C., Moser, D., Spassova, E., Goriwoda, W., Lagogiannis, G., Hoering, B., Ewers, R., and Redl, H. (2008). Bone regeneration using a naturally grown HA/TCP carrier loaded with rhBMP-2 is independent of barrier-membrane effects. *Journal of Biomedical Materials Research Part A*, 85A:954 – 963.

Schopper, C., Moser, D., Spassova-Tzekova, E., Russmueller, G., Goriwoda, W., Lagogiannis, G., Ewers, R., and Redl, H. (2009). Mineral apposition rates provide significant information on long-term effects in BMP-induced bone regeneration. *Journal of Biomedical Materials Research Part A*, 89A:679 – 686.

Verma, D., Katti, K., Katti, D., and Mohanty, B. (2008). Mechanical response and multilevel structure of biomimetic hydroxyapatite/polygalacturonic/chitosan nanocomposites. *Materials Science and Engineering C*, 28:399 – 405.

Wakashima, K. and Tsukamoto, H. (1991). Mean-field micromechanics model and its application to the analysis of thermomechanical behaviour of composite materials. *Materials Science and Engineering: A*, 146(1-2):291 – 316.

Weaver, J. (1966). The microscopic hardness of bone. *Journal of Bone and Joint Surgery*, 48:273–288.

Wiesmann, H., Meyer, U., Plate, U., and Höhling, H. (2005). Aspects of collagen mineralization in hard tissue formation. *International Review of Cytology*, 242:121–156.

Wolfram, U., Wilke, H.-J., and Zysset, P. (2010). Rehydration of vertebral trabecular bone: Influences on its anisotropy, its stiffness and the indentation work with a view to age, gender and vertebral level. *Bone*, 46:348 – 354.

Zaoui, A. (2002). Continuum micromechanics: survey. *Journal of Engineering Mechanics, (ASCE)*, 128(8):808 – 816.

3. Summary, Biological Review, and Perspective

The main focus of this thesis was to find a 'universal' pattern in fibrillogenesis and mineralization of bone and derive mechanical properties for biomaterial design. Analyzation of already available experimental data collected throughout 70 years of bone research and found a new persective to evaluate and interpret them. Bone is a living tissue underlying changes during growth and also during aging under normal physiological conditions. Kiebzak (1991) stated a few age-related changes of bone, such as mismatch between bone formation and resorption, changes of the bone mineral content (hyper- and hypomineralization) and alterations of the bone matrix (protein content and organization).

Osteoclasts and osteoblasts are types of bone cells being responsible for bone resorption and formation (Buckwalter *et al.* , 1995a; Loveridge, 1999). Osteoblast are a result of mesenchymal stem cell differentiation Lemaire *et al.* (2004) at the embryonic stadium. Initially they form an unmineralized osteoid, which is a mesh-like structure consisting of collagen and proteoglycans providing a basis for the aggregation of mineral crystals (Ozawa *et al.* , 2008; Hoshi *et al.* , 1999). During resorption the mineral component and the bone matrix is being decomposed and formation of the bone is the substitution of this resporbed matrix which then becomes again mineralized (Kazuhiko *et al.* , 2009). In the growing phase of an individual there is a correlation of these two mechanism. This correlation is still not well understood. When bone is being resorbed by the osteclasts, new bone is being formed by the osteoblasts, in other words there is a balance. At a high age however there is a so-called uncoupling between bone resorption and formation as being described by Kiebzak (1991) and bone formation rate decreases (Buckwalter *et al.* , 1995b; Jowsey, 1960). Osteoblasts either apoptose or differentiate into osteocytes trapped in lacunae after bone formation. In older individuals it may occur that a non-functional osteoblast is being formed, leading to an increase of area where bone cells can not be grown and thus a decrease of bone formation rate causing an imbalance (Sharpe, 1979; Kazuhiko *et al.* , 2009).

In order to determine what might cause the imbalance during aging, it is essential to know how osteoblasts and osteoclasts communicate with each other. Lemaire *et al.* (2004) developed a mathematical model to describe the interactions between osteoblast and osteoclasts under normal conditions and, amongst other diseases, also under aging (senescense). The model describes an interaction of osteoclast and osteoblast guided by the regulators parathyroid hormone (PTH), receptor activator of nuclear factor κB (RANK), ligand of RANK (RANKL),

osteoprotegerin (OPG) and transforming growth factor beta (TGF-β), see Fig. 1 in Lemaire *et al.* (2004). Osteoblasts originate from progenitors (mesenchymal stem cells) who commit themselves to differentiate into preosteoblasts stimulated by TGF-β. They further differentiate into osteoblasts with an interaction between PTH and TGF-β. The latter acts as an inhibitor of osteoblastic differentation. Osteoclasts have a different path of differentiation than osteoblasts. They stem from precursor which differentiate with cell contact of osteoblasts and precursor of osteoclasts via RANK and RANKL. Produced by preosteoblasts, OPGs are able to bind RANKL inhibiting the cell contact and thus regulating the differentiation of osteoclasts. TGF-β are produced and released by osteoclasts and might also induce apoptosis of their producer. Roholl *et al.* (1994) found out that maturation of preosteoblasts to osteoblasts decreases with age in rats. While the number of preosteoblasts and osteoclasts per 100 μm almost remain the same, the activity and the number of matured osteoblasts decreases dramatically due to lack of regulator stimuli.

The results of the apparent mass density of the mineral and the organic content show us that old bone has a higher degree of mineralization than young bone. The apparent mass density and the volume fraction of the mineral content keeps increasing at growth and at the aging process. These findings correlate well with the results from Reid & Boyde (1987), who investigated the mineral density distribution with age by analysing SEM images. A decreasing number of low-density tissues was found with progressing age while the reverse was found for high-density tissues. The localized distribution of the mineralized tissues also changes during aging. The canaliculae and the lacunae filled with osteocytes are empty at young individuals but are filled with mineralized tissue at high age (Frost, 1960). This phenomenon was also observed by Jowsey (1960) who used a microradiography to study human bones. A high number of lacunae filled with bone mineral, which most often appear in the interstitial bone and the central canal of the osteon filled with calcified tissue could be found at high age. In the same course of research an increased number of almost complete mineralized osteones was found in bones of individuals with an age higher than 60 years. As was summarized by Kiebzak (1991), our results also suggest that the apparent mass density of the mineral content increases with age.

The focus of the research of Smith (1963) was to determine the alteration of the bone inorganic and organic fraction with age by investigating the organic component in the primary and seondary osteons. Primary osteons are being laid down at the beginning of the growing process and are going through changes with age. Secondary osteons are being accreted at the center of new bone, which are being resorbed and new secondary osteons are being formed. The tissue surrounding the secondary osteons is called interstitial tissue and is always older than the secondary osteon, which is newly formed consistently. Smith (1963) discovered that the organic concentration in the interstitial tissue is lower than in the secondary osteon, whose concentration is also higher than that of the primary osteons. Since the inorganic fraction was also observed by Smith (1963) and an increase with age noted, it seemed obvious to suggest that progressing mineralization is accompanied by decrease of the organic fraction. Similar results were found by Bailey *et al.* (1999) who researched on male and female human anterior superior iliac spine to relate the collagen changes to age and to bone strength. It was found that the total collagen concentration decreases with age for both sexes which reflects the results of our evaluation indicating a decline of the organic apparent mass density after reaching

the turning point between growing and aging. It is hypothesized that this can be explained by the diminishment of bone turnover as was already indicated by the increase of mineralization degree.

Since about 90% of the organic matter of bone consists of collagen (Biltz & Pellegrino, 1969; Urist *et al.* , 1983; Lees, 1987; Weiner & Wagner, 1998; Teitelbaum, 2000; Kazuhiko *et al.* , 2009), it also makes sense to turn our attention to collagen in other tissues besides bone. Research has been done on collagen in rat skin, liver, tendon, etc. related to age and a consistent finding among the different experiments could be proven. Mays *et al.* (1991) used rat tissue to determine the change of collagen and found a decrease in turnover with increasing age which is consistent to the findings of Lindstedt & Prockop (1960) and Neuberger *et al.* (1950), who also investigated the collagen content of rat tissues independently. These experiments reflect that not only collagen content in bone but also in different tissues undergo a decline with progressing age.

The results, shown in this thesis, reflect very well the mechanism of growing and aging bone in consideration of the well-directed interaction between bone forming and resorbing cells. The concentration of water, mineral, organics and thus the overall mass density have a strong influence on the mechanical properties of the bone tissue, as can be seen in Figures 8–12. Biomaterials used in surgery, should integrate easily in their environment and should not be much different than the biological tissue they are replacing. These facts display a strong demand of providing an easy access to those mechanical properties, which are essential in biomaterial desgin. Eqs. (35)–(43) deliver an approach to calculate the elasticity tensor components with the overall mass density as a single input parameter.

A. Scientific Appendix

A.1. Precision of Eq. (16) for determination of extracellular mass density

The extracellular mass density of those bone samples, whose mass density ρ_{exp}^{ec} were determined via the Archimedes' principle, was also computed by using Eq.(16), see Chapter 2, delivering the weight fractions of the water, the hydroxyapatite mineral and the organic matter, on the basis of the predicted density ρ_{pred}^{ec}. The mean and the standard deviation of the relative errors between the predicted values ρ_{pred}^{ec} and the experimentally obtained extracellular bone density ρ_{exp}^{ec} given in the papers, which were collected for the data basis, was calculated according to

$$err_{mean} = \frac{1}{n} * \sum_{i=1}^{n} err_i = \frac{1}{n} * \sum_{i=1}^{n} \frac{\rho_{pred,i}^{ec} - \rho_{exp,i}^{ec}}{\rho_{exp,i}^{ec}}, \tag{A.1}$$

$$err_{std} = \sqrt{\frac{1}{n-1} * \sum_{i=1}^{n} (err_i - err_{mean})^2}, \tag{A.2}$$

where n is the total number of specimens from each experiment. These values amount to $-0.85 \pm 2.67\%$ [mean$\pm$standard deviation]. Given this mean relative error of even less than 1%, Eq. (16) in Chapter 2 is validated to be accurate enough to calculate the extracellular mass density for those bone samples, where the density was not determined in the course of the experiment or was not specifically stated in the used scientific paper itself.

Figure A.1.: Experimental and predicted extracellular bone density

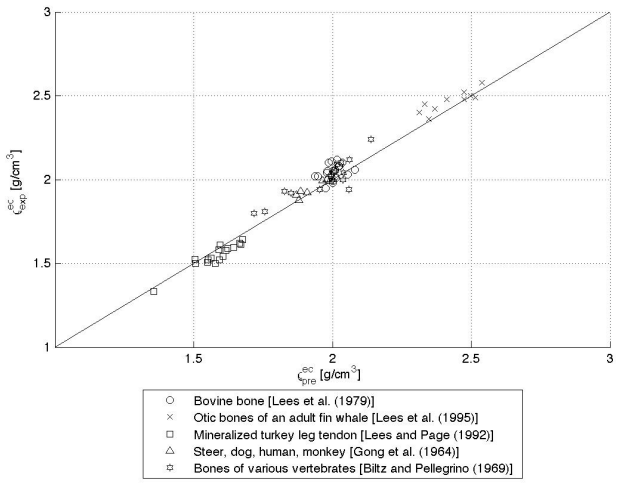

A.2. Detailled description of the four homogenization steps taken from Fritsch *et al.* (2009)

Based on the multistep microstructural homogenization scheme developed by Fritsch *et al.* (2009) and on the relations between mass density and constituent volume fraction of Chapter 2, we calculated the stiffness tensor components as functions of the experimentally accessible extracellular mass density ρ^{ec}.

We employ four homogenization steps at different observation scales, starting with the smallest scale, see Fig. 3 in Fritsch *et al.* (2009) or Fig. 6 of Chapter 2:

- First step: homogenization of cross-linked collagen molecules forming a matrix with water-filled intermolecular spaces (“wet collagen”)
- Second step: hydroxyapatite crystal agglomerations in the gap zone of the collagen fibrils and the “wet collagen” interpenetrate each other and form mineralized collagen fibrils
- Third step: needle-shaped hydroxyapatite crystal phases and the intercrystalline space form a porous polycrystal (“hydroxyapatite foam”)
- Fourth step: homogenization of extracellular bone matrix - the foam from the third step forms a matrix with embedded mineralized collagen fibrils from the second step.

A.2.1. First step - "wet collagen"

A Mori-Tanaka scheme was used to homogenize the wet collagen molecules, which are attached at their ends. For that scheme the transversely isotropic stiffness tensor of the collagen $\mathbb{c}_{col}$ was necessary for calculation. The values were taken from Table 1 of Fritsch & Hellmich (2007) based on experiments by Cusack & Miller (1979). The result from this homogenization step is the stiffness tensor of the "wet collagen" phase:

$$\begin{aligned}\mathbb{C}_{wetcol} = &\left\{(1-\mathring{f}_{im})\mathbb{c}_{col} + \mathring{f}_{im}\mathbb{c}_{im} : \left[\mathbb{I} + \mathbb{P}^{col}_{cyl} : (\mathbb{c}_{im} - \mathbb{c}_{col})\right]^{-1}\right\} \\ &: \left\{(1-\mathring{f}_{im})\mathbb{I} + \mathring{f}_{im}\left[\mathbb{I} + \mathbb{P}^{col}_{cyl} : (\mathbb{c}_{im} - \mathbb{c}_{col})\right]^{-1}\right\}^{-1}\end{aligned} \tag{A.3}$$

$\mathring{f}_{im} + \mathring{f}_{col} = 1$, where $\mathring{f}_{im}$ is the volume fraction of the intermolecular space and $\mathring{f}_{col}$ is the volume fraction of the molecular collagen. $\mathbb{I}$ is the fourth order unity tensor, $\mathbb{c}_{im}$ denotes the stiffness tensor of the intermolecular water and $\mathbb{P}^{col}_{cyl}$ is Hill's morphology tensor for cylindrical inclusions (intermolecular pores) in a matrix built up by molecular collagen.

A.2.2. Second step - "mineralized collagen fibril"

A self-consistent scheme is used here for homogenization of the wet collagen phase with stiffness $\mathbb{C}_{wetcol}$ and the mineral phase with stiffness $\mathbb{C}_{HA}$ (taken from experiments of Katz & Ukraincik (1971)):

$$\begin{aligned}\mathbb{C}_{fib} = &\left\{\breve{f}_{wetcol}\mathbb{C}_{wetcol} : \left[\mathbb{I} + \mathbb{P}^{fib}_{cyl} : (\mathbb{C}_{wetcol} - \mathbb{C}_{fib})\right]^{-1} + \breve{f}_{HA}\mathbb{c}_{HA}\right. \\ &: \left[\mathbb{I} + \mathbb{P}^{fib}_{sph} : (\mathbb{c}_{HA} - \mathbb{C}_{fib})\right]^{-1}\Big\} : \Big\{\breve{f}_{wetcol}\left[\mathbb{I} + \mathbb{P}^{fib}_{cyl} : (\mathbb{C}_{wetcol} - \mathbb{C}_{fib})\right]^{-1} \\ &\left.+\breve{f}_{HA}\left[\mathbb{I} + \mathbb{P}^{fib}_{sph} : (\mathbb{c}_{HA} - \mathbb{C}_{fib})\right]^{-1}\right\}^{-1}\end{aligned} \tag{A.4}$$

$\breve{f}_{HA} + \breve{f}_{wetcol} = 1$, whereas $\breve{f}_{HA}$ is the volume fraction of the hydroxyapatite crystals and $\breve{f}_{wetcol}$ is the volume fraction of the wet collagen phase. $\mathbb{c}_{HA}$ is the stiffness of the hydroxyapatite, $\mathbb{P}^{fib}_{cyl}$ and $\mathbb{P}^{fib}_{sph}$ are Hill's morphology tensors for a cylindrical (wet collagen) and spherical (mineral) inclusions in a matrix with the elastic properties of the mineralized collagen fibril.

A.2.3. Third step - "extrafibrillar hydroxyapatite foam"

In this step the homogenization occurs over the phase hydroxyapatite and the phase intercrystalline space to compose the extrafibrillar space (hydroxyapatite foam). Therefore a self-consistent scheme was used with uniform orientation distribution, needle-like inclusion phase for the mineral:

$$\begin{aligned}\mathbb{C}_{ef} =& \check{f}_{HA}\mathbb{c}_{HA} : \left\langle \left[\mathbb{I} + \mathbb{P}^{ef}_{cyl} : (\mathbb{c}_{HA} - \mathbb{C}_{ef})\right]^{-1} \right\rangle + (1 - \check{f}_{HA})\mathbb{c}_{H_2O} : \\ & \left[\mathbb{I} + \mathbb{P}^{ef}_{sph} : (\mathbb{c}_{H_2O} - \mathbb{C}_{ec})\right]^{-1} : \Bigg\{ \check{f}_{HA} \left\langle \left[\mathbb{I} + \mathbb{P}^{ef}_{cyl} : (\mathbb{c}_{HA} - \mathbb{C}_{ef})\right]^{-1} \right\rangle \\ & + (1 - \check{f}_{HA}) \left[(\mathbb{I} - \mathbb{P}^{ic}_{sph} : \mathbb{C}_{ef})\right]^{-1} \Bigg\}^{-1}\end{aligned} \tag{A.5}$$

where $\left\langle \left[\mathbb{I} + \mathbb{P}^{ef}_{cyl} : (\mathbb{c}_{HA} - \mathbb{C}_{ef})\right]^{-1} \right\rangle$ denotes the average over all crystal orientations ϑ and φ, see (Pichler *et al.* , 2008):

$$\int_{\varphi=0}^{2\pi} \int_{\vartheta=0}^{\pi} \left[\mathbb{I} + \mathbb{P}^{ef}_{cyl}(\varphi, \vartheta) : (\mathbb{c}_{HA} - \mathbb{C}_{ef})\right]^{-1} \frac{\sin\vartheta}{4\pi} d\vartheta d\varphi \tag{A.6}$$

$\check{f}_{HA}$ is the volume fraction of the hydroxyapatite crystals and $(1 - \check{f}_{HA})$ is the volume fraction of the intercrystalline space. $\mathbb{P}^{HA}_{cyl}$ and $\mathbb{P}^{ic}_{sph}$ are Hill's morphology tensors for cylindrical and spherical inclusions in a matrix of stiffness $\mathbb{C}_{ef}$.

A.2.4. Fourth step - "extracellular bone matrix"

Taking the mineralized collagen fibrils from step two and the hydroxyapatite foam calculated in the third step, we combine those two phases with their volume fractions $\bar{f}_{fib}$, $\bar{f}_{ef} = 1 - \bar{f}_{fib}$ and homogenize them using a Mori-Tanaka scheme, in order to obtain the extracellular (or ultrastructural) bone matrix, according to the following equation:

$$\begin{aligned}\mathbb{C}_{ultra} =& \left\{ (1 - \bar{f}_{fib})\mathbb{C}_{ef} + \bar{f}_{fib}\mathbb{C}_{fib} : \left[\mathbb{I} + \mathbb{P}^{ef}_{cyl} : (\mathbb{C}_{fib} - \mathbb{C}_{ef})\right]^{-1} \right\} \\ & : \left\{ (1 - \bar{f}_{fib})\mathbb{I} + \bar{f}_{fib} \left[\mathbb{I} + \mathbb{P}^{ef}_{cyl} : (\mathbb{C}_{fib} - \mathbb{C}_{ef})\right]^{-1} \right\}^{-1}\end{aligned} \tag{A.7}$$

$\mathbb{P}^{ef}_{cyl}$ denotes Hill's morphology tensor for a cylindrical inclusion in a matrix with stiffness $\mathbb{C}_{ef}$.

B. Source codes in MATLAB

The calculations were done with Matlab®, Version 7.7.0.471 (R2008b), Students license.

B.1. ExpData.m

This file is the collection of all differently obtained experimental data from literature and bringing them to a consistent level.

```
% ****************************************
% 01. EXTRACELLULAR EXPERIMENTAL DATAS
% ****************************************
% NEED FUNCTION: WFmtlt.m, ternaryc.m, terlabel.m, terplot.m
% ------------------------------------------------------
% OUTPUT: terData.jpg
% ------------------------------------------------------
clear all;
clc

if ispc
slash = '\';
else
slash = '/';
end;

% data from ultrasonic experiments done by Lees, Heeley and Cleary
% (1979) on bovine cortical bone tested in three different axis (axial,
% tangential, radial), microstructural weight fractions
WFminaxiallees79 = [0.658 0.656 0.621 0.627 0.643 0.643 0.671 0.664];
WForgaxiallees79 = [0.219 0.219 0.239 0.232 0.227 0.230 0.211 0.216];
WFwateraxiallees79 = [0.123 0.126 0.140 0.140 0.129 0.127 0.118 0.120];

WFmintanglees79 = [0.661 0.663 0.647 0.654 0.644 0.649 0.638 0.699];
WForgtanglees79 = [0.215 0.221 0.224 0.217 0.227 0.229 0.213 0.184];
WFwatertanglees79 = [0.123 0.116 0.129 0.128 0.129 0.122 0.123 0.117];

WFminradlees79 = [0.658 0.656 0.640 0.659 0.638 0.699];
```

```
WForgradlees79 = [0.219 0.219 0.228 0.218 0.242 0.210];
WFwaterradlees79 = [0.123 0.126 0.131 0.123 0.121 0.116];

% ----------------------------------------
% Lees95 - Some acoustical properties of the otic bones of a fin whale
% 1.-2. Maleus 3. Incus 4.-5. Stapes 6.-10. Periotic 11. T.bulla
WFminlees95 = [0.86 0.80 0.86 0.81 0.80 0.81 0.83 0.85 0.85 0.87 0.85];
WForglees95 = [0.1 0.13 0.09 0.13 0.14 0.13 0.11 0.1 0.1 0.09 0.1];
WFwaterlees95 = [0.04 0.07 0.05 0.06 0.06 0.07 0.06 0.05 0.05 0.04 0.05];

% ----------------------------------------
% Lees92
% WF from Figure 1 page 265

% MTLT
[rhoeclees92exp, WFminlees92, WForglees92] = WFmtlt();
WFwaterlees92 = 1 - WFminlees92 - WForglees92;

for i = 1:2
    rhoeclees92exp(i) = [];
    WFwaterlees92(i) = [];
    WFminlees92(i) = [];
    WForglees92(i) = [];
end

% ----------------------------------------
% Gong64 - Steer, Dog, Human, Monkey
% Density:
rhoectrabgong64exp = [1.93 1.911 1.924 1.878];
rhoeccorgong64exp = [1.995 2.003 1.991 2.035];

% Apparent density:
rhoappwatertrabgong64 = [0.281 0.292 0.27 0.271];
rhoappwatercorgong64 = [0.252 0.223 0.237 0.239];

rhoapporgtrabgong64 = [0.514 0.507 0.497 0.514];
rhoapporgcorgong64 = [0.486 0.519 0.476 0.487];

rhoappmintrabgong64 = rhoectrabgong64exp-rhoappwatertrabgong64 ...
                      -rhoapporgtrabgong64;
rhoappmincorgong64 = rhoeccorgong64exp-rhoappwatercorgong64 ...
                     -rhoapporgcorgong64;


% Weight fractions
WForgtrabgong64 = rhoapporgtrabgong64./rhoectrabgong64exp;
WFmintrabgong64 = rhoappmintrabgong64./rhoectrabgong64exp;
WFwatertrabgong64 = 1 - WForgtrabgong64 - WFmintrabgong64;

WForgcorgong64 = rhoapporgcorgong64./rhoeccorgong64exp;
WFmincorgong64 = rhoappmincorgong64./rhoeccorgong64exp;
WFwatercorgong64 = 1 - WForgcorgong64 - WFmincorgong64;
```

```
81
82 % ----------------------------------------
83 % DENSITY MISSING
84 % ----------------------------------------
85 % Hammett25 - Albino rats - no density, age in days
86 Agehammett25 = [23 30 50 65 75 100 150];
87
88 Mhummalehammett25 = [0.0557 0.0786 0.1018 0.1488 0.1591 0.1847 0.2556];
89 Mfemmalehammett25 = [0.0842 0.1373 0.2069 0.3255 0.3407 0.4050 0.5811];
90 Mhumfemhammett25 = [0.0537 0.0725 0.1008 0.1333 0.1417 0.1732 0.2033];
91 Mfemfemhammett25 = [0.0885 0.1258 0.2011 0.2866 0.3080 0.3818 0.4502];
92
93 WForghummalehammett25 = [0.1797 0.1906 0.1988 0.2097 0.2076 0.2149 0.2219];
94 WFminhummalehammett25 = [0.1707 0.1760 0.2347 0.3149 0.3367 0.3781 0.4241];
95 WFwaterhummalehammett25 = 1-WForghummalehammett25-WFminhummalehammett25;
96
97 WForgfemmalehammett25 = [0.1823 0.1909 0.2039 0.2171 0.2101 0.2174 0.2296];
98 WFminfemmalehammett25 = [0.1332 0.1437 0.2012 0.2833 0.3152 0.3558 0.4132];
99 WFwaterfemmalehammett25 = 1-WForgfemmalehammett25-WFminfemmalehammett25;
100
101 WForghumfemhammett25 = [0.1937 0.1929 0.2046 0.2093 0.2092 0.2192 0.2285];
102 WFminhumfemhammett25 = [0.1751 0.1797 0.2638 0.3151 0.3622 0.4201 0.4511];
103 WFwaterhumfemhammett25 = 1-WForghumfemhammett25-WFminhumfemhammett25;
104
105 WForgfemfemhammett25 = [0.1972 0.1949 0.2080 0.2127 0.2142 0.2223 0.2346];
106 WFminfemfemhammett25 = [0.1432 0.1502 0.2351 0.2884 0.3381 0.4012 0.4298];
107 WFwaterfemfemhammett25 = 1-WForgfemfemhammett25-WFminfemfemhammett25;
108
109 Morghummalehammett25 = WForghummalehammett25.*Mhummalehammett25;
110 Mminhummalehammett25 = WFminhummalehammett25.*Mhummalehammett25;
111 Mwaterhummalehammett25 = WFwaterhummalehammett25.*Mhummalehammett25;
112
113 Morgfemmalehammett25 = WForgfemmalehammett25.*Mfemmalehammett25;
114 Mminfemmalehammett25 = WFminfemmalehammett25.*Mfemmalehammett25;
115 Mwaterfemmalehammett25 = WFwaterfemmalehammett25.*Mfemmalehammett25;
116
117 Morghumfemhammett25 = WForghumfemhammett25.*Mhumfemhammett25;
118 Mminhumfemhammett25 = WFminhumfemhammett25.*Mhumfemhammett25;
119 Mwaterhumfemhammett25 = WFwaterhumfemhammett25.*Mhumfemhammett25;
120
121 Morgfemfemhammett25 = WForgfemfemhammett25.*Mfemfemhammett25;
122 Mminfemfemhammett25 = WFminfemfemhammett25.*Mfemfemhammett25;
123 Mwaterfemfemhammett25 = WFwaterfemfemhammett25.*Mfemfemhammett25;
124
125 % Lees03 - Mineralization of Type I Collagen
126 % third metacarpal of a horse
127 % ----------------------------------------
128 % Composition of the third horse metacarpal as a function of age and sex
129 % Male, age in months:
130 WFwatermlees03 = [0.2 0.17 0.19 0.18 0.12 0.11 0.12 0.13 0.13];
131 WFminmlees03 = [0.55 0.57 0.55 0.54 0.62 0.62 0.62 0.61 0.62];
132 WForgmlees03 = [0.25 0.26 0.26 0.28 0.26 0.27 0.26 0.26 0.25];
```

```
Agemlees03 = [0.1 0.13 0.33 0.4 7.0 12.0 12.0 17.0 19.0];
% Female, age in months:
WFwaterflees03 = [0.23 0.23 0.19 0.15 0.13 0.12 0.13 0.12 0.12 0.13];
WFminflees03 = [0.54 0.53 0.54 0.63 0.62 0.62 0.64 0.62 0.66 0.63];
WForgflees03 = [0.23 0.24 0.27 0.22 0.25 0.26 0.23 0.26 0.23 0.24];
Ageflees03 = [0.03 0.23 2.5 4.0 6.0 7.0 12.0 15.0 24.0 32.0];

% ---------------------------------------
% Burns29
% Rabbit: Duration of experiments: 17, 28
% last two data points of the control group was not taken since the % of
% fat was not determined
Mrabbitburns29 = [6.714 4.400];
WForgrabbitburns29f = [0.202 0.194];
WFfatrabbitburns29 = [0.138 0.014];
WFwaterrabbitburns29f = [0.392 0.581];
WFminrabbitburns29f = [0.267 0.21];

Morgrabbitburns29 = Mrabbitburns29.*WForgrabbitburns29f;
Mfatrabbitburns29 = Mrabbitburns29.*WFfatrabbitburns29;
Mwaterrabbitburns29 = Mrabbitburns29.*WFwaterrabbitburns29f;
Mminrabbitburns29 = Mrabbitburns29.*WFminrabbitburns29f;

WForgrabbitburns29 = Morgrabbitburns29./ ...
                     (Mrabbitburns29-Mfatrabbitburns29);
WFminrabbitburns29 = Mminrabbitburns29./ ...
                     (Mrabbitburns29-Mfatrabbitburns29);
WFwaterrabbitburns29 = Mwaterrabbitburns29./ ...
                       (Mrabbitburns29-Mfatrabbitburns29);

% Rat: Duration of experiments: 70, 70, 70, 70, 60 days
Mratburns29 = [2.461 2.510 2.269 2.313 1.944];
WForgratburns29f = [0.231 0.224 0.232 0.218 0.23];
WFfatratburns29 = [0.067 0.056 0.052 0.065 0.049];
WFwaterratburns29f = [0.313 0.375 0.318 0.334 0.344];
WFminratburns29f = [0.389 0.345 0.398 0.378 0.376];

Morgratburns29 = Mratburns29.*WForgratburns29f;
Mfatratburns29 = Mratburns29.*WFfatratburns29;
Mwaterratburns29 = Mratburns29.*WFwaterratburns29f;
Mminratburns29 = Mratburns29.*WFminratburns29f;

WForgratburns29 = Morgratburns29./(Mratburns29-Mfatratburns29);
WFminratburns29 = Mminratburns29./(Mratburns29-Mfatratburns29);
WFwaterratburns29 = Mwaterratburns29./(Mratburns29-Mfatratburns29);

% ***************************************
% DENSITY CALCULATIONS
% --------------------
% given in literature (Fritsch, Hellmich 2007)
% volume fractions of vascular and lacunar porosity

```

```
% In Literature:
rhowater = 1;
rhocoll = 1.41;
rhomin = 3;

% density from different experiments
% Lees 79
rhoecaxiallees79exp = [2.06 2.05 2.02 2.02 2.00 2.05 2.10 2.08];
rhoectanglees79exp = [2.12 2.08 2.10 1.98 2.05 2.11 2.03 2.06];
rhoecradlees79exp = [2.02 1.99 1.95 2.01 2.04 2.05];

rhoeclees79exp = [rhoecaxiallees79exp rhoecradlees79exp rhoectanglees79exp];

% Lees 95
rhoeclees95exp = [2.49 2.45 2.5 2.42 2.36 2.4 2.48 2.52 2.52 2.58 2.48];

% Lees(83 b)
% 1. porpoise t bulla 2.porpoise t bulla
% 3.whale t bulla 4.whale t bulla 5.horse t bulla 6.bovine dentin
rhoecwetlees87exp = [2.70 2.68 2.54 2.50 2.29 2.09];

% % Broz95
% rhoecbroz95exp = [2.02 2.01 1.99 1.95 1.95];

% Biltz and Pellegrino Biltz69
rhoecbiltz69exp = [1.8 1.81 1.93 1.92 1.94 2.0 2.09 2.05 2.02 2.04 ...
                   1.94 2.04 2.0 2.10 2.12 2.24];
tissuesbiltz69 = char(['Fish      '; 'Turtle    '; 'Frog      '; ...
                       'Polar Bear'; 'Man       '; 'Elephant  '; ...
                       'Monkey    '; 'Cat       '; 'Horse     '; ...
                       'Chicken   '; 'Dog       '; 'Goose     '; ...
                       'Cow       '; 'Guinea Pig'; 'Rabbit    '; ...
                       'Rat       ']);
vfwaterbiltz69 = [0.396 0.37 0.352 0.33 0.155 0.2 0.23 0.236 0.25 ...
                  0.245 0.28 0.23 0.262 0.25 0.245 0.202];
vfminbiltz69 = [0.295 0.292 0.345 0.362 0.399 0.411 0.426 0.422 ...
                0.41 0.417 0.387 0.427 0.426 0.435 0.45 0.499];
vforgbiltz69 = [0.369 0.401 0.385 0.401 0.418 0.415 0.411 0.405 0.405 ...
                0.387 0.355 0.376 0.362 0.37 0.372 0.383];
WFcabiltz69 = [0.2326 0.245 0.2469 0.2475 0.2569 0.2601 0.2614 0.266 ...
               0.2644 0.2631 0.2668 0.2694 0.2759 0.2701 0.2821 0.2881];
WFashdrybiltz69 = [0.61 0.624 0.656 0.66 0.67 0.686 0.688 0.691 0.694 ...
                   0.696 0.698 0.7077 0.71 0.712 0.727 0.735];
WFmindrybiltz69 = WFashdrybiltz69*1.066;

% Taken von Hellmich and Ulm 2003
rhoappwaterbiltz69 = vfwaterbiltz69.*rhowater;
rhoappminbiltz69 = WFmindrybiltz69.*(rhoecbiltz69exp-rhoappwaterbiltz69);
rhoapporgbiltz69 = rhoecbiltz69exp-rhoappwaterbiltz69-rhoappminbiltz69;
WFminbiltz69 = rhoappminbiltz69./rhoecbiltz69exp;
WFwaterbiltz69 = rhoappwaterbiltz69./rhoecbiltz69exp;
WForgbiltz69 = 1-WFwaterbiltz69-WFminbiltz69;
```

```
237
238 % ****************************************************************
239 % PLOT DATA IN A TERNARY DIAGRAM
240 % ****************************************************************
241
242 % Plot axis
243 [h,hg,htick] = terplot;
244
245 % Plot the data
246 % Lees79
247 terWFaxiallees79 = ternaryc(WFminaxiallees79, WForgaxiallees79, ...
248                     WFwateraxiallees79);
249 terWFradlees79  = ternaryc(WFminradlees79, WForgradlees79, ...
250                    WFwaterradlees79);
251 terWFtanglees79  = ternaryc(WFmintanglees79, WForgtanglees79, ...
252                     WFwatertanglees79);
253
254 set(terWFaxiallees79,'marker','o','markerfacecolor', 'none', 'color', ...
255     'black', 'markersize', 6)
256 set(terWFradlees79,'marker','o','markerfacecolor', 'none', 'color', ...
257     'black','markersize', 6)
258 set(terWFtanglees79,'marker','o','markerfacecolor', 'none', 'color', ...
259     'black','markersize', 6)
260
261 % Lees95
262 terWFlees95 = ternaryc(WFminlees95, WForglees95, WFwaterlees95);
263
264 set(terWFlees95,'marker','x','markerfacecolor', 'none', 'color', ...
265     'black', 'markersize', 6)
266
267 % Lees92
268 terWFlees92 = ternaryc(WFminlees92, WForglees92, WFwaterlees92);
269
270 set(terWFlees92,'marker','s','markerfacecolor', 'none', 'color', ...
271     'black', 'markersize', 6)
272
273 % Lees03
274 terWFflees03 = ternaryc(WFminflees03, WForgflees03, WFwaterflees03);
275 set(terWFflees03,'marker','d','markerfacecolor', 'none', 'color', ...
276     'black', 'markersize', 6)
277
278 terWFmlees03 = ternaryc(WFminmlees03, WForgmlees03, WFwatermlees03);
279 set(terWFmlees03,'marker','d','markerfacecolor', 'none', 'color', ...
280     'black', 'markersize', 6)
281
282 % Hammett25
283 terWFhummalehammett25 = ternaryc(WFminhummalehammett25, ...
284                       WForghummalehammett25, WFwaterhummalehammett25);
285 set(terWFhummalehammett25,'marker','*','markerfacecolor', 'none', ...
286     'color', 'black', 'markersize', 6)
287
288 terWFfemmalehammett25 = ternaryc(WFminfemmalehammett25, ...
```

```
                        WForgfemmalehammett25, WFwaterfemmalehammett25);
set(terWFfemmalehammett25,'marker','*','markerfacecolor', 'none', ...
    'color', 'black', 'markersize', 6)

terWFfemfemhammett25 = ternaryc(WFminfemfemhammett25, ...
                        WForgfemfemhammett25, WFwaterfemfemhammett25);
set(terWFfemfemhammett25,'marker','*','markerfacecolor', 'none', ...
    'color', 'black', 'markersize', 6)

terWFhumfemhammett25 = ternaryc(WFminhumfemhammett25, ...
                        WForghumfemhammett25, WFwaterhumfemhammett25);
set(terWFhumfemhammett25,'marker','*','markerfacecolor', 'none', ...
    'color', 'black', 'markersize', 6)

% gong64
terWFtrabgong64 = ternaryc(WFmintrabgong64, WForgtrabgong64, ...
                  WFwatertrabgong64);
set(terWFtrabgong64,'marker','^','markerfacecolor', 'none', 'color', ...
    'black', 'markersize', 6)

terWFcorgong64 = ternaryc(WFmincorgong64, WForgcorgong64, ...
                 WFwatercorgong64);
set(terWFcorgong64,'marker','^','markerfacecolor', 'none', 'color', ...
    'black', 'markersize', 6)

% burns29
terWFrabbitburns29 = ternaryc(WFminrabbitburns29, WForgrabbitburns29, ...
                     WFwaterrabbitburns29);
set(terWFrabbitburns29,'marker','v','markerfacecolor', 'none', ...
    'color', 'black', 'markersize', 6)
terWFratburns29 = ternaryc(WFminratburns29, WForgratburns29, ...
                  WFwaterratburns29);
set(terWFratburns29,'marker','v','markerfacecolor', 'none', 'color', ...
    'black', 'markersize', 6)

% biltz69
terWFbiltz69 = ternaryc(WFminbiltz69, WForgbiltz69, WFwaterbiltz69);
set(terWFbiltz69,'marker','h','markerfacecolor', 'none', 'color', ...
    'black', 'markersize', 6)

hlabels=terlabel('Mineral','Organic','Water');

hlegend = legend([terWFaxiallees79(1) terWFlees95(1) terWFlees92(1) ...
 terWFflees03(1) terWFhummalehammett25(1) terWFtrabgong64(1) ...
 terWFrabbitburns29(1) terWFbiltz69(1)], ...
 'Bovine bone [Lees et al. (1979)]', ...
 'Otic bones of a fine whale [Lees et al. (1995)]', ...
 'Mineralized turkey leg tendon [Lees (1992)]', ...
 'Horse metacarpal [Lees (2003)]', ...
 'Femur and humeris of albino rats (female and male) [Hammett (1925)]', ...
 'Bone from steer, dog, human, monkey [Gong et al. (1964)]', ...
 'Rabbit and rat bones [Burns (1929)]', ...
```

```
 'Bone from various vertebrates [Biltz and Pellegrino (1969)]', ...
 'location', 'northoutside');

filename = 'terData.jpg';
currentDir = pwd;
absPathPlot = strcat(pwd, slash, 'LatexFiles', slash, filename);
print('-djpeg', absPathPlot);
```

B.1.1. WFmtlt.m

The purpose of this function, is to import Fig. 1 in Lees & Page (1992) and automatically determine the overall mass density, the weight fractions for hydroxyapatite, water and the organic matter.

```
% ************************************************
% Lees 92: Turkey Leg Tendon
% Reading weight fractions from Figure 1
% ************************************************
% Original image measures 113 x 204 mm

function[rhomuLees92, WFmuminLees92, WFmuorgLees92]=WFmtlt()
imgOrg = imread('WF_Org.gif', 'gif');
k = 1;
sizeOrg = size(imgOrg);

for i = 1:sizeOrg(:,2);
    for j = 1:sizeOrg(:,1)
       if imgOrg(j, i) < 240; % 255 = white, else counts as black
           y = (j * 113/sizeOrg(:,1)); % converting indices into mm
           WFmuorgLees92temp(k) = ((113-y-10) * 0.0078);
           % converting into scale of picture

           x = i * 204/sizeOrg(:,2);
           rhomuorgLees92temp(k) = ((x * 0.0039) + 1);

           k = k + 1;
       else
       end
    end
end


imgMin = imread('WF_Min.gif', 'gif');
k = 1;
sizeMin = size(imgOrg);

for i = 1:sizeMin(:,2);
```

```
    for j = 1:sizeMin(:,1)
       if imgMin(j, i) < 240; % 255 = white, else counts as black
           y = (j * 113/sizeMin(:,1)); % converting indices into mm
           WFmuminLees92temp(k) = ((113-y-10) * 0.0078);
           % converting into scale of picture (

           if WFmuminLees92temp(k) < 0
               WFmuminLees92temp(k) = 0;
           end

           x = i * 204/sizeMin(:,2);
           rhomuminLees92temp(k) = ((x * 0.0039) + 1);

           k = k + 1;
       end
    end
end

% Mapping of weight fractions organic and mineral to the corresponding
% density

n = 1;

for l=1:length(rhomuminLees92temp)
    for m=1:length(rhomuorgLees92temp)
        if (rhomuminLees92temp(l)-rhomuorgLees92temp(m)) == 0
            rhomuLees92(n) = rhomuminLees92temp(l);
            WFmuminLees92(n) = WFmuminLees92temp(l);
            WFmuorgLees92(n) = WFmuorgLees92temp(m);

            rhomuminLees92temp(l) = 100;
            rhomuorgLees92temp(m) = 50;
            WFmuminLees92temp(l) = 0;
            WFmuorgLees92temp(m) = 0;


            n = n + 1;
        elseif  (rhomuminLees92temp(l)-rhomuorgLees92temp(m)) <= 0.005 ...
                && (rhomuminLees92temp(l)-rhomuorgLees92temp(m)) > -0.005

                rhomuLees92(n) = rhomuminLees92temp(l);
                WFmuminLees92(n) = WFmuminLees92temp(l);
                WFmuorgLees92(n) = WFmuorgLees92temp(m);

                rhomuminLees92temp(l) = 1000;
                rhomuorgLees92temp(m) = 500;
                WFmuminLees92temp(l) = 0;
                WFmuorgLees92temp(m) = 0;

                n = n + 1;
        end
    end
```

```
86 end
87 end
```

B.1.2. Ternary Diagram

The functions **ternaryc.m**, **terlabel.m** and **terplot.m**, required for **ExpData.m** were taken from MATLAB®
CENTRAL - An open exchange for the MATLAB and SIMULINK user community, with thanks to the author Ulrich Theune:

(http://www.mathworks.com/matlabcentral/fileexchange/7210, 2010)

B.2. DensityPrediction.m

This file was written to predict the extracellular density. The experimental and predicted density was then compared to obtain the relative mean error and the standard deviation to determine the accuracy.

```
% ************************************************************************
% PREDICTION: Density of extracellular bone matrix
% ------------------------------------------------------------------------
% RUN: ExpData.m
% NEED FUNCTION: funcRhoecpre.m
% ------------------------------------------------------------
% OUTPUT: boneDensities.jpg
% ----------------------------------------------------------
% Data from Lees79, bovine cortical bone

rhoecaxiallees79pre = funcRhoecpre(WForgaxiallees79, WFminaxiallees79, ...
                       WFwateraxiallees79, rhocoll, rhomin, rhowater);
rhoecradlees79pre = funcRhoecpre(WForgradlees79, WFminradlees79, ...
                     WFwaterradlees79, rhocoll, rhomin, rhowater);
rhoectanglees79pre = funcRhoecpre(WForgtanglees79, WFmintanglees79, ...
                      WFwatertanglees79, rhocoll, rhomin, rhowater);

% ----------------------------------------------------------
% Data from Lees95
% Whale
rhoeclees95pre = funcRhoecpre(WForglees95, WFminlees95, WFwaterlees95, ...
                 rhocoll, rhomin, rhowater);

% Data from Lees92 MTLT
rhoeclees92pre = funcRhoecpre(WForglees92, WFminlees92, WFwaterlees92, ...
                 rhocoll, rhomin, rhowater);

% Data from gong64
rhoectrabgong64pre = funcRhoecpre(WForgtrabgong64, WFmintrabgong64, ...
                      WFwatertrabgong64, rhocoll, rhomin, rhowater);
rhoeccorgong64pre = funcRhoecpre(WForgcorgong64, WFmincorgong64, ...
                     WFwatercorgong64, rhocoll, rhomin, rhowater);

% Data from biltz69
rhoecbiltz69pre = funcRhoecpre(WForgbiltz69, WFminbiltz69, ...
                   WFwaterbiltz69, rhocoll, rhomin, rhowater);

% Data from burns29
rhoecrabbitburns29pre = funcRhoecpre(WForgrabbitburns29, ...
                         WFminrabbitburns29, WFwaterrabbitburns29, ...
                         rhocoll, rhomin, rhowater);
rhoecratburns29pre = funcRhoecpre(WForgratburns29, WFminratburns29, ...
                      WFwaterratburns29, rhocoll, rhomin, rhowater);

% Data from Hammett 25
```

```
rhoecfemfemhammett25pre = funcRhoecpre(WForgfemfemhammett25, ...
                          WFminfemfemhammett25, WFwaterfemfemhammett25, ...
                          rhocoll, rhomin, rhowater);
rhoechumfemhammett25pre = funcRhoecpre(WForghumfemhammett25, ...
                          WFminhumfemhammett25, WFwaterhumfemhammett25, ...
                          rhocoll, rhomin, rhowater);
rhoecfemmalehammett25pre = funcRhoecpre(WForgfemmalehammett25, ...
                           WFminfemmalehammett25, ...
                           WFwaterfemmalehammett25, rhocoll, rhomin, ...
                           rhowater);
rhoechummalehammett25pre = funcRhoecpre(WForghummalehammett25, ...
                           WFminhummalehammett25, ...
                           WFwaterhummalehammett25, rhocoll, rhomin, ...
                           rhowater);


rhoechammett25pre = [rhoechumfemhammett25pre rhoechummalehammett25pre ...
                     rhoecfemfemhammett25pre rhoecfemmalehammett25pre];

% Data from Lees03
rhoecmlees03pre = funcRhoecpre(WForgmlees03, WFminmlees03, ...
                  WFwatermlees03, rhocoll, rhomin, rhowater);
rhoecflees03pre = funcRhoecpre(WForgflees03, WFminflees03, ...
                  WFwaterflees03, rhocoll, rhomin, rhowater);

rhoeclees03pre = [rhoecmlees03pre rhoecflees03pre];


% ********************************************************
% Calculate error of all calculated and experimental density
% ********************************************************
% calculate error in subgroups
% Lees79: bovine bones
rhoeclees79 = ([rhoecaxiallees79pre rhoecradlees79pre ...
                rhoectanglees79pre; rhoecaxiallees79exp ...
                rhoecradlees79exp rhoectanglees79exp]');
err_rholees79 = (rhoeclees79(:,1)-rhoeclees79(:,2))./rhoeclees79(:,2);
meanerr_rholees79 = mean(err_rholees79);
stderr_rholees79 = std(err_rholees79);
varerr_rholees79 = var(err_rholees79);

% Lees95: otic wale bones
rhoeclees95 = ([rhoeclees95pre; rhoeclees95exp]');
err_rholees95 = (rhoeclees95(:,1)-rhoeclees95(:,2))./rhoeclees95(:,2);
meanerr_rholees95 = mean(err_rholees95);
stderr_rholees95 = std(err_rholees95);
varerr_rholees95 = var(err_rholees95);

% Lees92: MTLT
rhoeclees92 = ([rhoeclees92pre; rhoeclees92exp]');
err_rholees92 = (rhoeclees92(:,1)-rhoeclees92(:,2))./rhoeclees92(:,2);
meanerr_rholees92 = mean(err_rholees92);
```

```
stderr_rholees92 = std(err_rholees92);
varerr_rholees92 = var(err_rholees92);

% gong64
rhoecgong64 = ([rhoectrabgong64pre rhoeccorgong64pre; ...
                rhoectrabgong64exp rhoeccorgong64exp]');
err_rhogong64 = (rhoecgong64(:,1)-rhoecgong64(:,2))./rhoecgong64(:,2);
meanerr_rhogong64 = mean(err_rhogong64);
stderr_rhogong64 = std(err_rhogong64);
varerr_rhogong64 = var(err_rhogong64);

% biltz69
rhoecbiltz69 = ([rhoecbiltz69pre; rhoecbiltz69exp]');
err_rhobiltz69 = (rhoecbiltz69(:,1)-rhoecbiltz69(:,2))./rhoecbiltz69(:,2);
meanerr_rhobiltz69 = mean(err_rhobiltz69);
stderr_rhobiltz69 = std(err_rhobiltz69);
varerr_rhobiltz69 = var(err_rhobiltz69);

% All errors
rhoecall = ([rhoeclees79' rhoeclees92' rhoeclees95' rhoecgong64' ...
             rhoecbiltz69']');
err_all = (rhoecall(:,1)-rhoecall(:,2))./rhoecall(:,2);
meanerr_all = mean(err_all)
stderr_all = std(err_all)
varerr_all = var(err_all)

% ********************************************************
% Plot results
% ********************************************************

hold on
plot([rhoecaxiallees79pre rhoectanglees79pre rhoecradlees79pre], ...
     [rhoecaxiallees79exp rhoectanglees79exp rhoecradlees79exp], ...
     'o', 'color', 'black')
plot(rhoeclees95pre, rhoeclees95exp, 'x', 'color', 'black')
plot(rhoeclees92pre, rhoeclees92exp, 's', 'color', 'black')
plot([rhoectrabgong64pre rhoeccorgong64pre], ...
      [rhoectrabgong64exp rhoeccorgong64exp], '^', 'color', 'black')
plot(rhoecbiltz69pre, rhoecbiltz69exp, 'h', 'color', 'black')
plot([1 3], [1 3], 'color', 'black')
hlegend = legend('Bovine bone [Lees et al. (1979)]', ...
        'Otic bones of an adult fin whale [Lees et al. (1995)]', ...
        'Mineralized turkey leg tendon [Lees and Page (1992)]', ...
        'Steer, dog, human, monkey [Gong et al. (1964)]', ...
        'Bones of various vertebrates [Biltz and Pellegrino (1969)]', ...
        'location', 'southoutside');
set(hlegend, 'fontsize', 10);

set(gca, 'XTick', 1.5:0.5:3, 'XTickLabel',{'1.5','2','2.5','3'}, ...
    'YTick', 0:0.5:3.5, 'YTickLabel',{'0','0.5','1','1.5','2','2.5', ...
    '3','3.5'})
xlabel('\rho^{ec}_{pre} [g/cm^3]')
```

```
150 ylabel('\rho^{ec}_{exp} [g/cm^3]')
151 grid('on')
152
153 filename = 'boneDensities.jpg';
154 absPathPlot = strcat(pwd, slash, 'LatexFiles', slash, filename);
155 print('-djpeg', absPathPlot);
```

B.2.1. funcRhoecpre.m

This function predicts the extracellular density on the basis of the hydroxyapatite, water and organic weight fractions and their density.

```
1 % Calculation of predicted extracecullar density
2
3 function[rhoecpre] = funcRhoecpre(WForg,WFmin,WFwater,rhocoll,rhomin,rhowater)
4     rhoecpre = (WForg/rhocoll + WFmin/rhomin + WFwater/rhowater).^-1;
5 end
```

B.3. AppRho.m

This file was written to calculate the concentration of the three bone components, namely the apparent mass density and delivers 4 EPS graphic files as Output. It also compares the correlation of each apparent mass density to the other and determines a growing and aging pattern of bone by finding the best coefficient of determination.

```
% ************************************************************
% 03. APPARENT MASS DENSITIES of components of microstructure!
% ************************************************************
% RUN: ExpData.m, DensityPrediction.m
% NEED FUNCTION: funcappRho.m, rsquare.m, funcVF.m, funcWF.m
% ------------------------------------------------------------
% OUTPUT: appDensity_WaterMin.eps, appDensity_MinOrg.eps,
% appDensity_WaterOrg.eps, appDensity_rhoc.eps
% ------------------------------------------------------------
% DATA FROM GONG 64 IN ExpData.m

[rhoappwaterlees79, rhoapporglees79, rhoappminlees79] = ...
  funcappRho([WFwateraxiallees79 WFwaterradlees79 WFwatertanglees79], ...
  [WForgaxiallees79 WForgradlees79 WForgtanglees79], [WFminaxiallees79 ...
  WFminradlees79 WFmintanglees79], [rhoecaxiallees79exp ...
  rhoecradlees79exp rhoectanglees79exp]);
[rhoappwaterlees03, rhoapporglees03, rhoappminlees03] = ...
  funcappRho([WFwatermlees03 WFwaterflees03], [WForgmlees03 ...
  WForgflees03], [WFminmlees03 WFminflees03], [rhoecmlees03pre ...
  rhoecflees03pre]);
[rhoappwaterhammett25, rhoapporghammett25, rhoappminhammett25] = ...
  funcappRho([WFwaterfemmalehammett25 WFwaterfemfemhammett25 ...
  WFwaterhummalehammett25 WFwaterhumfemhammett25], ...
  [WForgfemmalehammett25 WForgfemfemhammett25 WForghummalehammett25 ...
  WForghumfemhammett25], [WFminfemmalehammett25 WFminfemfemhammett25 ...
  WFminhummalehammett25 WFminhumfemhammett25], ...
  [rhoecfemmalehammett25pre rhoecfemfemhammett25pre ...
  rhoechummalehammett25pre rhoechumfemhammett25pre]);
[rhoappwaterrabbitburns29, rhoapporgrabbitburns29, ...
  rhoappminrabbitburns29] = funcappRho(WFwaterrabbitburns29, ...
  WForgrabbitburns29, WFminrabbitburns29, rhoecrabbitburns29pre);
[rhoappwaterratburns29, rhoapporgratburns29, rhoappminratburns29] = ...
  funcappRho(WFwaterratburns29,WForgratburns29, WFminratburns29, ...
  rhoecratburns29pre);
[rhoappwaterlees95, rhoapporglees95, rhoappminlees95] = ...
  funcappRho(WFwaterlees95,WForglees95, WFminlees95, rhoeclees95exp);
[rhoappwaterlees92, rhoapporglees92, rhoappminlees92] = ...
  funcappRho(WFwaterlees92,WForglees92, WFminlees92, rhoeclees92exp);

% Biltz69: apparent mass density given in ExpData.m (taken from Hellmich
% and Ulm)

% ------------------------------------------------
% REGRESSION
```

```
% ------------------------------------------------

rhoapp = [rhoapporglees95 rhoapporgbiltz69 rhoapporgcorgong64 ...
    rhoapporghammett25 rhoapporglees03 rhoapporglees79 rhoapporglees92 ...
    rhoapporgrabbitburns29 rhoapporgratburns29 ...
    rhoapporgtrabgong64; ...
    rhoappminlees95 rhoappminbiltz69 rhoappmincorgong64 ...
    rhoappminhammett25 rhoappminlees03 rhoappminlees79 rhoappminlees92 ...
    rhoappminrabbitburns29 rhoappminratburns29 ...
    rhoappmintrabgong64; ...
    rhoappwaterlees95 rhoappwaterbiltz69 rhoappwatercorgong64 ...
    rhoappwaterhammett25 rhoappwaterlees03 rhoappwaterlees79 ...
    rhoappwaterlees92 rhoappwaterrabbitburns29 ...
    rhoappwaterratburns29 rhoappwatertrabgong64; ...
    rhoeclees95exp rhoecbiltz69exp rhoeccorgong64exp ...
    rhoechammett25pre rhoeclees03pre rhoeclees79exp ...
    rhoeclees92exp rhoecrabbitburns29pre ...
    rhoecratburns29pre rhoectrabgong64exp]';

% Find threshold between Growing and Aging - Algorithm comparing the R^2
% with each other and determine the threshold with the highest R^2

% Define maximum rhoapp organic and determine matching rhoapp
% mineral-boundaries of +/- 25.
[maxrhoapporg,Ind]=max(rhoapp(:,1));
TSrhoappmin = rhoapp(Ind,2);
TSrhoappminlow = rhoapp(Ind,2)/100*75;
TSrhoappminhigh = rhoapp(Ind,2)*1.25;
TS = (TSrhoappminlow:0.01:TSrhoappminhigh);

% Calculate R^2 for different threshold (threshold defines, where process
% Growing stops and process Aging begins)
for m = (1:length(TS))
    j = 1;
    k = 1;
    for i = 1:length(rhoapp)
        if rhoapp(i,2) <= TS(m)
            rhoapporgminGrowthtemp(j,1) = rhoapp(i,1);
            rhoapporgminGrowthtemp(j,2) = rhoapp(i,2);
            j = j+1;
        else
            rhoapporgminAgetemp(k,1) = rhoapp(i,1);
            rhoapporgminAgetemp(k,2) = rhoapp(i,2);
            k = k+1;
        end
    end
    polyGrowthtemp = polyfit(rhoapporgminGrowthtemp(:,2), ...
                     rhoapporgminGrowthtemp(:,1), 1);
    rhoapporgGrowthtemp = polyGrowthtemp(:,1)* ...
                          rhoapporgminGrowthtemp(:,2) + polyGrowthtemp(:,2);

    rhoapporgAgetemp = (polyGrowthtemp(:,1)* TS(m) + polyGrowthtemp(:,2)).*...
```

```
                        (1-(rhoapporgminAgetemp(:,2)-TS(m))./(rhomin-TS(m)));

    testTS(m,1) = TS(m);
    testTS(m,2) = rsquare([rhoapporgminGrowthtemp(:,1); ...
        rhoapporgminAgetemp(:,1)], [rhoapporgGrowthtemp; rhoapporgAgetemp]);
    clear rhoapporgminGrowthtemp;
    clear rhoapporgminAgetemp;
end

% Find out best R^2 in the values with different thresholds
[bestRR, indbestRR] = max(testTS(:,2));
bestTSrhoappmin = testTS(indbestRR,1);

bestRR

% separate values in two groups with the best threshold (best R^2) in Aging
% and Growing process
j=1; k=1;
for i = 1:length(rhoapp)
    if rhoapp(i,2) <= bestTSrhoappmin
        rhoappGrowth(j,1) = rhoapp(i,1);
        rhoappGrowth(j,2) = rhoapp(i,2);
        rhoappGrowth(j,3) = rhoapp(i,3);
        rhoappGrowth(j,4) = rhoapp(i,4);
        j = j+1;
    elseif rhoapp(i,2) > bestTSrhoappmin
        rhoappAge(k,1) = rhoapp(i,1);
        rhoappAge(k,2) = rhoapp(i,2);
        rhoappAge(k,3) = rhoapp(i,3);
        rhoappAge(k,4) = rhoapp(i,4);
        k=k+1;
    end
end

clear j k;

% Calculate regression with the best mineral threshold between Aging and
% Growing
polyrhoappGrowth = polyfit(rhoappGrowth(:,2), ...
                                rhoappGrowth(:,1), 1);
rhoappminGrowth = (0.1:0.01:bestTSrhoappmin);
rhoapporgGrowth = polyrhoappGrowth(:,1)*rhoappminGrowth ...
                +polyrhoappGrowth(:,2);

% Regression for Aging is simply a regression between start point (which is
% end point of Aging process) and end point (which is were rhoapp organic =
% 0 and rhoapp mineral = 3, since pure mineral density is 3 g/cm^2
minAging = [bestTSrhoappmin; 3];
orgAging = [(polyrhoappGrowth(:,2)*bestTSrhoappmin ...
            +polyrhoappGrowth(:,2)); 0];
polyrhoappAge = polyfit(minAging, orgAging, 1);

```

```
rhoappminAge = (bestTSrhoappmin:0.01:3);
rhoapporgAge = (polyrhoappGrowth(:,1)*bestTSrhoappmin ...
                  +polyrhoappGrowth(:,2)).*...
                (1-(rhoappminAge-bestTSrhoappmin)./(rhomin-bestTSrhoappmin));


% CALCULATIONS OF DATA FROM REGRESSION

[vfminregAge, vforgregAge, vfwaterregAge] = ...
    funcVF(rhoappminAge, rhoapporgAge, rhomin, rhocoll);
[vfminregGrowth, vforgregGrowth, vfwaterregGrowth] = ...
    funcVF(rhoappminGrowth, rhoapporgGrowth, rhomin, rhocoll);
rhoappwaterAge = vfwaterregAge.*rhowater;
rhoappwaterGrowth = vfwaterregGrowth.*rhowater;

rhoecregAge = (rhoappwaterAge+rhoappminAge+rhoapporgAge);
rhoecregGrowth = (rhoappwaterGrowth+rhoappminGrowth+rhoapporgGrowth);

[WFwaterregAge, WForgregAge, WFminregAge] = ...
    funcWF(rhoappwaterAge, rhoappminAge, rhoapporgAge, ...
    (rhoappwaterAge+rhoappminAge+rhoapporgAge));
[WFwaterregGrowth, WForgregGrowth, WFminregGrowth] = ...
    funcWF(rhoappwaterGrowth, rhoappminGrowth, rhoapporgGrowth, ...
    (rhoappwaterGrowth+rhoappminGrowth+rhoapporgGrowth));

% for determination coefficient of water vs. organic, water vs. mineral

polyrhoapporgwaterAge = polyfit(rhoappwaterAge, rhoapporgAge, 1);
polyrhoapporgwaterGrowth = polyfit(rhoappwaterGrowth, rhoapporgGrowth, 1);

polyrhoappminwaterAge = polyfit(rhoappwaterAge, rhoappminAge, 1);
polyrhoappminwaterGrowth = polyfit(rhoappwaterGrowth, rhoappminGrowth, 1);

rhoapporgAgerr = polyrhoapporgwaterAge(:,1).*rhoappAge(:,3) + ...
    polyrhoapporgwaterAge(:,2);
rhoapporgGrowthrr = polyrhoapporgwaterGrowth(:,1).*rhoappGrowth(:,3) + ...
    polyrhoapporgwaterGrowth(:,2);

rhoappminAgerr = polyrhoappminwaterAge(:,1).*rhoappAge(:,3) + ...
    polyrhoappminwaterAge(:,2);
rhoappminGrowthrr = polyrhoappminwaterGrowth(:,1).*rhoappGrowth(:,3) + ...
    polyrhoappminwaterGrowth(:,2);

RRorgwater = rsquare([rhoappGrowth(:,1); rhoappAge(:,1)], ...
                  [rhoapporgGrowthrr; rhoapporgAgerr])

RRminwater = rsquare([rhoappGrowth(:,2); rhoappAge(:,2)], ...
                  [rhoappminGrowthrr; rhoappminAgerr])

% coefficient of determination for rhoapp vs. rhoec


```

```
polyrhoapporgecAge = polyfit(rhoecregAge, rhoapporgAge, 1);
polyrhoappminecAge = polyfit(rhoecregAge, rhoappminAge, 1);
polyrhoappwaterecAge = polyfit(rhoecregAge, rhoappwaterAge, 1);

polyrhoapporgecGrowth = polyfit(rhoecregGrowth, rhoapporgGrowth, 1);
polyrhoappminecGrowth = polyfit(rhoecregGrowth, rhoappminGrowth, 1);
polyrhoappwaterecGrowth = polyfit(rhoecregGrowth, rhoappwaterGrowth, 1);

rhoapporgecAge = polyrhoapporgecAge(:,1).*rhoappAge(:,4)+...
                 polyrhoapporgecAge(:,2);
rhoapporgecGrowth = polyrhoapporgecGrowth(:,1).*rhoappGrowth(:,4)+...
                 polyrhoapporgecGrowth(:,2);

rhoappminecAge = polyrhoappminecAge(:,1).*rhoappAge(:,4)+...
                 polyrhoappminecAge(:,2);
rhoappminecGrowth = polyrhoappminecGrowth(:,1).*rhoappGrowth(:,4)+...
                 polyrhoappminecGrowth(:,2);

rhoappwaterecAge = polyrhoappwaterecAge(:,1).*rhoappAge(:,4)+...
                 polyrhoappwaterecAge(:,2);
rhoappwaterecGrowth = polyrhoappwaterecGrowth(:,1).*rhoappGrowth(:,4)+...
                 polyrhoappwaterecGrowth(:,2);

RRrhoecwater = rsquare([rhoappGrowth(:,3); rhoappAge(:,3)], ...
                  [rhoappwaterecGrowth; rhoappwaterecAge])

RRrhoecmin = rsquare([rhoappGrowth(:,2); rhoappAge(:,2)], ...
                  [rhoappminecGrowth; rhoappminecAge])

RRrhoecorg = rsquare([rhoappGrowth(:,1); rhoappAge(:,1)], ...
                  [rhoapporgecGrowth; rhoapporgecAge])

% PLOT RHOAPP WATER VS. RHOAPP MIN

hold on
plot(rhoappwaterlees79, rhoappminlees79, 'o', 'color', 'black')
plot(rhoappwaterlees03, rhoappminlees03, 'd', 'color', 'black')
plot(rhoappwaterhammett25, rhoappminhammett25, '*', 'color', 'black')
plot([rhoappwatertrabgong64 rhoappwatercorgong64], ...
     [rhoappmintrabgong64 rhoappmincorgong64], '^', 'color', 'black')
plot(rhoappwaterlees92, rhoappminlees92, 's', 'color', 'black')
plot([rhoappwaterrabbitburns29 rhoappwaterratburns29], ...
     [rhoappminrabbitburns29 rhoappminratburns29], 'v', 'color', 'black')
plot(rhoappwaterbiltz69, rhoappminbiltz69, 'h', 'color', 'black')
plot(rhoappwaterlees95, rhoappminlees95, 'x', 'color', 'black')

plot(rhoappwaterGrowth, rhoappminGrowth, '-', 'color', 'black', ...
    'linewidth', 1)
plot(rhoappwaterAge, rhoappminAge, '-', 'color', 'black', 'linewidth', 1)
plot(0,0)
xlabel('\rho^*_{H_2O} [g/cm^3]')
ylabel('\rho^*_{HA} [g/cm^3]')
```

```
grid('on')

hlegend = legend('Bovine tibia [Lees et al. (1979)]', ...
 'Horse metacarpals [Lees (2003)]', ...
 'Femur and humeris of albino rats [Hammett (1925)]', ...
 'Bones from steers, dogs, humans, monkeys [Gong et al. (1964)]', ...
 'Mineralized turkey leg tendon [Lees and Page (1992)]', ...
 'Bones from rabbits, rats [Burns (1929)]', ...
 'Bones from various vertebrates [Biltz and Pellegrino (1969)]', ...
 'Otic bones of a fine whale [Lees et al. (1995)]', ...
 'location', 'southoutside');
set(hlegend, 'fontsize', 10);

filename = 'appDensity_WaterMin.eps';
absPathPlot = strcat(pwd, slash, 'LatexFiles', slash, filename);
print('-depsc', absPathPlot);

% PLOT RHOAPP MIN VS. RHOAPP ORG

figure
hold on
plot(rhoappminlees79, rhoapporglees79, 'o', 'color', 'black')
plot(rhoappminlees03, rhoapporglees03, 'd', 'color', 'black')
plot(rhoappminhammett25, rhoapporghammett25, '*', 'color', 'black')
plot([rhoappmintrabgong64 rhoappmincorgong64], ...
     [rhoapporgtrabgong64 rhoapporgcorgong64], '^', 'color', 'black')
plot(rhoappminlees92, rhoapporglees92, 's', 'color', 'black')
plot([rhoappminrabbitburns29 rhoappminratburns29], ...
     [rhoapporgrabbitburns29 rhoapporgratburns29],  'v', 'color', 'black')
plot(rhoappminbiltz69, rhoapporgbiltz69, 'h', 'color', 'black')
plot(rhoappminlees95, rhoapporglees95, 'x', 'color', 'black')

plot(rhoappminGrowth, rhoapporgGrowth, '-', 'color', 'black', ...
    'linewidth', 1)
plot(rhoappminAge, rhoapporgAge, '-', 'color', 'black', 'linewidth', 1)
plot(0,0)
xlabel('\rho^*_{HA} [g/cm^3]')
ylabel('\rho^*_{org} [g/cm^3]')
grid('on')

hlegend = legend('Bovine tibia [Lees et al. (1979)]', ...
 'Horse metacarpals [Lees (2003)]', ...
 'Femur and humeris of albino rats [Hammett (1925)]', ...
 'Bones from steers, dogs, humans, monkeys [Gong et al. (1964)]', ...
 'Mineralized turkey leg tendon [Lees and Page (1992)]', ...
 'Bones from rabbits, rats [Burns (1929)]', ...
 'Bones from various vertebrates [Biltz and Pellegrino (1969)]', ...
 'Otic bones of a fine whale [Lees et al. (1995)]', ...
 'location', 'southoutside');
set(hlegend, 'fontsize', 10);

filename = 'appDensity_MinOrg.eps';
```

```
absPathPlot = strcat(pwd, slash, 'LatexFiles', slash, filename);
print('-depsc', absPathPlot);

% PLOT RHOAPP WATER VS. RHOAPP ORG

figure
hold on
plot(rhoappwaterlees79, rhoapporglees79, 'o', 'color', 'black')
plot(rhoappwaterlees03, rhoapporglees03, 'd', 'color', 'black')
plot(rhoappwaterhammett25, rhoapporghammett25, '*', 'color', 'black')
plot([rhoappwatertrabgong64 rhoappwatercorgong64], ...
     [rhoapporgtrabgong64 rhoapporgcorgong64], '^', 'color', 'black')
plot(rhoappwaterlees92, rhoapporglees92, 's', 'color', 'black')
plot([rhoappwaterrabbitburns29 rhoappwaterratburns29], ...
     [rhoapporgrabbitburns29 rhoapporgratburns29],  'v', 'color', 'black')
plot(rhoappwaterbiltz69, rhoapporgbiltz69, 'h', 'color', 'black')
plot(rhoappwaterlees95, rhoapporglees95, 'x', 'color', 'black')

plot(rhoappwaterGrowth, rhoapporgGrowth, '-', 'color', 'black', ...
    'linewidth', 1)
plot(rhoappwaterAge, rhoapporgAge, '-', 'color', 'black', 'linewidth', 1)
plot(0,0)
xlabel('\rho^*_{H_2O} [g/cm^3]')
ylabel('\rho^*_{org} [g/cm^3]')
grid('on')

hlegend = legend('Bovine tibia [Lees et al. (1979)]', ...
 'Horse metacarpals [Lees (2003)]', ...
 'Femur and humeris of albino rats [Hammett (1925)]', ...
 'Bones from steers, dogs, humans, monkeys [Gong et al. (1964)]', ...
 'Mineralized turkey leg tendon [Lees and Page (1992)]', ...
 'Bones from rabbits, rats [Burns (1929)]', ...
 'Bones from various vertebrates [Biltz and Pellegrino (1969)]', ...
 'Otic bones of a fine whale [Lees et al. (1995)]', ...
 'location', 'southoutside');
set(hlegend, 'fontsize', 10);

filename = 'appDensity_WaterOrg.eps';
absPathPlot = strcat(pwd, slash, 'LatexFiles', slash, filename);
print('-depsc', absPathPlot);

% Plot all data as a function of rhoec

figure
hold on
plot([rhoecaxiallees79exp rhoecradlees79exp rhoectanglees79exp], ...
    rhoapporglees79, 'o', 'color', 'black')
plot(rhoeclees95exp, rhoapporglees95, 'x','color', 'black')
plot(rhoeclees92exp, rhoapporglees92, 's', 'color', 'black')
plot([rhoectrabgong64exp rhoeccorgong64exp], [rhoapporgtrabgong64 ...
    rhoapporgcorgong64], '^', 'color', 'black')
plot([rhoecrabbitburns29pre rhoecratburns29pre], ...
```

```
    [rhoapporgrabbitburns29 rhoapporgratburns29], 'v', 'color', 'black')
plot(rhoecbiltz69exp, rhoapporgbiltz69, 'h', 'color', 'black')
plot([rhoecmlees03pre rhoecflees03pre], rhoapporglees03, 'd', ...
    'color', 'black')
plot([rhoecfemmalehammett25pre rhoecfemfemhammett25pre ...
    rhoechummalehammett25pre rhoechumfemhammett25pre], ...
    rhoapporghammett25, '*', 'color', 'black')
plot([rhoecregGrowth rhoecregAge], [rhoapporgGrowth rhoapporgAge], ...
    '-', 'color', 'black', 'linewidth', 1)
plot([rhoecregGrowth rhoecregAge], [rhoappminGrowth rhoappminAge], ...
    '-.', 'color', 'black', 'linewidth', 1)
plot([rhoecregGrowth rhoecregAge], [rhoappwaterGrowth rhoappwaterAge], ...
    '--', 'color', 'black', 'linewidth', 1)

plot([rhoecaxiallees79exp rhoecradlees79exp rhoectanglees79exp], ...
    rhoappminlees79, 'o', 'color', 'black')
plot(rhoeclees95exp, rhoappminlees95, 'x','color', 'black')
plot(rhoeclees92exp, rhoappminlees92, 's', 'color', 'black')
plot([rhoectrabgong64exp rhoeccorgong64exp], [rhoappmintrabgong64 ...
    rhoappmincorgong64], '^', 'color', 'black')
plot([rhoecrabbitburns29pre rhoecratburns29pre], ...
    [rhoappminrabbitburns29 rhoappminratburns29], 'v', 'color', 'black')
plot(rhoecbiltz69exp, rhoappminbiltz69, 'h', 'color', 'black')
plot([rhoecmlees03pre rhoecflees03pre], rhoappminlees03, 'd', ...
    'color', 'black')
plot([rhoecfemmalehammett25pre rhoecfemfemhammett25pre ...
    rhoechummalehammett25pre rhoechumfemhammett25pre], ...
    rhoappminhammett25, '*', 'color', 'black')

plot([rhoecaxiallees79exp rhoecradlees79exp rhoectanglees79exp], ...
    rhoappwaterlees79, 'o', 'color', 'black')
plot(rhoeclees95exp, rhoappwaterlees95, 'x','color', 'black')
plot(rhoeclees92exp, rhoappwaterlees92, 's', 'color', 'black')
plot([rhoectrabgong64exp rhoeccorgong64exp], [rhoappwatertrabgong64 ...
    rhoappwatercorgong64], '^', 'color', 'black')
plot([rhoecrabbitburns29pre rhoecratburns29pre], ...
    [rhoappwaterrabbitburns29 rhoappwaterratburns29], 'v', 'color', 'black')
plot(rhoecbiltz69exp, rhoappwaterbiltz69, 'h', 'color', 'black')
plot([rhoecmlees03pre rhoecflees03pre], rhoappwaterlees03, 'd', ...
    'color', 'black')
plot([rhoecfemmalehammett25pre rhoecfemfemhammett25pre ...
    rhoechummalehammett25pre rhoechumfemhammett25pre], ...
    rhoappwaterhammett25, '*', 'color', 'black')

xlabel('\rho^{ec} [g/cm^3]')
ylabel('\rho^* [g/cm^3]')
grid('on')

hlegend = legend('Bovine bone [Lees et al. (1979)]', ...
 'Otic bones of a fin whale [Lees et al. (1995)]', ...
 'Mineralized turkey leg tendon [Lees and Page (1992)]', ...
 'Bones from steers, dogs, humans, monkeys [Gong et al. (1964)]', ...
```

```
 'Bones from rabbits, rats [Burns (1929)]', ...
 'Bones from various vertebrates [Biltz and Pellegrino (1969)]', ...
 'Horse metacarpals [Lees (2003)]', ...
 'Femur and humeris of albino rats (female and male) [Hammett (1925)]', ...
 'Organic', ...
 'Mineral', ...
 'Water', ...
 'location', 'southoutside');
set(hlegend, 'fontsize', 10);

filename = 'appDensity_rhoec.eps';
absPathPlot = strcat(pwd, slash, 'LatexFiles', slash, filename);
print('-depsc', absPathPlot);
```

B.3.1. funcappRho.m

This function calculates the apparent mass density.

```
% calculation of apparent density

function[rhoappwater, rhoapporg, rhoappmin] = ...
                              funcappRho(WFmuwater, WFmuorg, WFmumin, rhomu)
    rhoappwater = WFmuwater .* rhomu;
    rhoapporg = WFmuorg .*rhomu;
    rhoappmin = WFmumin .* rhomu;
end
```

B.3.2. rsquare.m

This function calculates the coefficient of determination.

```
% Function to calculate the coefficient of determination R^2

function[rr] = rsquare(y, f)

    SStot = sum((y-mean(y)).^2);
    SSerr = sum((y-f).^2);

    rr = 1-(SSerr/SStot);
```

B.3.3. funcVF.m

This function calculates the volume fractions of water, hydroxyapatite and the organic matter.

```
function[vfmin, vforg, vfwater] = ...
                              funcVF(rhoappmin, rhoapporg, rhomin, rhocoll)
    vfmin = rhoappmin./rhomin;
    vforg = rhoapporg./rhocoll;
    vfwater = 1 - (vforg + vfmin);
end
```

B.3.4. funcWF.m

This function calculates the weight fraction on the basis of the apparent mass densities.

```
% calculation of weight fractions for biltz and pellegrino 69

function[WFmuwater, WFmuorg, WFmumin] = ...
                            funcWF(rhoappwater, rhoappmin, rhoapporg, rhomu)
    WFmuwater = rhoappwater ./ rhomu;
    WFmuorg = rhoapporg ./rhomu;
    WFmumin = rhoappmin ./ rhomu;
end
```

B.4. VF.m

This file was written to calculate the extracellular volume fractions.

```
% ********************************************************
% 04. Calculation of extracellular VOLUME FRACTIONS
% ********************************************************
% RUN: ExpData.m, DensityPrediction.m, AppRho.m
% NEED FUNCTION: funcVF.m
% --------------------------------------------------------
% OUTPUT: VF.eps
% --------------------------------------------------------
% Data from Lees79: Bovine tibia
% wet volume fractions HA and collagen Fritsch, Hellmich eq (25) and (26)
% axial
[vfminlees79, vforglees79, vfwaterlees79] = funcVF(rhoappminlees79, ...
    rhoapporglees79, rhomin, rhocoll);

% --------------------------------------------------------
% Data from Lees95, otic bones of a fin whale
[vfminlees95, vforglees95, vfwaterlees95] = funcVF(rhoappminlees95, ...
    rhoapporglees95, rhomin, rhocoll);

% --------------------------------------------------------
% Data from Lees92, MTLT
[vfminlees92, vforglees92, vfwaterlees92] = funcVF(rhoappminlees92, ...
    rhoapporglees92, rhomin, rhocoll);

% --------------------------------------------------------
% Data from gong64; Steer, Dog, Human, Monkey
% trabecular bone
vfmintrabgong64 = [0.042+0.335 0.042+0.326 0.042+0.339 0.04+0.329];
vforgtrabgong64 = [0.342 0.345 0.349 0.361];
vfwatertrabgong64 = [0.281 0.288 0.27 0.271];
vfmincorgong64 = [0.046+0.366 0.046+0.368 0.046+0.377 0.047+0.382];
vforgcorgong64 = [0.336 0.363 0.338 0.337];
vfwatercorgong64 = [0.252 0.223 0.329 0.237];

% Burns29 - no density was given in paper, therefore predicted density
% for calculation
[vfminrabbitburns29, vforgrabbitburns29, vfwaterrabbitburns29] = ...
    funcVF(rhoappminrabbitburns29, rhoapporgrabbitburns29, rhomin, ...
    rhocoll);
[vfminratburns29, vforgratburns29, vfwaterratburns29] = ...
    funcVF(rhoappminratburns29, rhoapporgratburns29, rhomin, rhocoll);

% Biltz69: volume fractions in ExpData.m (given in paper)

% --------------------------------------------------------
% Lees03
[vfminlees03, vforglees03, vfwaterlees03] = funcVF(rhoappminlees03, ...
```

```
    rhoapporglees03, rhomin, rhocoll);

% ---------------------------------------------------------
% Hammett25
[vfminhammett25, vforghammett25, vfwaterhammett25] = ...
    funcVF(rhoappminhammett25, rhoapporghammett25, rhomin, rhocoll);

% Data from regression
[vfminAge, vforgAge, vfwaterAge] = ...
    funcVF(rhoappminAge, rhoapporgAge, rhomin, rhocoll);
[vfminGrowth, vforgGrowth, vfwaterGrowth] = ...
    funcVF(rhoappminGrowth, rhoapporgGrowth, rhomin, rhocoll);

% *********************************************************
% PLOT RESULTS
% *********************************************************
% calulate correlation coefficient
R = corrcoef(rhoecall);

% Calculate regression
rhoecexp = [rhoecaxiallees79exp rhoecradlees79exp rhoectanglees79exp ...
           rhoeclees95exp rhoeclees92exp rhoectrabgong64exp ...
           rhoeccorgong64exp rhoecrabbitburns29pre rhoecratburns29pre ...
           rhoecbiltz69exp rhoecmlees03pre rhoecflees03pre ...
           rhoecfemmalehammett25pre rhoecfemfemhammett25pre ...
           rhoechummalehammett25pre rhoechumfemhammett25pre];

vforg = [vforglees79 vforglees95 vforglees92...
         vforgtrabgong64 vforgcorgong64 vforgrabbitburns29 ...
         vforgratburns29 vforgbiltz69 vforglees03 vforghammett25];

vfmin = [vfminlees79 vfminlees95 vfminlees92...
         vfmintrabgong64 vfmincorgong64 vfminrabbitburns29 ...
         vfminratburns29 vfminbiltz69 vfminlees03 vfminhammett25];

vfwater = [vfwaterlees79 vfwaterlees95 vfwaterlees92...
         vfwatertrabgong64 vfwatercorgong64 vfwaterrabbitburns29 ...
         vfwaterratburns29 vfwaterbiltz69 vfwaterlees03 vfwaterhammett25];

% Correlation coefficient
rmin = corr2([rhoecregGrowth rhoecregAge], [vfminGrowth vfminAge])
rwater = corr2([rhoecregGrowth rhoecregAge], [vfwaterGrowth vfwaterAge])
rorg = corr2([rhoecregGrowth rhoecregAge], [vforgGrowth vforgAge])

% PLOT DATA

figure
hold on
plot([rhoecaxiallees79exp rhoecradlees79exp rhoectanglees79exp], ...
    vforglees79, 'o', 'color', 'black')
plot(rhoeclees95exp, vforglees95, 'x','color', 'black')
plot(rhoeclees92exp, vforglees92, 's', 'color', 'black')
```

```
plot([rhoectrabgong64exp rhoeccorgong64exp], [vforgtrabgong64 ...
    vforgcorgong64], '^', 'color', 'black')
plot([rhoecrabbitburns29pre rhoecratburns29pre], [vforgrabbitburns29 ...
    vforgratburns29], 'v', 'color', 'black')
plot(rhoecbiltz69exp, vforgbiltz69, 'h', 'color', 'black')
plot([rhoecmlees03pre rhoecflees03pre], vforglees03, 'd', 'color', 'black')
plot([rhoecfemmalehammett25pre rhoecfemfemhammett25pre ...
    rhoechummalehammett25pre rhoechumfemhammett25pre], vforghammett25, ...
    '*', 'color', 'black')

plot([rhoecregGrowth rhoecregAge], [vforgGrowth vforgAge], '-', ...
    'color', 'black', 'linewidth', 1)
plot([rhoecregGrowth rhoecregAge], [vfminGrowth vfminAge], '-.', ...
    'color', 'black', 'linewidth', 1)
plot([rhoecregGrowth rhoecregAge], [vfwaterGrowth vfwaterAge], '--', ...
    'color', 'black', 'linewidth', 1)

plot([rhoecaxiallees79exp rhoecradlees79exp rhoectanglees79exp], ...
    vfminlees79, 'o', 'color', 'black')
plot(rhoeclees95exp, vfminlees95, 'x','color', 'black')
plot(rhoeclees92exp, vfminlees92, 's', 'color', 'black')
plot([rhoectrabgong64exp rhoeccorgong64exp], [vfmintrabgong64 ...
    vfmincorgong64], '^', 'color', 'black')
plot([rhoecrabbitburns29pre rhoecratburns29pre], [vfminrabbitburns29 ...
    vfminratburns29], 'v', 'color', 'black')
plot(rhoecbiltz69exp, vfminbiltz69, 'h', 'color', 'black')
plot([rhoecmlees03pre rhoecflees03pre], vfminlees03, 'd', ...
    'color', 'black')
plot([rhoecfemmalehammett25pre rhoecfemfemhammett25pre ...
    rhoechummalehammett25pre rhoechumfemhammett25pre], vfminhammett25, ...
    '*', 'color', 'black')

plot([rhoecaxiallees79exp rhoecradlees79exp rhoectanglees79exp], ...
    vfwaterlees79, 'o', 'color', 'black')
plot(rhoeclees95exp, vfwaterlees95, 'x','color', 'black')
plot(rhoeclees92exp, vfwaterlees92, 's', 'color', 'black')
plot([rhoectrabgong64exp rhoeccorgong64exp], [vfwatertrabgong64 ...
    vfwatercorgong64], '^', 'color', 'black')
plot([rhoecrabbitburns29pre rhoecratburns29pre], [vfwaterrabbitburns29 ...
    vfwaterratburns29], 'v', 'color', 'black')
plot(rhoecbiltz69exp, vfwaterbiltz69, 'h', 'color', 'black')
plot([rhoecmlees03pre rhoecflees03pre], vfwaterlees03, 'd', ...
    'color', 'black')
plot([rhoecfemmalehammett25pre rhoecfemfemhammett25pre ...
    rhoechummalehammett25pre rhoechumfemhammett25pre], ...
    vfwaterhammett25, '*', 'color', 'black')

plot(1.2,0)
hlegend = legend('Bovine bone [Lees et al. (1979)]', ...
 'Otic bones of a fin whale [Lees et al. (1995)]', ...
 'Mineralized turkey leg tendon [Lees and Page (1992)]', ...
 'Bones from steers, dogs, humans, monkeys [Gong et al. (1964)]', ...
```

```
 'Bones from rabbits, rats [Burns (1929)]', ...
 'Bones from various vertebrates [Biltz and Pellegrino (1969)]', ...
 'Horse metacarpals [Lees (2003)]', ...
 'Femur and humeris of albino rats (female and male) [Hammett (1925)]', ...
 'Organic', ...
 'Mineral', ...
 'Water', ...
 'location', 'southoutside');
set(hlegend, 'fontsize', 10);
set(gca, 'XTick', 1.2:0.2:4, 'YTick', 0:0.1:1)
xlabel('Extracellular mass density \rho^{ec} [g/cm^3]')
ylabel('f_{HA}, f_{org}, f_{H_2O}')
grid('on')

filename = 'VF.eps';
absPathPlot = strcat(pwd, slash, 'LatexFiles', slash, filename);
print('-depsc', absPathPlot);
```

B.5. Ctensor.m

This file was written to calculate the elasticity tensor components $\mathbb{C}^{ec}_{ijkl}$ for growing and aging bone with the modified 4-step homogenization scheme by Fritsch & Hellmich (2007).

```
% *********************************************************
% 05. CALCULATION OF ELASTIC COMPONENTS
% *********************************************************
% Taken from Fritsch, Hellmich 2007
% RUN: ExpData.m, DensityPrediction.m, AppRho.m, VF.m
% NEED FUNCTION: func_5stephom.m, funccirclefcol.m, func_hom_wetcol_MT.m
% func_hom_fib_SCS.m, func_hom_ef.m, func_hom_ultra_MT.m
% fun_Psph_1111m, fun_Psph_1122m, fun_Psph_3333.m, fun_Psph_1122.m
% fun_Psph_2323.m, xcirc.m, fun_kSCS.m, fun_muSCS.m, barffib.m
% ---------------------------------------------------------
% Data from AppRho-Regression

starttime = clock;
fprintf('Start time: %d:%d\n', starttime(4), starttime(5))


[circlefcolGrowth, circlefwaterGrowth, brevefwetcolGrowth, brevefHAGrowth, ...
    checkfHAGrowth, barfefGrowth, barffibGrowth] = ...
    funccirclefcol(rhoecregGrowth, vforgregGrowth, vfminregGrowth);

[C1111regGrowth, C3333regGrowth, C2323regGrowth, C1122regGrowth, ...
    C1133regGrowth, E1regGrowth, E3regGrowth, nu12regGrowth, nu13regGrowth, ...
    G12regGrowth, cefGrowth, E3cefGrowth] = func_5stephom(circlefcolGrowth, ...
    circlefwaterGrowth, brevefwetcolGrowth, ...
    brevefHAGrowth, checkfHAGrowth, barfefGrowth, barffibGrowth);

save workspace_DA.mat

halftime = clock;
fprintf('Half time: %d:%d\n', halftime(4), halftime(5))

[circlefcolAge, circlefwaterAge, brevefwetcolAge, brevefHAAge, ...
    checkfHAAge, barfefAge, barffibAge] = ...
    funccirclefcol(rhoecregAge, vforgregAge, vfminregAge);

[C1111regAge, C3333regAge, C2323regAge, C1122regAge, C1133regAge, ...
 E1regAge, E3regAge, nu12regAge, nu13regAge, G12regAge, cefAge, E3cefAge] = ...
    func_5stephom(circlefcolAge, circlefwaterAge, brevefwetcolAge, ...
    brevefHAAge, checkfHAAge, barfefAge, barffibAge);

save workspace_DA.mat

endtime = clock;
fprintf('End time: %d:%d\n', endtime(4), endtime(5))
```

B.5.1. funccirclefcol.m

This function calculates all the volume fraction needed for calculation of the elasticity tensor $\mathbb{C}^{ec}$.

```
function[circlefcol, circlefwater, brevefwetcol, brevefHA, checkfHA, ...
                    barfef, barffib]=funccirclefcol(rhoecexp, vforg, vfmin)
    ds = 1.57*rhoecexp.^-(1/3); % nm
    % ds = -0.2*rhoecexp+1.6580
    % volume of one rhomboidal fibrillar unit
    nufib = 1.47*ds*5*64;
    % volume of a single collagen molecule
    nucol = 335.6;
    % ultrastructural volume fraction of the fibril
    barffib = vforg .* (nufib/nucol);
    % ultrastructural volume fraction of the extrafibrillar space
    barfef = 1-barffib;
    % volume fraction of HA in the extrafibrillar space Eq 39
    phiHAef = (1-barffib)./(1-vforg);
    % mineral volume fraction in the fibrillar space
    brevefHA = vfmin.*(1-phiHAef)./barffib;
    % mineral volume fraction in the extrafibrillar space
    checkfHA = (phiHAef.*vfmin)./barfef;
    % volume fraction of wet collagen Eq. 40
    brevefwetcol = 1-brevefHA;
    circlefcol = vforg./brevefwetcol;
    circlefwater = 1-circlefcol;
end
```

B.5.2. func_5stephom.m

This function is the actual function, which carries out the homogenization and calls all the homogenization functions required step-by-step.

```
function[C1111, C3333, C2323, C1122, C1133, E1, E3, nu12, nu13, ...
             G12, cef, E3cef] = func_5stephom(circlefcol, circlefwater, ...
             brevefwetcol, brevefHA, checkfHA, barfef, barffib)

% Start timer
tic

% CONSTANTS

% HA
% unity tensor
I=[1 0 0 0 0 0; ...
```

```
    0 1 0 0 0 0; ...
    0 0 1 0 0 0; ...
    0 0 0 1 0 0; ...
    0 0 0 0 1 0; ...
    0 0 0 0 0 1];
% volumetric part of unity tensor
K=[1/3 1/3 1/3 0 0 0; ...
    1/3 1/3 1/3 0 0 0; ...
    1/3 1/3 1/3 0 0 0; ...
    0 0 0 0 0 0; ...
    0 0 0 0 0 0; ...
    0 0 0 0 0 0];

% deviatoric part of unity tensor
J=I-K;

% Stiffness tensor of collagen
ccol(1,1)=11.7;
ccol(2,2)=ccol(1,1);
ccol(3,3)=17.9;
ccol(1,2)=5.1;
ccol(2,1)=ccol(1,2);
ccol(1,3)=7.1;
ccol(3,1)=ccol(1,3);
ccol(3,2)=ccol(3,1);
ccol(2,3)=ccol(3,2);
ccol(4,4)=2*3.3;
ccol(5,5)=ccol(4,4);
ccol(6,6)=2*0.5*(ccol(1,1)-ccol(1,2));

% Bulk and shear modulus
kHA=82.6;
muHA=44.9;
cHA=2*muHA*J+3*kHA*K;

% water
kwater=2.3;
muwater=0.001;
cwater=3*kwater*K;
%cwater=2*muwater*J;

% ---------------------------------------------------------
% 5-step homogenization procedure

for i = 1:length(circlefcol)
    if checkfHA(i)~=0 || brevefHA(i)~=0
        % 1. wet collagen
        [cwetcol, kwetcol, muwetcol] = func_hom_wetcol_MT...
                        (I, J, ccol, cwater, circlefcol(i), circlefwater(i));

        % 2. Mineralized collagen fibril
        cfib = func_hom_fib_SCS ...
```

```
65              (I, J, K, cHA, cwetcol, muwetcol, kwetcol, brevefwetcol(i), ...
66              brevefHA(i));
67
68          % 3. Extrafibrillar space: hydroxyapatite foam
69          [cef, khom, muhom] = func_hom_ef_cyl...
70                               (I, J, K, kHA, cwater, muHA, cHA, checkfHA(i));
71
72
73          % 4. Extracellular bone matrix (ultrastructure)
74          Cultra = func_hom_ultra_MT...
75                           (I, khom, muhom, cef, cfib, barfef(i), barffib(i));
76
77      % Elastic constants:
78      D=inv(Cultra);
79      E1(i)=1/D(1,1);
80      E3(i)=1/D(3,3);
81      nu12(i)=-D(1,2)*E1(i);
82      nu13(i)=-D(1,3)*E3(i);
83      G12(i)=E1(i)/(2*(1+nu12(i)));
84
85      C1111(i)=Cultra(1,1);
86      C1133(i)=Cultra(1,3);
87      C3333(i)=Cultra(3,3);
88      C1122(i)=Cultra(1,2);
89      C2323(i)=0.5*Cultra(4,4);
90
91      Dcef = inv(cef);
92      E3cef(i)=1/Dcef(3,3);
93
94      end
95
96      fprintf('%d Durchlauf von func_5stephom.m\n', i)
97
98  end
99
100 ti=toc;
101 fprintf('Elapsed time: %3.1f min\n', ti/60)
102 end
```

B.5.2.1. func_hom_wetcol_MT.m

This function was originally written and used for the publications (Hellmich *et al.* , 2004) and (Hellmich, 2005). It was modified for the publication (Fritsch & Hellmich, 2007) and was further modified for this master thesis.

```
1  % Homogenization of wet collagen
2  % Mori-Tanaka-scheme, collagen matrix with cylindrical water inclusions
```

```
function[Chom, kwetcol, muwetcol] = ...
           func_hom_wetcol_MT(I, J, ccol, cwater, circlefcol, circlefwater)
C0=ccol;

% evaluate P-tensor for cylindrical inclusions
% in transversely isotropic matrix
%-----------------------------------------
P1111=1/8*(5*C0(1,1)-3*C0(1,2))/C0(1,1)/(C0(1,1)-C0(1,2));
P1122=-1/8*(C0(1,1)+C0(1,2))/C0(1,1)/(C0(1,1)-C0(1,2));
P2222=1/8*(5*C0(1,1)-3*C0(1,2))/C0(1,1)/(C0(1,1)-C0(1,2));
P2323=1/8*1/(0.5*C0(4,4));    % 0.5*C0(4,4)=C0_2323
P1313=1/8*1/(0.5*C0(4,4));    % 0.5*CO(4,4)=C0_2323
P1212=1/8*(3*C0(1,1)-C0(1,2))/C0(1,1)/(C0(1,1)-C0(1,2));
Pcyl=zeros(6,6);
Pcyl(1,1)=P1111;
Pcyl(2,2)=P2222;
Pcyl(1,2)=P1122;
Pcyl(2,1)=Pcyl(1,2);
Pcyl(4,4)=2*P2323;
Pcyl(5,5)=2*P1313;
Pcyl(6,6)=2*P1212;
% evaluate [I+P:(c-C0)]^-1 for water
%-------------------------------
helpwater=(I+Pcyl*(cwater-ccol))^-1; %cylindrical inclusions!!!
% evaluate homogenized stiffness
%-------------------------------
Chom=(circlefcol*ccol+circlefwater*cwater*helpwater)...
                                  *(circlefcol*I+circlefwater*helpwater)^-1;

muwetcol=Chom(5,5)/2;
kwetcol=Chom(1,1)-J(1,1)*2*muwetcol;
end
```

B.5.2.2. func_hom_fib_SCS.m

This function was originally written and used for the publications (Hellmich *et al.* , 2004) and (Hellmich, 2005). It was modified for the publication of (Fritsch & Hellmich, 2007) and was further modified for this master thesis.

```
% Homogenization of fibrils
% self-consistent-scheme, wetcol=cylindrical, transversely isotropic
% inclusions
% HA=isotropic, cylindrical inclusions
function[C0] = func_hom_fib_SCS(I, J, K, cHA, cwetcol, muwetcol, ...
                                          kwetcol, brevefwetcol, brevefHA)
i=0;
% start with cwetcol as the C0-matrix
```

```
%-------------------------------------
C0=cwetcol;
C0_old=0;

khom_temp = kwetcol;
muhom_temp = muwetcol;

% iteration for calculation of self-consistent stiffness
%-------------------------------------------------------
while abs((norm(C0)-norm(C0_old))/norm(C0))>0.000001
 i=i+1;

 P1111=quad('fun_Psph_1111',-1,1,[],[],C0(1,1),C0(1,2),C0(1,3), ...
                                                    C0(3,3),C0(4,4)/2);
 P1122=quad('fun_Psph_1122',-1,1,[],[],C0(1,1),C0(1,2),C0(1,3), ...
                                                    C0(3,3),C0(4,4)/2);
 P1133=quad('fun_Psph_1133',-1,1,[],[],C0(1,1),C0(1,2),C0(1,3), ...
                                                    C0(3,3),C0(4,4)/2);
 P3333=quad('fun_Psph_3333',-1,1,[],[],C0(1,1),C0(1,2),C0(1,3), ...
                                                    C0(3,3),C0(4,4)/2);
 P2323=quad('fun_Psph_2323',-1,1,[],[],C0(1,1),C0(1,2),C0(1,3), ...
                                                    C0(3,3),C0(4,4)/2);
 Psph=zeros(6,6);
 Psph(1,1)=P1111;
 Psph(2,2)=Psph(1,1);
 Psph(3,3)=P3333;
 Psph(1,2)=P1122;
 Psph(1,3)=P1133;
 Psph(2,3)=Psph(1,3);
 Psph(2,1)=Psph(1,2);
 Psph(3,1)=Psph(1,3);
 Psph(3,2)=Psph(2,3);
 Psph(4,4)=2*P2323;
 Psph(5,5)=Psph(4,4);
 Psph(6,6)=2*0.5*(P1111-P1122);

 % evaluate P-tensor for cylindrical inclusions
 % in transversely isotropic matrix
 %-----------------------------------------
 P1111=1/8*(5*C0(1,1)-3*C0(1,2))/C0(1,1)/(C0(1,1)-C0(1,2));
 P1122=-1/8*(C0(1,1)+C0(1,2))/C0(1,1)/(C0(1,1)-C0(1,2));
 P2222=1/8*(5*C0(1,1)-3*C0(1,2))/C0(1,1)/(C0(1,1)-C0(1,2));
 P2323=1/8*1/(0.5*C0(4,4));     % 0.5*C0(4,4)=C0_2323
 P1313=1/8*1/(0.5*C0(4,4));     % 0.5*CO(4,4)=C0_2323
 P1212=1/8*(3*C0(1,1)-C0(1,2))/C0(1,1)/(C0(1,1)-C0(1,2));
 Pcyl=zeros(6,6);
 Pcyl(1,1)=P1111;
 Pcyl(2,2)=P2222;
 Pcyl(1,2)=P1122;
 Pcyl(2,1)=Pcyl(1,2);
 Pcyl(4,4)=2*P2323;
 Pcyl(5,5)=2*P1313;
```

```
 Pcyl(6,6)=2*P1212;

 % evaluate [I+P:(c-C0)]^-1 for wetcol
 %---------------------------
 helpwetcol=(I+Pcyl*(cwetcol-C0))^-1;

 % evaluate [I+P:(c-C0)]^-1 for HA
 %---------------------------
 helpHA=(I+Psph*(cHA-C0))^-1;

 % Homogenization
 Chom=(brevefwetcol*cwetcol*helpwetcol+brevefHA*cHA*helpHA)*...
                              (brevefwetcol*helpwetcol+brevefHA*helpHA)^-1;

 muhom_temp=Chom(5,5)/2;
 khom_temp = Chom(1,1)-J(1,1)*2*muhom_temp;

 C0_old=C0;
 C0=Chom;
end
end
```

B.5.2.2.1. fun_Psph_1111.m

This function was originally written and used for the publication (Hellmich *et al.* , 2004).

```
% P1111 for spherical inclusions
% in transversely isotropic matrix
%----------------------------------
function y=fun_Psph1111(x,C1111,C1122,C1133,C3333,C2323);
y=-1/16.*(-5.*C1111.*x.^4.*C3333-3.*C1122.*x.^2.*C3333-3.*C1122.*x.^4.*C2323+...
  3.*C1122.*x.^4.*C3333+5.*C1111.*x.^4.*C2323-10.*C1111.*C2323.*x.^2+...
  2.*x.^4.*C1133.^2+8.*C2323.*x.^4.*C3333-6.*C2323.^2.*x.^4+...
  4.*C2323.*x.^4.*C1133+6.*C1122.*C2323.*x.^2+5.*C1111.*C2323+...
  5.*C1111.*x.^2.*C3333-4.*C2323.*x.^2.*C1133+6.*C2323.^2.*x.^2-...
  2.*x.^2.*C1133.^2-3.*C1122.*C2323).*(-1+x.^2)./(-2*C1111.^2*x.^4*C3333+...
  2*C2323.^2*x.^6*C3333-4*C1111*C2323.^2*x.^4-3*C1111.^2*C2323*x.^2+...
  C1111.^2*x.^2*C3333+2*C1111*C2323.^2*x.^2-2*C2323*x.^4*C1133.^2-...
  C1111*C1133.^2*x.^6+2*C1111*C1133.^2*x.^4+4*C2323.^2*x.^6*C1133-...
  2*C1122*C1133.^2*x.^4+2*C2323*x.^6*C1133.^2+3*C1111.^2*x.^4*C2323+...
  C1122*C1133.^2*x.^6-C1111.^2*x.^6*C2323+2*C1111*x.^6*C2323.^2+...
  C1111.^2*x.^6*C3333-C1111*C1133.^2*x.^2-4*C2323.^2*x.^4*C1133+...
  C1122*C1133.^2*x.^2+C1111.^2*C2323-C1122*C1111*C2323-C1122*x.^6*C1111*C3333+...
  4*C1111*x.^4*C2323*C1133-2*C1111*x.^2*C2323*C1133-4*C1122*x.^4*C2323*C1133+...
  2*C1122*x.^2*C2323*C1133+2*C1122*x.^6*C2323*C1133-2*C1111*x.^6*C2323*C1133-...
  3*C1111*x.^6*C2323*C3333+2*C1122*C1111*x.^4*C3333-C1122*C2323*x.^4*C3333-...
  3*C1122*C1111*x.^4*C2323-C1122*C1111*x.^2*C3333+3*C1122*C1111*C2323*x.^2+...
  3*C1111*C2323*x.^4*C3333+C1122*x.^6*C1111*C2323+C1122*x.^6*C2323*C3333);
```

B.5.2.2.2. fun_Psph_3333.m

This function was originally written and used for the publication (Hellmich *et al.* , 2004).

```
% P3333 for spherical inclusions
% in transversely isotropic matrix
%---------------------------------
function y=fun_Psph3333(x,C1111,C1122,C1133,C3333,C2323);
y=1./2.*x.^2.*(x.^2.*C2323-C1111.*x.^2+C1111)./...
  (2.*C2323.*x.^4.*C1133+C2323.*x.^4.*C3333+C1111.*x.^4.*C2323-...
  2.*C2323.*x.^2.*C1133-2.*C1111.*C2323.*x.^2+C1111.*C2323+...
  x.^4.*C1133.^2-C1111.*x.^4.*C3333-x.^2.*C1133.^2+C1111.*x.^2.*C3333);
```

B.5.2.2.3. fun_Psph_1122.m

This function was originally written and used for the publication (Hellmich *et al.* , 2004).

```
% P1122 for spherical inclusions
% in transversely isotropic matrix
%---------------------------------
function y=fun_Psph1122(x,C1111,C1122,C1133,C3333,C2323);
y=1./16.*(C1111.*C2323-2.*C1111.*C2323.*x.^2+C1111.*x.^2.*C3333+...
 C1122.*C2323-2.*C1122.*C2323.*x.^2+C1122.*x.^2.*C3333+C1111.*x.^4.*C2323-...
 C1111.*x.^4.*C3333+C1122.*x.^4.*C2323-C1122.*x.^4.*C3333-...
 2.*C2323.^2.*x.^2+2.*C2323.^2.*x.^4-4.*C2323.*x.^2.*C1133+...
 4.*C2323.*x.^4.*C1133-2.*x.^2.*C1133.^2+2.*x.^4.*C1133.^2).*(-1+x.^2)./...
 (-2.*C1111.^2.*x.^4.*C3333+2.*C2323.^2.*x.^6.*C3333-...
 4.*C1111.*C2323.^2.*x.^4-3.*C1111.^2.*C2323.*x.^2+C1111.^2.*x.^2.*C3333+...
 2.*C1111.*C2323.^2.*x.^2-2.*C2323.*x.^4.*C1133.^2-C1111.*C1133.^2.*x.^6+...
 2.*C1111.*C1133.^2.*x.^4+4.*C2323.^2.*x.^6.*C1133-2.*C1122.*C1133.^2.*x.^4+...
 2.*C2323.*x.^6.*C1133.^2+3.*C1111.^2.*x.^4.*C2323+C1122.*C1133.^2.*x.^6-...
 C1111.^2.*x.^6.*C2323+2.*C1111.*x.^6.*C2323.^2+C1111.^2.*x.^6.*C3333-...
 C1111.*C1133.^2.*x.^2-4.*C2323.^2.*x.^4.*C1133+C1122.*C1133.^2.*x.^2+...
 C1111.^2.*C2323-C1122.*C1111.*C2323-C1122.*x.^6.*C1111.*C3333+...
 4.*C1111.*x.^4.*C2323.*C1133-2.*C1111.*x.^2.*C2323.*C1133-...
 4.*C1122.*x.^4.*C2323.*C1133+2.*C1122.*x.^2.*C2323.*C1133+...
 2.*C1122.*x.^6.*C2323.*C1133-2.*C1111.*x.^6.*C2323.*C1133-...
 3.*C1111.*x.^6.*C2323.*C3333+2.*C1122.*C1111.*x.^4.*C3333-...
 C1122.*C2323.*x.^4.*C3333-3.*C1122.*C1111.*x.^4.*C2323-...
 C1122.*C1111.*x.^2.*C3333+3.*C1122.*C1111.*C2323.*x.^2+...
 3.*C1111.*C2323.*x.^4.*C3333+C1122.*x.^6.*C1111.*C2323+...
 C1122.*x.^6.*C2323.*C3333);
```

B.5.2.2.4. fun_Psph_1133.m

This function was originally written and used for the publication (Hellmich *et al.* , 2004).

```
% P1133 for spherical inclusions
% in transversely isotropic matrix
%---------------------------------
function y=fun_Psph1133(x,C1111,C1122,C1133,C3333,C2323);
y=1./4.*(-1+x.^2).*x.^2.*(C2323+C1133)./...
  (2.*C2323.*x.^4.*C1133+C2323.*x.^4.*C3333+C1111.*x.^4.*C2323-...
  2.*C2323.*x.^2.*C1133-2.*C1111.*C2323.*x.^2+C1111.*C2323+...
  x.^4.*C1133.^2-C1111.*x.^4.*C3333-x.^2.*C1133.^2+C1111.*x.^2.*C3333);
```

B.5.2.2.5. fun_Psph_2323.m

This function was originally written and used for the publication (Hellmich *et al.* , 2004).

```
% P2323 for spherical inclusions
% in transversely isotropic matrix
%---------------------------------
function y=fun_Psph2323(x,C1111,C1122,C1133,C3333,C2323);
y=1./16.*(4.*C1111.*C2323.*x.^2-8.*C2323.*x.^4.*C1133-...
  2.*x.^4.*C1133.^2-C1122.*x.^4.*C3333-8.*C1111.*x.^4.*C2323+...
  3.*C1111.*x.^4.*C3333+4.*C1111.*x.^4.*C1133-4.*C1122.*x.^4.*C1133+...
  2.*C1122.*x.^6.*C1133-2.*C1111.*x.^6.*C1133+C1122.*x.^6.*C1111-...
  3.*C1122.*x.^4.*C1111+3.*C1122.*C1111.*x.^2-2.*C1111.*x.^2.*C1133+...
  2.*C1122.*x.^2.*C1133+8.*x.^6.*C2323.*C1133-3.*x.^6.*C1111.*C3333+...
  4.*x.^6.*C2323.*C3333+4.*C1111.*x.^6.*C2323+C1122.*x.^6.*C3333+...
  3.*C1111.^2.*x.^4-C1111.^2.*x.^6+2.*C1133.^2.*x.^6-...
  3.*C1111.^2.*x.^2+C1111.^2-C1122.*C1111)./...
  (-2.*C1111.^2.*x.^4.*C3333+2.*C2323.^2.*x.^6.*C3333-...
  4.*C1111.*C2323.^2.*x.^4-3.*C1111.^2.*C2323.*x.^2+...
  C1111.^2.*x.^2.*C3333+2.*C1111.*C2323.^2.*x.^2-...
  2.*C2323.*x.^4.*C1133.^2-C1111.*C1133.^2.*x.^6+...
  2.*C1111.*C1133.^2.*x.^4+4.*C2323.^2.*x.^6.*C1133-...
  2.*C1122.*C1133.^2.*x.^4+2.*C2323.*x.^6.*C1133.^2+...
  3.*C1111.^2.*x.^4.*C2323+C1122.*C1133.^2.*x.^6-...
  C1111.^2.*x.^6.*C2323+2.*C1111.*x.^6.*C2323.^2+...
  C1111.^2.*x.^6.*C3333-C1111.*C1133.^2.*x.^2-...
  4.*C2323.^2.*x.^4.*C1133+C1122.*C1133.^2.*x.^2+...
  C1111.^2.*C2323-C1122.*C1111.*C2323-C1122.*x.^6.*C1111.*C3333+...
  4.*C1111.*x.^4.*C2323.*C1133-2.*C1111.*x.^2.*C2323.*C1133-...
  4.*C1122.*x.^4.*C2323.*C1133+2.*C1122.*x.^2.*C2323.*C1133+...
  2.*C1122.*x.^6.*C2323.*C1133-2.*C1111.*x.^6.*C2323.*C1133-...
  3.*C1111.*x.^6.*C2323.*C3333+2.*C1122.*C1111.*x.^4.*C3333-...
  C1122.*C2323.*x.^4.*C3333-3.*C1122.*C1111.*x.^4.*C2323-...
  C1122.*C1111.*x.^2.*C3333+3.*C1122.*C1111.*C2323.*x.^2+...
  3.*C1111.*C2323.*x.^4.*C3333+C1122.*x.^6.*C1111.*C2323+...
  C1122.*x.^6.*C2323.*C3333);
```

B.5.2.3. func_hom_ef_cyl.m

This function was originally written and used for the publications (Hellmich *et al.* , 2004) and (Hellmich, 2005). It was modified for the publication (Fritsch & Hellmich, 2007) and was further modified for this master thesis.

```
%-------------------------------------------------------------------------
% This function needs the following functions:
% fun_Psph_1111, fun_Psph_1122, fun_Psph_1133, fun_Psph_3333,
% fun_Psph_2323, rot2retour, compress, expand
% evaluate P-tensor for cylindrical inclusions
% in transversely isotropic matrix
%----------------------------------------
function[Cef, muhom, khom] = ...
                func_hom_ef_cyl(I, J, K, kHA, cwater, muHA, cHA, checkfHA)
% start with cHA as the C0-matrix
%-------------------------------------
C0=cHA;
C0_old=0;

helpHA = zeros(6,6);
% helpIPcHA_global=zeros(6,6);
%
% dtheta=pi/40;
% number_incr_theta=pi/2/dtheta;
% number_incr_phi=40;
%
% incr_theta=dtheta;
% incr_phi=2*pi/number_incr_phi;

khom_temp = kHA;
muhom_temp = muHA;

r = 1/2;
t = (sqrt(5)-1)/4;
s = (sqrt(5)+1)/4;

% see paper Pichler_Scheiner_Hellmich_2008_ActaGeotechnica, p278
coor1=[+r +r -r -r ...
       +t +t -t -t ...
       +s +s -s -s ...
       1 0 0];
coor2=[+s -s +s -s ...
       +r -r +r -r ...
       +t -t +t -t ...
       0 1 0];
coor3=[+t +t +t +t ...
       +s +s +s +s ...
       +r +r +r +r ...
       0 0 1];

```

```
% % iteration for calculation of self-consistent stiffness
% %-------------------------------------------------------
while abs((norm(C0)-norm(C0_old))/norm(C0))>0.001

 % construct Eshelby's tensor for cylindrical, compressible inclusions in
 % compressible matrix in local base
 % calculate Poisson's ratio of polycrystalline matrix
 %---------------------------
 nup=(3*khom_temp-2*muhom_temp)/(6*khom_temp+2*muhom_temp);
 % construct Eshelby's tensor for cylindrical, compressible
 % inclusions in compressible matrix
 %---------------------------
 Qesh=3/(8*pi*(1-nup));
 Resh=(1-2*nup)/(8*pi*(1-nup));
 a=1;
 Ia=2*pi;
 Iab=4*pi/(3*(2*a)^2);
 Iaa=4*pi/(3*a^2)-Iab;
 Sesh11=Qesh*a^2*Iaa+Resh*Ia;
 Sesh22=Sesh11;
 Sesh33=0;
 Sesh12=Qesh*a^2*Iab-Resh*Ia;
 Sesh21=Sesh12;
 Sesh13=Qesh/3*Ia-Resh*Ia;
 Sesh23=Sesh13;
 Sesh31=0;
 Sesh32=Sesh31;
 Sesh44=1/4;
 Sesh55=Sesh44;
 Sesh66=Qesh/2*(2*a^2)*Iab+Resh*Ia;
 Sesh=[Sesh11 Sesh12 Sesh13 0 0 0; ...
       Sesh21 Sesh22 Sesh23 0 0 0; ...
       Sesh31 Sesh32 Sesh33 0 0 0; ...
       0 0 0 2*Sesh44 0 0;...
       0 0 0 0 2*Sesh55 0; ...
       0 0 0 0 0 2*Sesh66];

 Pcyl_local=Sesh*(C0)^-1;

 for i = 1:length(coor1)
    Pcyl_global = ...
        compress(rot2retour(coor1(i),coor2(i),coor3(i),expand(Pcyl_local)));
    %see Fritsch_Dormieux_Hellmich_Sanahuja_2008_JoBMR.pdf p 153
    helpHA=helpHA+((I+Pcyl_global*(cHA-C0))^-1);
 end

 % evaluate P-tensor for spherical inclusions
 % in isotropic matrix
 %-----------------------------------------

 alpha = (3*khom_temp)/(3*khom_temp+4*muhom_temp);
 beta = (6*(khom_temp+2*muhom_temp))/(5*(3*khom_temp+4*muhom_temp));
```

```
98
99  Sesh_sph = alpha*K+beta*J;
100
101 Psph=Sesh_sph*(C0)^-1;
102
103 % evaluate [I+P:(c-C0)]^-1 for HA
104 %---------------------------
105 % see above in loop
106 helpHA=helpHA/length(coor1);
107
108 % evaluate [I+P:(c-C0)]^-1 for ic
109 %---------------------------
110 helpic=(I-Psph*C0)^-1;
111
112 % volume fraction of intercrystalline space
113 checkfic = 1-checkfHA;
114
115 % Homogenization
116 Cef=(checkfHA*cHA*helpHA+checkfic*cwater*(I+Psph*(cwater-C0))^-1) ...
117                                     *(checkfHA*helpHA+checkfic*helpic)^-1;
118
119 muhom_temp=Cef(6,6)/2;
120 khom_temp=Cef(1,1)-J(1,1)*2*muhom_temp;
121
122 C0_old=C0;
123 C0=Cef;
124
125 end
126 muhom=muhom_temp;
127 khom=khom_temp;
128 end
```

B.5.2.3.1. compress.m

This function was originally developed for the publication (Hofstetter *et al.* , 2006), and was also used for the publication (Fritsch *et al.* , 2009).

```
1  % function for determination of compressed matrix representation
2  % of fourth-order tensor
3  %
4  %-------------------------------------------------------------------------
5  % INPUT:
6  % I ... forth-order tensor
7  %
8  % OUTPUT:
9  % Ic ... tensor in compressed matrix representation
10 %-------------------------------------------------------------------------
11
```

```
function [Ic] = compress(I)
%
W = sqrt(2) ;
%
Ic = [ 1*I(1,1,1,1) 1*I(1,1,2,2) 1*I(1,1,3,3) ...
       W*I(1,1,2,3) W*I(1,1,1,3) W*I(1,1,1,2) ; ...
       1*I(2,2,1,1) 1*I(2,2,2,2) 1*I(2,2,3,3) ...
       W*I(2,2,2,3) W*I(2,2,1,3) W*I(2,2,1,2) ; ...
       1*I(3,3,1,1) 1*I(3,3,2,2) 1*I(3,3,3,3) ...
       W*I(3,3,2,3) W*I(3,3,1,3) W*I(3,3,1,2) ; ...
       W*I(2,3,1,1) W*I(2,3,2,2) W*I(2,3,3,3) ...
       2*I(2,3,2,3) 2*I(2,3,1,3) 2*I(2,3,1,2) ; ...
       W*I(1,3,1,1) W*I(1,3,2,2) W*I(1,3,3,3) ...
       2*I(1,3,2,3) 2*I(1,3,1,3) 2*I(1,3,1,2) ; ...
       W*I(1,2,1,1) W*I(1,2,2,2) W*I(1,2,3,3) ...
       2*I(1,2,2,3) 2*I(1,2,1,3) 2*I(1,2,1,2) ] ;
%
```

B.5.2.3.2. expand.m

This function was originally developed for the publication (Hofstetter *et al.* , 2006), and was also used for the publication (Fritsch *et al.* , 2009).

```
% function for determination of components of fourth-order
% tensor from compressed matrix representation
%
%--------------------------------------------------------------------------
% INPUT:
% I ... tensor in compressed matrix representation
%
% OUTPUT:
% Ie ... fourth-order tensor
%--------------------------------------------------------------------------

function [Ie] = expand(I)
%
W=sqrt(2);
%
Ie(1,1,1,1)=I(1,1);
Ie(1,1,2,2)=I(1,2);
Ie(1,1,3,3)=I(1,3);
Ie(1,1,2,3)=I(1,4)/W;
Ie(1,1,3,2)=I(1,4)/W;
Ie(1,1,1,3)=I(1,5)/W;
Ie(1,1,3,1)=I(1,5)/W;
Ie(1,1,1,2)=I(1,6)/W;
Ie(1,1,2,1)=I(1,6)/W;
Ie(2,2,1,1)=I(2,1);
```

```
Ie(2,2,2,2)=I(2,2);
Ie(2,2,3,3)=I(2,3);
Ie(2,2,2,3)=I(2,4)/W;
Ie(2,2,3,2)=I(2,4)/W;
Ie(2,2,1,3)=I(2,5)/W;
Ie(2,2,3,1)=I(2,5)/W;
Ie(2,2,1,2)=I(2,6)/W;
Ie(2,2,2,1)=I(2,6)/W;
Ie(3,3,1,1)=I(3,1);
Ie(3,3,2,2)=I(3,2);
Ie(3,3,3,3)=I(3,3);
Ie(3,3,2,3)=I(3,4)/W;
Ie(3,3,3,2)=I(3,4)/W;
Ie(3,3,1,3)=I(3,5)/W;
Ie(3,3,3,1)=I(3,5)/W;
Ie(3,3,1,2)=I(3,6)/W;
Ie(3,3,2,1)=I(3,6)/W;
Ie(2,3,1,1)=I(4,1)/W;
Ie(3,2,1,1)=I(4,1)/W;
Ie(2,3,2,2)=I(4,2)/W;
Ie(3,2,2,2)=I(4,2)/W;
Ie(2,3,3,3)=I(4,3)/W;
Ie(3,2,3,3)=I(4,3)/W;
Ie(2,3,2,3)=I(4,4)/2;
Ie(2,3,3,2)=I(4,4)/2;
Ie(3,2,3,2)=I(4,4)/2;
Ie(3,2,2,3)=I(4,4)/2;
Ie(2,3,1,3)=I(4,5)/2;
Ie(2,3,3,1)=I(4,5)/2;
Ie(3,2,3,1)=I(4,5)/2;
Ie(3,2,1,3)=I(4,5)/2;
Ie(2,3,1,2)=I(4,6)/2;
Ie(2,3,2,1)=I(4,6)/2;
Ie(3,2,2,1)=I(4,6)/2;
Ie(3,2,1,2)=I(4,6)/2;
Ie(1,3,1,1)=I(5,1)/W;
Ie(3,1,1,1)=I(5,1)/W;
Ie(1,3,2,2)=I(5,2)/W;
Ie(3,1,2,2)=I(5,2)/W;
Ie(1,3,3,3)=I(5,3)/W;
Ie(3,1,3,3)=I(5,3)/W;
Ie(1,3,2,3)=I(5,4)/2;
Ie(1,3,3,2)=I(5,4)/2;
Ie(3,1,3,2)=I(5,4)/2;
Ie(3,1,2,3)=I(5,4)/2;
Ie(1,3,1,3)=I(5,5)/2;
Ie(1,3,3,1)=I(5,5)/2;
Ie(3,1,3,1)=I(5,5)/2;
Ie(3,1,1,3)=I(5,5)/2;
Ie(1,3,1,2)=I(5,6)/2;
Ie(1,3,2,1)=I(5,6)/2;
Ie(3,1,2,1)=I(5,6)/2;
```

```
Ie(3,1,1,2)=I(5,6)/2;
Ie(1,2,1,1)=I(6,1)/W;
Ie(2,1,1,1)=I(6,1)/W;
Ie(1,2,2,2)=I(6,2)/W;
Ie(2,1,2,2)=I(6,2)/W;
Ie(1,2,3,3)=I(6,3)/W;
Ie(2,1,3,3)=I(6,3)/W;
Ie(1,2,2,3)=I(6,4)/2;
Ie(1,2,3,2)=I(6,4)/2;
Ie(2,1,3,2)=I(6,4)/2;
Ie(2,1,2,3)=I(6,4)/2;
Ie(1,2,1,3)=I(6,5)/2;
Ie(1,2,3,1)=I(6,5)/2;
Ie(2,1,3,1)=I(6,5)/2;
Ie(2,1,1,3)=I(6,5)/2;
Ie(1,2,1,2)=I(6,6)/2;
Ie(1,2,2,1)=I(6,6)/2;
Ie(2,1,2,1)=I(6,6)/2;
Ie(2,1,1,2)=I(6,6)/2;
```

B.5.2.3.3. rot2retour.m

This function was originally developed for the publication (Hofstetter *et al.* , 2006), and was also used for the publication (Fritsch *et al.* , 2009).

```
function [Inew] = rot2retour(coor1,coor2,coor3,I)
%
% geï¿½ndert von AF (phi und theta getauscht)!!!!
%
theta = acos(coor3);
%
if coor1<0
   theta = -theta ;
end
%theta
%
if coor1 == 1
   phi = 0 ;
elseif coor2 == 1
   phi = pi/2 ;
elseif coor3 == 1
   theta = 0 ;
   phi = 0 ;
else
   phi = asin(coor2/sin(theta));
end
%phi
%
```

```
% new base-vectors
%
e1 = [cos(phi)*cos(theta) ; sin(phi)*cos(theta) ; -sin(theta)];
e2 = [-sin(phi)           ; cos(phi)            ;  0         ];
e3 = [cos(phi)*sin(theta) ; sin(phi)*sin(theta) ;  cos(theta)];

%
% check calculations performed so far
%
if abs(e3(1,1)-coor1)>1.0e-7
   abs(e3(1,1)-coor1)
   error('error #1 in file rot2.m')
elseif abs(e3(2,1)-coor2)>1.0e-7
   error('error #2 in file rot2.m')
elseif abs(e3(3,1)-coor3)>1.0e-7
   error('error #3 in file rot2.m')
elseif dot(e1,e2)>1.0e-7
   error('error #4 in file rot2.m')
elseif dot(e2,e3)>1.0e-7
   error('error #5 in file rot2.m')
elseif dot(e3,e1)>1.0e-7
   error('error #6 in file rot2.m')
elseif abs(e1)-1>1.0e-7
   error('error #7 in file rot2.m')
elseif abs(e2)-1>1.0e-7
   error('error #8 in file rot2.m')
elseif abs(e3)-1>1.0e-7
   error('error #9 in file rot2.m')
end
%
% components nij
%
nn(1,1) = e1(1,1) ;
nn(2,1) = e1(2,1) ;
nn(3,1) = e1(3,1) ;
%
nn(1,2) = e2(1,1) ;
nn(2,2) = e2(2,1) ;
nn(3,2) = e2(3,1) ;
%
nn(1,3) = e3(1,1) ;
nn(2,3) = e3(2,1) ;
nn(3,3) = e3(3,1) ;
%
%nn=nn';
%
for i=1:3
   for j=1:3
      for k=1:3
     for l=1:3
        Inew(i,j,k,l) = 0 ;
        for m=1:3
```

```
            for n=1:3
           for p=1:3
              for q=1:3
             Inew(i,j,k,l) = Inew(i,j,k,l) + ...
             nn(i,m)*nn(j,n)*nn(k,p)*nn(l,q)*I(m,n,p,q) ;
              end
           end
            end
         end
      end
       end
   end
end
```

B.5.2.4. func_hom_ultra_MT.m

This function was originally written and used for the publications (Hellmich *et al.* , 2004) and (Hellmich, 2005). It was modified for the publication (Fritsch & Hellmich, 2007) and was further modified for this master thesis.

```
% Homogenization of ultrastructure
% Mori-Tanaka-scheme, ef=matrix, fib = inclusions
function[Chom]=func_hom_ultra_MT(I, khom, muhom, cef, cfib, barfef, barffib)
a=1;
% calculate Poisson's ratio of polycrystalline matrix
%----------------------------
nup=(3*khom-2*muhom)/(6*khom+2*muhom);
% construct Eshelby's tensor for cylindrical, compressible
% inclusions in compressible matrix
%----------------------------
Qesh=3/(8*pi*(1-nup));
Resh=(1-2*nup)/(8*pi*(1-nup));
% a=3.224 % help value
Ia=2*pi;
Iab=4*pi/(3*(2*a)^2);
Iaa=4*pi/(3*a^2)-Iab;
Sesh11=Qesh*a^2*Iaa+Resh*Ia;
Sesh22=Sesh11;
Sesh33=0;
Sesh12=Qesh*a^2*Iab-Resh*Ia;
Sesh21=Sesh12;
Sesh13=Qesh/3*Ia-Resh*Ia;
Sesh23=Sesh13;
Sesh31=0;
Sesh32=Sesh31;
Sesh44=1/4;
Sesh55=Sesh44;
```

```
Sesh66=Qesh/2*(2*a^2)*Iab+Resh*Ia;
Sesh=[Sesh11 Sesh12 Sesh13 0 0 0; Sesh21 Sesh22 Sesh23 0 0 0; ...
      Sesh31 Sesh32 Sesh33 0 0 0; 0 0 0 2*Sesh44 0 0;...
      0 0 0 0 2*Sesh55 0; 0 0 0 0 0 2*Sesh66];
Pcyl=Sesh*(cef)^-1;

% evaluate [I+P:(c-C0)]^-1 for fib
%--------------------------
helpfib=(I+Pcyl*(cfib-cef))^-1;                %cylindrical inclusions!!!

Chom=(barfef*cef+barffib*cfib*helpfib)*(barfef*I+barffib*helpfib)^-1;
end
```

B.6. CTensorPlots.m

This file was written to plot all the data calculated in *Ctensor.m*.

```
% ------------------------------------------------------------------------
% PLOTS FOR C-TENSOR
% ------------------------------------------------------------------------

figure
hold on
grid on
plot(rhoecregGrowth, C1111regGrowth, '-.', 'color', 'black', 'linewidth', 2)
plot(rhoecregGrowth, C3333regGrowth, '-', 'color', 'black', 'linewidth', 4)
plot(rhoecregGrowth, C2323regGrowth, '--', 'color', 'black', 'linewidth', 2)
plot(rhoecregGrowth, C1122regGrowth, '-', 'color', 'black', 'linewidth', 2)
plot(rhoecregGrowth, C1133regGrowth, ':', 'color', 'black', 'linewidth', 2)
hlegend = legend('C^{ec}_{1111}', ...
                 'C^{ec}_{3333}', ...
                 'C^{ec}_{2323}', ...
                 'C^{ec}_{1122}', ...
                 'C^{ec}_{1133}', ...
                 'location', 'NorthWest');
set(hlegend,'FontSize', 21);
%resize_legend(hlegend,2)
legend boxoff
set(gca, 'XTick', 1:0.2:2, 'YTick', 0:5:25, 'fontsize', 16)
xlabel('Extracellular mass density \rho^{ec} [g/cm^3]', 'fontsize', 18)
ylabel('Elasticity tensor components [GPa]', 'fontsize', 18)

filename = 'Ctens_Growing.eps';
absPathPlot = strcat(pwd, slash, 'LatexFiles', slash, filename);
print('-depsc', absPathPlot);

% Aging
```

```
31
32 figure
33 hold on
34 grid on
35 plot(rhoecregAge, C1111regAge, '-.', 'color', 'black', 'linewidth', 2)
36 plot(rhoecregAge, C3333regAge, '-', 'color', 'black', 'linewidth', 4)
37 plot(rhoecregAge, C2323regAge, '--', 'color', 'black', 'linewidth', 2)
38 plot(rhoecregAge, C1122regAge, '-', 'color', 'black', 'linewidth', 2)
39 plot(rhoecregAge, C1133regAge, ':', 'color', 'black', 'linewidth', 2)
40 plot(3.02,120)
41 hlegend = legend('C^{ec}_{1111}', ...
42                  'C^{ec}_{3333}', ...
43                  'C^{ec}_{2323}', ...
44                  'C^{ec}_{1122}', ...
45                  'C^{ec}_{1133}', ...
46                  'location', 'NorthWest');
47 set(hlegend,'FontSize', 21);
48 %resize_legend(hlegend,2)
49 legend boxoff
50 set(gca, 'XTick', 1.9:0.2:3.1, 'YTick', 0:20:150, 'fontsize', 16)
51 xlabel('Extracellular mass density \rho^{ec} [g/cm^3]', 'fontsize', 18)
52 ylabel('Elasticity tensor components [GPa]', 'fontsize', 18)
53
54 filename = 'Ctens_Aging.eps';
55 absPathPlot = strcat(pwd, slash, 'LatexFiles', slash, filename);
56 print('-depsc', absPathPlot);
57
58 % % ------------------------------------------------------------------------
59 figure
60 hold on
61 grid on
62 plot(rhoecregGrowth, nu12regGrowth, '-.', 'color', 'black', 'linewidth', 2)
63 plot(rhoecregGrowth, nu13regGrowth, '-', 'color', 'black', 'linewidth', 2)
64 plot(1,1)
65 hlegend = legend('\nu_{12}', ...
66    '\nu_{13}', ...
67    'location', 'West');
68 resize_legend(hlegend,2)
69 legend boxoff
70 set(gca, 'XTick', 1:0.2:1.9, 'YTick', 0:0.1:1, 'fontsize', 16)
71 xlabel('Extracellular mass density \rho^{ec} [g/cm^3]', 'fontsize', 18)
72 ylabel('\nu_{13} and \nu_{12}', 'fontsize', 18)
73
74
75 filename = 'nu_growing.eps';
76 absPathPlot = strcat(pwd, slash, 'LatexFiles', slash, filename);
77 print('-depsc', absPathPlot);
78
79 % Aging
80
81 figure
82 hold on
```

```
grid on
plot(rhoecregAge, nu12regAge, '-.', 'color', 'black', 'linewidth', 2)
plot(rhoecregAge, nu13regAge, '-', 'color', 'black', 'linewidth', 2)
plot(3.1,0)
plot(1.9,0)
plot(1.9,1)
hlegend = legend('\nu_{12}', ...
   '\nu_{13}', ...
   'location', 'West');
resize_legend(hlegend,2)
legend boxoff
set(gca, 'XTick', 1.9:0.2:3, 'YTick', 0:0.1:3, 'fontsize', 16)
xlabel('Extracellular mass density \rho^{ec} [g/cm^3]', 'fontsize', 18)
ylabel('\nu_{13} and \nu_{12}', 'fontsize', 18)


filename = 'nu_aging.eps';
absPathPlot = strcat(pwd, slash, 'LatexFiles', slash, filename);
print('-depsc', absPathPlot);

% ------------------------------------------------------------------------
figure
hold on
grid on
plot(rhoecregGrowth, E1regGrowth, '-', 'color', 'black', 'linewidth', 2)
plot(rhoecregGrowth, E3regGrowth, '--', 'color', 'black', 'linewidth', 2)
plot(rhoecregGrowth, G12regGrowth, '-.', 'color', 'black', 'linewidth', 2)

hlegend = legend('E^{ec}_{1}', ...
   'E^{ec}_{3}', ...
   'G_{12}', ...
   'location', 'West');
resize_legend(hlegend,2)
legend boxoff
set(gca, 'XTick', 1:0.2:2, 'YTick', 0:2:25, 'fontsize', 16)
xlabel('Extracellular mass density \rho^{ec} [g/cm^3]', 'fontsize', 18)
ylabel('E^{ec}_{1}, E^{ec}_{3}, G_{12} [GPa]', 'fontsize', 18)

filename = 'EG_Growing.eps';
absPathPlot = strcat(pwd, slash, 'LatexFiles', slash, filename);
print('-depsc', absPathPlot);


% Aging

figure
hold on
grid on
plot(rhoecregAge, E1regAge, '-', 'color', 'black', 'linewidth', 2)
plot(rhoecregAge, E3regAge, '--', 'color', 'black', 'linewidth', 2)
plot(rhoecregAge, G12regAge, '-.', 'color', 'black', 'linewidth', 2)

```

```
plot(3.02, 120)
hlegend = legend('E^{ec}_{1}', ...
   'E^{ec}_{3}', ...
   'G_{12}', ...
   'location', 'West');
resize_legend(hlegend,2)
legend boxoff
set(gca, 'XTick', 1.9:0.2:3.1, 'YTick', 0:20:120, 'fontsize', 16)
xlabel('Extracellular mass density \rho^{ec} [g/cm^3]', 'fontsize', 18)
ylabel('E^{ec}_{1}, E^{ec}_{3}, G_{12} [GPa]', 'fontsize', 18)

filename = 'EG_Aging.eps';
absPathPlot = strcat(pwd, slash, 'LatexFiles', slash, filename);
print('-depsc', absPathPlot);


% ------------------------------------------------

figure
hold on
grid on
plot(rhoecregAge, C1111modelnorm, '-.', 'color', 'black', 'linewidth', 2)
plot(rhoecregAge, C2323modelnorm, '--', 'color', 'black', 'linewidth', 2)
plot(rhoecregAge, C1133modelnorm, ':', 'color', 'black', 'linewidth', 2)
plot(rhoecregAge, G12modelnorm, '-', 'color', 'black', 'linewidth', 2)
plot(1.93, Chumanashman84norm(1,1), 'd', 'color', 'black')
plot(1.93, Chumanashman84norm(4,4), 's', 'color', 'black')
plot(1.93, Chumanashman84norm(1,3), 'x', 'color', 'black')
plot(1.93, Chumanashman84norm(6,6), 'o', 'color', 'black')
plot((rhoeclees83_3333(3) + rhoeclees83_1111(4))/2, ...
                        C1111lees83(4)/C3333lees83(3),'p', 'color', 'black')

hlegend = legend('C^{norm}_{1111}', ...
                 'C^{norm}_{2323}', ...
                 'C^{norm}_{1133}', ...
                 'G^{norm}_{12}', ...
                 'C^{norm,exp}_{1111}', ...
                 'C^{norm,exp}_{2323}', ...
                 'C^{norm,exp}_{1133}', ...
                 'G^{norm,exp}_{12}', ...
                 'C^{norm}_{1111} (Lees83)');
set(hlegend, 'fontsize', 14);
resize_legend(hlegend,2)

legend boxoff
set(gca, 'XTick', 1.8:0.05:2.1, 'YTick', 0.1:0.1:0.7, 'fontsize', 16)
axis([1.8,2.1,0.1,0.7])
set(hlegend, 'location', 'West');

xlabel('Extracellular mass density \rho^{ec} [g/cm^3]', 'fontsize', 16)
ylabel('Elasticity tensor components normalized to C_{3333}', ...
                                                        'fontsize', 16)
```

```
187
188 filename = 'Ctens_ashman.eps';
189 absPathPlot = strcat(pwd, slash, 'LatexFiles', slash, filename);
190 print('-depsc', absPathPlot);
```

B.6.1. resize_legend.m

This function was taken from MATLAB®CENTRAL - An open exchange for the MATLAB and SIMULINK user community, with thanks to the author Denis Gilbert:

(http://www.mathworks.com/matlabcentral/fileexchange/2190-resizelegend, 2010)

B.7. ultrasoundData.m

This file was written to collect all the data to verify the model predicted elasticity tensor with those found in ultrasound experiments.

```
1  % ***************************************************************
2  % CALCULATIONS OF DATA FROM ULTRASOUND TESTS
3  % ***************************************************************
4  % Needs function: funcC, round2
5  % DATA
6  % Lees79
7  soslees79_3333 = [3.92 3.92 3.81 3.86 3.90 3.88 3.88 3.92];
8  soslees79_2222= [3.46 3.49 3.27 3.26 3.42 3.48 3.18 3.21];
9  soslees79_1111 = [3.18 3.18 3.18 3.16 3.27 3.26];
10
11 for i = 1:length(soslees79_3333)
12     rhoeclees79_3333(i) = rhoeclees79exp(i);
13 end
14
15 for i = 1:length(soslees79_2222)
16     rhoeclees79_2222(i) = rhoeclees79exp(i+length(soslees79_3333));
17 end
18
19 for i = 1:length(soslees79_1111)
20     rhoeclees79_1111(i) = rhoeclees79exp(i+length(soslees79_3333) ...
21                           +length(soslees79_2222));
22 end
23
24 C3333lees79 = funcC(soslees79_3333, rhoeclees79_3333);
```

```
C2222lees79 = funcC(soslees79_2222, rhoeclees79_2222);
C1111lees79 = funcC(soslees79_1111, rhoeclees79_1111);

% Lees82
tissueslees82 = ['Bovine tibia      '; 'Fin whale t. bulla'];
soslees82_3333 = [3.89 4.53]; % km/s
soslees82_1111 = [3.21 4.53]; % radial
rhoeclees82 = [2.04 2.53];

C1111lees82 = funcC(soslees82_1111, rhoeclees82);
C3333lees82 = funcC(soslees82_3333, rhoeclees82);

% Lees83
tissueslees83_3333 = ['Bovine tibia   '; 'Elephant radius'; ...
                      'Human femur    '];
soslees83_3333 = [4.18 3.89 3.76];
rhoeclees83_3333 = [2.06 1.93 1.96];

tissueslees83_1111 = ['Bovine tibia   '; 'Dugong rib     '; ...
                      'Elephant radius'; 'Human femur    '];
soslees83_1111 = [3.32 3.00 3.05 3.13];
rhoeclees83_1111 = [2.07 2.02 1.94 1.93];

C3333lees83 = funcC(soslees83_3333, rhoeclees83_3333);
C1111lees83 = funcC(soslees83_1111, rhoeclees83_1111);

% Lees92
% Cow bone
soslees92_3333 = 3.89; % axial
soslees92_2222 = 2.85; % tang
soslees92_1111 = 3.21; % rad
rhoeclees92us = 2.04;

C1111lees92 = funcC(soslees92_1111, rhoeclees92us);
C3333lees92 = funcC(soslees92_3333, rhoeclees92us);
C2222lees92 = funcC(soslees92_2222, rhoeclees92us);

[rhoecmtltlees92us,sosmtltlees92us] = ...
                       funcDataGraph('lees92_mtlt_us', 1.0, 1.6, 1.7, 2.4);

C1111mtltlees92 = funcC(sosmtltlees92us, rhoecmtltlees92us);


% Lees95
soslees95_1111 = [4.85 4.89 4.55 4.61 4.79 4.7 4.15 4.6 4.53 4.65 4.84 ...
                  4.60 4.53 4.53 4.54 4.48];
rhoeclees95us = [2.49 2.53 2.51 2.45 2.50 2.46 2.40 2.48 2.50 2.52 2.58 ...
                 2.54 2.50 2.53 2.54 2.49];

C1111lees95 = funcC(soslees95_1111, rhoeclees95us);

% % Not used as measured with 2.25 MHz
```

```
% % Ashman88
% tissuesashman88 = ['Human femur '; 'Human femur '; 'Human femur '; ...
%                    'Bovine femur'];
% sosashman88_3333 = [2.639 2.721 2.754 2.501];
% rhoecashman88 = [1.803 1.777 1.73 1.739]; % g/cm^3
%
% C3333ashman88 = funcC(sosashman88_3333, rhoecashman88);

% % Not used as measured with 5 MHz
% % Katz84
% % bovine femur
% soskatz84_1111 = [2.863 2.767];
% soskatz84_2222 = [3.189 2.849];
% soskatz84_3333 = [3.771 3.483];
% rhoeckatz84_1111 = [2.105 2.010];
% rhoeckatz84_2222 = [2.1 2.025];
% rhoeckatz84_3333 = [2.093 2.032];
%
% C3333katz84 = funcC(soskatz84_3333, rhoeckatz84_3333);
% C1111katz84 = funcC(soskatz84_1111, rhoeckatz84_1111);
% C2222katz84 = funcC(soskatz84_2222, rhoeckatz84_2222);

% % Not used as measured with 2.25 MHz
% % McCarthy data taken from Andreas Fritsch
% % experiments of McCarthy et al. (1990)
% % material:
% % cortical bone from dorsal cortex of horse
% % solid bone matrix wet; marrow removed
% % from Fig. 4, Fig. 3
% % Porosity
% pormccarthy90temp = [5 6 6 7 7 7 8 9 9 9 9 10 10 10 10 10 10.5 11 11 11 ...
%                      12 12 12 13 14 14 18 18 22 25 30 44];
% rhomccarthy90temp = [2.03  2.02  2.01  2.01  2.00  2.00  2.00  1.98  ...
%                      1.98  1.98  1.98  1.97  1.97  1.96  1.96  1.95  ...
%                      1.95  1.95  1.95  1.95  1.95  1.93  1.93  1.93  ...
%                      1.92  1.92  1.92  1.92  1.91  1.91  1.91  1.90  ...
%                      1.90  1.82  1.76  1.65];
%
% % speed of sound in relation to porosity
% sos1111mccarthy90_2 = [3.550 3.575 3.625 3.675 3.400 3.400 3.550 3.325 ...
%                        3.400 3.425 3.550 3.400 3.500 3.525 3.525 3.600 ...
%                        3.450 3.400 3.425 3.500 3.350 3.400 3.425 3.500 ...
%                        3.525 3.550 3.425 3.450 3.500 3.150 3.200 2.950];
%
% % speed of sound in 2  directions
% sos3333mccarthy90temp = [4.300 4.200 4.100 4.400 4.200 4.200 4.300 ...
%                          4.100 4.150 4.150 4.300 4.025 4.200 4.025 ...
%                          4.200 3.950 4.025 4.100 4.100 4.150 4.150 ...
%                          4.025 4.100 4.250 4.000 4.025 4.200 4.200 ...
%                          4.125 4.175 4.350 3.950 4.000 4.000 3.850 3.650];
%
% sos1111mccarthy90temp = [3.600 3.550 3.450 3.650 3.550 3.400 3.575 ...
```

```
% 3.425 3.350 3.500 3.600 3.500 3.350 3.500 ...
% 3.600 3.525 3.400 3.350 3.425 3.450 3.550 ...
% 3.350 3.300 3.475 3.350 3.400 3.350 3.400 ...
% 3.350 3.475 3.450 3.125 3.400 3.300 3.200 2.950];
%
% j=1;
%
% for i = 1:length(sos1111mccarthy90_2)
%     for k = 1:length(sos1111mccarthy90temp)
%         if (sos1111mccarthy90_2(i)-sos1111mccarthy90temp(k)) == 0 ...
%                                             && sos1111mccarthy90_2(i) ~= 0
%             sos1111mccarthy90old(j)=sos1111mccarthy90_2(i);
%             sos3333mccarthy90old(j)=sos3333mccarthy90temp(i);
%             rhomumccarthy90(j)=rhomccarthy90temp(i);
%             pormccarthy90(j)=pormccarthy90temp(i);
%
%             sos1111mccarthy90_2(i) = 0;
%             j=j+1;
%         end
%     end
% end
%
% flac = 0.0;
% fvas = (pormccarthy90/100-flac)/(1-flac);
% rhoexvasmccarthy90=rhomumccarthy90./(1-fvas);
% rhoecmccarthy90temp=(rhoexvasmccarthy90-rhowater*flac)/(1-flac);
%
% k = 1;
% for i = 1:length(rhoecmccarthy90temp)
%     if rhoecmccarthy90temp(rhoecmccarthy90temp(i)<3)
%         rhoecmccarthy90(k)=rhoecmccarthy90temp(i);
%         sosmccarthy90_1111(k)=sos1111mccarthy90old(i);
%         sosmccarthy90_3333(k)=sos3333mccarthy90old(i);
%         k = k+1;
%     end
%
%
% end
%
% C3333mccarthy90 = funcC(sosmccarthy90_3333, rhoecmccarthy90);
% C1111mccarthy90 = funcC(sosmccarthy90_1111, rhoecmccarthy90);

% ********************************************************
% Calculate error of all calculated and experimental Cijkl
% ********************************************************
% calculate error in subgroups

% Error in C1111
rhoecC1111us = round2([rhoeclees79_1111 rhoeclees83_1111 rhoeclees95us]', 0.01);

C1111us = ([C1111lees79 C1111lees83 C1111lees95]);

```

```
181
182 % round to 2 decimal places
183 rhoecregGrowthAge=round2([rhoecregGrowth rhoecregAge], 0.01);
184 C1111GrowthAge=[C1111regGrowth C1111regAge];
185 C3333GrowthAge=[C3333regGrowth C3333regAge];
186
187 % modelC1111=unique([rhoecregGrowthAge; C1111GrowthAge]');
188 % delete same values in rhoecregGrowthAge
189 [rhoecGrowthAge_unique, indexrhoec]=unique(rhoecregGrowthAge, 'first');
190
191 for i = 1:length(indexrhoec)
192     C1111unique(i)=C1111GrowthAge(indexrhoec(i));
193 end
194
195
196 % find corresponding C1111 values with respect to rho^ec, compare rho^ec
197 % experimental and rho^ec predicted to find corresponding C1111model to the
198 % C1111 experimental
199 j=1;
200 m=1;
201 for i = 1:length(rhoecC1111us)
202     for k = 1:length(rhoecGrowthAge_unique)
203         if (rhoecC1111us(i)-rhoecGrowthAge_unique(k))==0
204             C1111model(j)=C1111unique(k);
205             j=j+1;
206         end
207     end
208 end
209
210 errC1111_all = (C1111model-C1111us)./C1111us;
211 meanerrC1111_all = mean(errC1111_all)
212 stderrC1111_all = std(errC1111_all)
213 varerrC1111_all = var(errC1111_all)
214
215 % ------------------------------
216 % Error in C3333
217 rhoecC3333us = round2([rhoeclees79_3333 rhoeclees83_3333]', 0.01);
218 C3333us = ([C3333lees79 C3333lees83]);
219
220
221 % round to 2 decimal places
222 rhoecregGrowthAge=round2([rhoecregGrowth rhoecregAge], 0.01);
223 C3333GrowthAge=[C3333regGrowth C3333regAge];
224 C3333GrowthAge=[C3333regGrowth C3333regAge];
225
226 % modelC3333=unique([rhoecregGrowthAge; C3333GrowthAge]');
227 % delete same values in rhoecregGrowthAge
228 [rhoecGrowthAge_unique, indexrhoec]=unique(rhoecregGrowthAge, 'first');
229
230 for i = 1:length(indexrhoec)
231     C3333unique(i)=C3333GrowthAge(indexrhoec(i));
232 end
```

```
233
234
235 % find corresponding C3333 values with respect to rho^ec, compare rho^ec
236 % experimental and rho^ec predicted to find corresponding C3333model to the
237 % C3333 experimental
238 j=1;
239 m=1;
240 for i = 1:length(rhoecC3333us)
241     for k = 1:length(rhoecGrowthAge_unique)
242         if (rhoecC3333us(i)-rhoecGrowthAge_unique(k))==0
243             C3333model(j)=C3333unique(k);
244             j=j+1;
245         end
246     end
247 end
248
249 errC3333_all = (C3333model-C3333us)./C3333us;
250 meanerrC3333_all = mean(errC3333_all)
251 stderrC3333_all = std(errC3333_all)
252 varerrC3333_all = var(errC3333_all)
253
254 % --------------------------------
255 % Ashman84
256 % mean of human and canine
257 C1111ashman84 = [18.0 19.0];
258 C3333ashman84 = [27.6 29.7];
259 C3333humanashman84 = [26.9 28.2 27.0 28.0 26.9];
260 C3333canineashman84 = [28.5 30.6 30.7 29.6 28.5];
261 rhoechumanashman84 = [1.88 1.92 1.895 1.923 1.88];
262 rhoeccanineashman84 = [1.875 1.89 1.88 1.877 1.875];
263 rhoecC1111ashman84 = [mean(rhoechumanashman84) mean(rhoeccanineashman84)];
264
265 % full tensor
266
267 Chumanashman84norm = [18.0 09.98 10.10 0 0 0; ...
268                   09.98 20.20 10.70 0 0 0; ...
269                   10.10 10.70 27.60 0 0 0; ...
270                   0 0 0 6.23 0 0;...
271                   0 0 0 0 5.61 0 ; ...
272                   0 0 0 0 0 4.52]/C3333ashman84(1);
273
274 rhoashman84norm =[1.93 1.93 1.93 0 0 0; ...
275                   1.93 1.93 1.93 0 0 0; ...
276                   1.93 1.93 1.93 0 0 0; ...
277                   0 0 0 1.93 0 0;...
278                   0 0 0 0 1.93 0 ; ...
279                   0 0 0 0 0 1.93];
280
281 C3333modelnorm = C3333regAge./C3333regAge;
282 C1111modelnorm = C1111regAge./C3333regAge;
283 C1122modelnorm = C1122regAge./C3333regAge;
284 C1133modelnorm = C1133regAge./C3333regAge;
```

```
285 C2323modelnorm = C2323regAge./C3333regAge;
286 G12modelnorm = G12regAge./C3333regAge;
```

B.7.1. funcC.m

This function calculates the elasticity tensor components on the basis of the velocity of acoustic plane waves.

```
1 % stiffness components
2 function[C]=funcC(sos,rho)
3     C = rho.*(sos.*sos);
4 end
```

B.7.2. round2.m

This function was taken from MATLAB®CENTRAL - An open exchange for the MATLAB and SIMULINK user community, with thanks to the author Robert Bemis:

(http://www.mathworks.com/matlabcentral/fileexchange/4261-round2, 2010)

B.8. AttenCoeff.m

This file calculates and plots the X-ray attenuation coefficient. This file also requires the function *resize_legend.m* described in Chapter B.6.1.

```
1 % ********************************************************
2 % X-Ray: attenuation coefficient
3 % ********************************************************
4 muwater = 5.33;
5 mumin = 142;
6 muorg = 5.71;
7 muecAge = vfwaterAge*muwater+vfminAge*mumin+vforgAge*muorg;
8 muecGrowth = vfwaterGrowth*muwater+vfminGrowth*mumin+vforgGrowth*muorg;
9
10 % PLOT
11 figure
12 hold on
```

```
grid on
plot(muecGrowth, C1111regGrowth, '-.', 'color', 'black', 'linewidth', 2)
plot(muecGrowth, C3333regGrowth, '.', 'color', 'black', 'linewidth', 2)
plot(muecGrowth, C2323regGrowth, '--', 'color', 'black', 'linewidth', 2)
plot(muecGrowth, C1122regGrowth, '-', 'color', 'black', 'linewidth', 2)
plot(muecGrowth, C1133regGrowth, ':', 'color', 'black', 'linewidth', 2)
hlegend = legend('C^{ec}_{1111}', ...
                 'C^{ec}_{3333}', ...
                 'C^{ec}_{2323}', ...
                 'C^{ec}_{1122}', ...
                 'C^{ec}_{1133}', ...
                 'location', 'SouthWest');
resize_legend(hlegend,2)
legend boxoff
set(gca, 'XTick', 5:5:60, 'YTick', 0:5:25, 'fontsize', 16)
xlabel('Attenuation coefficient \mu^{ec} [cm^{-1}]', 'fontsize', 18)
ylabel('Elasticity tensor components [GPa]', 'fontsize', 18)

filename = 'Ctens_AttenCoeff_Growing.eps';
absPathPlot = strcat(pwd, slash, 'LatexFiles', slash, filename);
print('-depsc', absPathPlot);

% Aging

figure
hold on
grid on
plot(muecAge, C1111regAge, '-.', 'color', 'black', 'linewidth', 2)
plot(muecAge, C3333regAge, '.', 'color', 'black', 'linewidth', 2)
plot(muecAge, C2323regAge, '--', 'color', 'black', 'linewidth', 2)
plot(muecAge, C1122regAge, '-', 'color', 'black', 'linewidth', 2)
plot(muecAge, C1133regAge, ':', 'color', 'black', 'linewidth', 2)
hlegend = legend('C^{ec}_{1111}', ...
                 'C^{ec}_{3333}', ...
                 'C^{ec}_{2323}', ...
                 'C^{ec}_{1122}', ...
                 'C^{ec}_{1133}', ...
                 'location', 'West');
resize_legend(hlegend,2)
legend boxoff
set(gca, 'XTick', 55:10:145, 'YTick', 0:10:150, 'fontsize', 16)
xlabel('Attenuation coefficient \mu^{ec} [cm^{-1}]', 'fontsize', 18)
ylabel('Elasticity tensor components [GPa]', 'fontsize', 18)

filename = 'Ctens_AttenCoeff_Aging.eps';
absPathPlot = strcat(pwd, slash, 'LatexFiles', slash, filename);
print('-depsc', absPathPlot);
```

B.9. CTensorPlots_ultrasound.m

This file plots the data calculated in *Ctensor_ultrasound.m* and *Ctensor.m*. This file also requires the function *resize_legend.m* described in Chapter B.6.1.

```
% ------------------------------------------------------------------------
% PLOT ULTRASOUND DATA
% ------------------------------------------------------------------------

% Mapping of C1111model to the experimental data

for i = 1:length(rhoeclees79_1111)
    C1111lees79pre(i)=C1111model(i);
end

[C1111lees83pre,lengthloop] = funcCus_map(length(rhoeclees79_1111)+1, ...
                                          C1111model, rhoeclees83_1111);

% [C1111lees92pre,lengthloop] = funcCus_map(lengthloop, ...
%                                           C1111model, rhoeclees92us);

[C1111lees95pre,lengthloop] = funcCus_map(lengthloop, ...
                                          C1111model, rhoeclees95us);

% [C1111katz84pre,lengthloop] = funcCus_map(lengthloop, ...
%                                           C1111model, rhoeckatz84_1111);
%
% [C1111mccarthy90pre,lengthloop] = funcCus_map(lengthloop, ...
%                                           C1111model, rhoecmccarthy90);


% Mapping of C1111model to the experimental data

for i = 1:length(rhoeclees79_3333)
    C3333lees79pre(i)=C3333model(i);
end


[C3333lees83pre,lengthloop] = funcCus_map(length(rhoeclees79_3333)+1, ...
                                          C3333model, rhoeclees83_3333);

% [C3333lees92pre,lengthloop] = funcCus_map(lengthloop, ...
%                                           C3333model, rhoeclees92us);
%
% [C3333katz84pre,lengthloop] = funcCus_map(lengthloop, ...
%                                           C3333model, rhoeckatz84_3333);
%
% [C3333mccarthy90pre,lengthloop] = funcCus_map(lengthloop, ...
%                                           C3333model, rhoecmccarthy90);
%
% [C3333ashman88pre,lengthloop] = funcCus_map(lengthloop, ...
```

```
% C3333model, rhoecashman88);

figure
hold on
grid on
plot(C1111lees79pre, C1111lees79, 'x', 'color', 'black')
plot(C1111lees95pre, C1111lees95, '>', 'color', 'black')
plot(C1111lees83pre, C1111lees83, 'd', 'color', 'black')
plot(C3333lees79pre, C3333lees79, 'x', 'color', 'black', 'linewidth', 3)
plot(C3333lees83pre, C3333lees83, 'd', 'color', 'black', 'linewidth', 3)


plot([10 70], [10 70],'-', 'color', 'black')


hlegend = legend('C_{1111}: Bovine bone - [Lees et al. (1979)]', ...
   'C_{1111}: Whale bones - [Lees et al. (1995)]', ...
   'C_{1111}: Bones from various vertebrates - [Lees et al. (1983)]', ...
   'C_{3333}: Bovine bone - [Lees et al. (1979)]', ...
   'C_{3333}: Bones from various vertebrates - [Lees et al. (1983)]', ...
   'location', 'NorthOutside');
set(hlegend, 'fontsize', 12);
legend boxoff
set(gca, 'XTick', 10:10:70, 'YTick', 10:10:70, 'fontsize', 16)
axis equal
axis tight
xlabel('model-predicted stiffness [GPa]', 'fontsize', 17)
ylabel('experimental stiffness [GPa]', 'fontsize', 17)

filename = 'C_ultrasound_undrained.eps';
absPathPlot = strcat(pwd, slash, 'LatexFiles', slash, filename);
print('-depsc', absPathPlot);
```

B.10. FittingFunctions.m

This file was written to calculate the polynomial functions with the optimal order for the elasticity components by finding the optimal coefficient of determination.

```
% ************************************************************************
% Calculate fitting functions for C1111, C3333 and E1, E2 as a function of
% rho
% Run ultrasoundData.m
% Needs fucntion: func_bestfit.m
% ************************************************************************

Cha1111 = 137;
```

```
9
10 [polyC1111, regC1111, meanerrC1111fit, stdC1111fit]= ...
11     func_bestfit([rhoecregGrowth rhoecregAge], ...
12     [C1111regGrowth C1111regAge], meanerrC1111_all);
13
14 [polyC3333, regC3333, meanerrC3333fit, stdC3333fit]= ...
15     func_bestfit([rhoecregGrowth rhoecregAge], ...
16     [C3333regGrowth C3333regAge], meanerrC3333_all);
17
18 [polyC1122, regC1122, meanerrC1122fit, stdC1122fit]= ...
19     func_bestfit([rhoecregGrowth rhoecregAge], ...
20     [C1122regGrowth C1122regAge], meanerrC3333_all);
21
22 [polyC1133, regC1133, meanerrC1133fit, stdC1133fit]= ...
23     func_bestfit([rhoecregGrowth rhoecregAge], ...
24     [C1133regGrowth C1133regAge], meanerrC3333_all);
25
26 [polyC2323, regC2323, meanerrC2323fit, stdC2323fit]= ...
27     func_bestfit([rhoecregGrowth rhoecregAge], ...
28     [C2323regGrowth C2323regAge], meanerrC3333_all);
29
30 % dimensionless:
31
32 polyC1111_dl=func_dimless(polyC1111,Cha1111,rhomin)
33 polyC3333_dl=func_dimless(polyC3333,Cha1111,rhomin)
34 polyC1122_dl=func_dimless(polyC1122,Cha1111,rhomin)
35 polyC1133_dl=func_dimless(polyC1133,Cha1111,rhomin)
36 polyC2323_dl=func_dimless(polyC2323,Cha1111,rhomin)
```

B.10.1. func_bestfit.m

This function finds the optimal order of the polynomial function.

```
1  function [polynom, regValue, errmean, stdValue]=func_bestfit(x,y,meanerr)
2
3     errmean = 100;
4     stdValue = 0;
5     i = 2;
6
7   while abs(errmean) > abs(meanerr/10)
8      polynom = polyfit(x, y, i);
9      regValue = 0;
10     m = i;
11         for k = 1:i
12             regValue_old=polynom(:,k)*x.^(m);
13             regValue=regValue_old+regValue;
14             m = m - 1;
```

```
        end
    regValue = regValue + polynom(:,i+1);

    err = (regValue-y)./y;
    errmean = mean(err);
    stdValue = std(err);
    i = i+1;
 end

end
```

B.11. parry.m

This file was written to calculate the organic apposition rate for the data of Parry & Craig (1978).

```
% Parry Craig
% Number of fibrils per print
% ageParry = [0 0.75 1.25 2 3.50 13 24]; % Months
ageParry = [0 0.75 1.25 2 3.50];
% area fraction fibrillar of all fibrils
% vfibtot = [0.38 0.41 0.50 0.64 0.67 0.63 0.64];
vfibtot = [0.38 0.41 0.50 0.64 0.67];
magnification = 65000;

dw = 1.33; % neutron diffraction spacing between collagen molecules
b = 1.47; % length
D = 64; % axial macroperiod
vfibparry = 5*dw*b*D;
vcollparry = 335.6;
vfcollparry = vfibtot./(vfibparry/vcollparry);
vforgparry = vfcollparry/90*100;
rhoapporgparry=vforgparry.*rhocoll;

z = (0:4);
polyparryorg = polyfit(ageParry, rhoapporgparry, 1);
regparryorg = polyparryorg(:,1).*z + polyparryorg(:,2);


figure
hold on
plot(z, regparryorg, '-', 'color', 'black', 'linewidth', 3);
for i = 1:length(ageParry)
    plot(ageParry(i), rhoapporgparry(i), 'p', 'color', 'black')
end
plot(5,0.3)
```

```
set(gca, 'XTick', 0:1:5, 'YTick', 0.3:0.05:0.6, 'fontsize', 18)
xlabel('Age [months]', 'fontsize', 18)
ylabel('\rho^*_{org} [g/cm^3]', 'fontsize', 18)
grid('on')

hlegend = legend('Regression line', ...
        'Experimental data', ...
        'location', 'NorthWest');
set(hlegend, 'fontsize', 18);

filename = 'parry_age_rhoapporg.eps';
absPathPlot = strcat(pwd, slash, 'LatexFiles', slash, filename);
print('-depsc', absPathPlot);
```

B.12. hammett25.m

This file was written to calculate the organic apposition rate for the data of Hammett (1925).

```
% ********************************************************
% run ExpData.m, appRho.m
% Apparent mass densities of components of microstructure!
% ********************************************************

for i=1:6
    rhoapporgfemhammett25(i) = rhoapporghammett25(i);
end

for i=8:13
    rhoapporgfemhammett25(i-1) = rhoapporghammett25(i);
end

for i=15:20
    rhoapporghumhammett25(i-14) = rhoapporghammett25(i);
end

for i=22:27
    rhoapporghumhammett25(i-15) = rhoapporghammett25(i);
end

% Mineral

for i=1:6
    rhoappminfemhammett25(i) = rhoappminhammett25(i);
end

for i=8:13
    rhoappminfemhammett25(i-1) = rhoappminhammett25(i);
```

```
end

for i=15:20
    rhoappminhumhammett25(i-14) = rhoappminhammett25(i);
end

for i=22:27
    rhoappminhumhammett25(i-15) = rhoappminhammett25(i);
end

% Water

for i=1:6
    rhoappwaterfemhammett25(i) = rhoappwaterhammett25(i);
end

for i=8:13
    rhoappwaterfemhammett25(i-1) = rhoappwaterhammett25(i);
end

for i=15:20
    rhoappwaterhumhammett25(i-14) = rhoappwaterhammett25(i);
end

for i=22:27
    rhoappwaterhumhammett25(i-15) = rhoappwaterhammett25(i);
end

z = (0:5);
polyhammettorg = polyfit([Agehammett25 Agehammett25 Agehammett25 ...
    Agehammett25]/30, rhoapporghammett25, 1);
reghammettorg = polyhammettorg(:,1).*z + polyhammettorg(:,2);

figure
hold on
plot(z, reghammettorg, '-', 'color', 'black', 'linewidth', 3)
plot([Agehammett25 Agehammett25 Agehammett25 Agehammett25]/30, ...
    rhoapporghammett25, '*', 'color', 'black')
plot(0,0.2)
grid on;

hlegend = legend('Regression line', ...
                 'Experimental data', ...
                 'location', 'NorthWest');
set(hlegend, 'fontsize', 18);
set(gca, 'XTick', 0:1:5, 'YTick', 0:0.05:0.5, 'fontsize', 18)
xlabel('Age [months]', 'fontsize', 18)
ylabel('\rho^*_{org} [g/cm^3]', 'fontsize', 18)

filename = 'hammett_age_appOrgDensity.eps';
absPathPlot = strcat(pwd, slash, 'LatexFiles', slash, filename);
print('-depsc', absPathPlot);
```

Bibliography

Bailey, A.J., Paul, R.G., & Knott, L. 1998. Mechanisms of maturation and ageing of collagen. *Mechanisms of Aging and Development*, **106**, 1 – 56.

Bailey, A.J., Sims, T.J., Ebbesen, E.N., Mansell, J.P., Thomsen, & Mosekilde, Li. 1999. Age-related changes in the biochemical properties of human cancellous bone collagen: relationship to bone strength. *Cacified Tissue Int.*, **65**, 203 – 210.

Biltz, R.M., & Pellegrino, E.D. 1969. The chemical anatomy of bone. *Journal of Bone and Joint Surgery*, **51-A**(3), 456 – 466.

Buckwalter, J.A., Glimcher, M.J., Cooper, R.R., & Recker, R. 1995a. Bone Biology, Part I: Structure, blood supply, cells, matrix, and mineralization. *The Journal of Bone and Joint Surgery*, **77-A**(8), 1256 – 1275.

Buckwalter, J.A., Glimcher, M.J., Cooper, R.R., & Recker, R. 1995b. Bone Biology, Part II: Formation, form, modeling, remodeling, and regulation of cell functions. *The Journal of Bone and Joint Surgery*, **77-A**(8), 1276 – 1288.

Burns, C. M. 1929. XCIV. The effect of the continued ingestion of mineral acid on growth of body and bone and on the composition of bone and of the soft tissues. *Biochemical Journal*, **23**(5), 860 – 867.

Cusack, S., & Miller, A. 1979. Determination of the elastic constants of collagen by Brillouin light scattering. *Journal of Molecular Biology*, **135**, 39 – 51.

Fritsch, A., & Hellmich, Ch. 2007. 'Universal' microstructural patterns in cortical and trabecular, extracellular and extravacular bone materials: Micromechanics-based prediction of anisotropic elasticity. *Journal of Theoretical Biology*, **244**, 597 – 620.

Fritsch, A., Hellmich, Ch., & Dormieux, L. 2009. Ductile sliding between mineral crystals followed by rupture of collagen crosslinks: experimentally supported micromechanical explanation of bone strength. *Journal of Theoretical Biology*, **260**, 230 – 252.

Frost, H.M. 1960. Micropetrosis. *Journal of Bone and Joint Surgery*, **42**, 144 – 150.

Gong, J.K., Arnold, J.S., & Cohn, S, H. 1964. Composition of trabecular and cortical bone. *The Anatomical Record*, **149**, 325 – 332.

Hammett, F. S. 1925. A Biochemical Study of Bone Growth. I. Changes in the ash, organic matter and water during growth (mus norvegicus albinus). *The Journal of Biological Chemistry*, **64**, 409 – 428.

Hellmich, Ch. 2005. Microelasticity of Bone. *Pages 289 – 332 of:* Dormieux, L., & Ulm, F.-J. (eds), *Applied Micromechanics of Porous Media*, vol. 480. Springer, Wien - New York.

Hellmich, Ch., Barthélémy, J.-F., & Dormieux, L. 2004. Mineral-collagen interactions in elasticity of bone ultrastructure – a continuum micromechanics approach. *European Journal of Mechanics A-Solids*, **23**, 783 – 810.

Hofstetter, K., Hellmich, C., & Eberhardsteiner, J. 2006. The influence of the microfibril angle on wood stiffness: a continuum micromechanics approach. *Computer Assisted Mechanics and Engineering Sciences*, **13**, 523 – 536.

Hoshi, K., Kemmotsu, S., Takeuchi, Y., Amizuka, N., & Ozawa, H. 1999. The primary calcification in bones follows removal of decorin and fusion of collagen fibrils. *Journal of Bone and Mineral Research*, **14**(2), 273 – 280.

Jowsey, J. 1960. Age changes in human bone. *Clinical Orthopaedics*, **17**, 210 – 218.

Katz, J.L., & Ukraincik, K. 1971. On the anisotropic elastic properties of hydroxyapatite. *Journal of Biomechanics*, **4**, 221 – 227.

Kazuhiko, K., Buchanan, A.V., & Weiss, K.M. 2009. Biomineralization in humans: making the hard choices in life. *Annual Review of Genetics*, **43**, 119 – 142.

Kiebzak, G.M. 1991. Age-related bone changes. *Experimental Gerontology*, **26**, 171 – 187.

Lees, S. 1987. Considerations regarding the structure of the mammalian mineralized osteoid from viewpoint of the generalized packing model. *Connective Tissue Research*, **16**, 281 – 303.

Lees, S. 2003. Mineralization of type I collagen. *Biophysical Journal*, **85**, 204 – 207.

Lees, S., & Page, E.A. 1992. A study of some properties of mineralized turkey leg tendon. *Connective Tissue Research*, **28**, 263 – 287.

Lemaire, V., Tobin, F.L., Greller, L.D., Cho, C.R., & Suva, L.J. 2004. Modeling the interactions between osteoblast and osteoclast activities in bone remodeling. *Journal of Theoretical Biology*, **229**, 293 – 309.

Lindstedt, S., & Prockop, D.J. 1960. Isotopic studies on urinary hydroxyproline as evidence for rapidly catabolized forms of collagen in the young rat. *The Journal of Biological Chemistry*, **236**, 1399 – 1403.

Loveridge, N. 1999. Bone: more than a stick. *Journal of animal science*, **77**, 190 – 196.

Mays, P.K., McAnulty, R.J., Campa, J.S., & Laurent, G.J. 1991. Age-related changes in collagen synthesis and degradation in rat tissue. *Biochemical Journal*, **276**, 307 – 313.

Neuberger, A., Perrone, J.C., & Slack, H.G.B. 1950. The relative metabolic inertia of tendon collagen in the rat. *Biochemical Journal*, **49**, 199 – 204.

Ozawa, H., Hoshi, K., & Amizuka, N. 2008. Current concepts of bone biomineralization. *Journal of Oral Biosciences*, **50**(1), 1 – 14. Invited Review.

Parfitt, A.M. 1983. The physiologic and clinical significance of bone histomorphometric data. *Pages 143–223 of:* Recker, R.R. (ed), *Histomorphometry, Techniques and Interpretation*. CRC Press Inc, Boca Raton, FL, USA.

Parry, D.A.D., & Craig, A.S. 1978. Collagen fibrils and elastic fibers in rat-tail tendon: an electron microscopic investigation. *Biopolymers*, **17**, 843 – 855.

Pichler, B., Scheiner, S., & Hellmich, C. 2008. From micron-sized needle-shaped hydrates to meter-sized shotcrete tunnel shells: micromechanical upscaling of stiffness and strength of hydrating shotcrete. *Acta Geotechnica*, **3**, 273 – 294.

Reid, S.A., & Boyde, A. 1987. Changes in the mineral density distribution in human bone with age: Image analysis using backscattered electrons in the SEM. *Journal of bone and mineral research*, **2**(1), 13 – 22.

Roholl, P.J.M, Blauw, E., Zurcher, C., Dormans, J.A.M.A., & Theuns, H.M. 1994. Evidence for a diminished maturation of preosteoblasts into osteoblasts during aging in rats: an ultrastructural analysis. *Journal of bone and mineral research*, **9**(3), 355 – 366.

Sharpe, W.D. 1979. Age changes in human bone: an overview. *Bulletin of the New York Academy of Medicine*, **55**(8), 757 – 773.

Smith, J.W. 1963. Age changes in the organic fraction of bone. *The Journal of Bone and Joint Surgery*, **45B**, 761 – 769.

Teitelbaum, S. 2000. Bone resorption by osteoclasts. *Science*, **289**, 1504 – 1508.

Urist, M.R., DeLange, R.J., & Finerman, G.A.M. 1983. Bone Cell Differentiation and Growth Factors. *Science*, **220**, 680 – 686.

Weiner, S., & Wagner, H.D. 1998. The material bone: structure - mechanical function relations. *Annual Review of Materials Science*, **28**, 271 – 298.